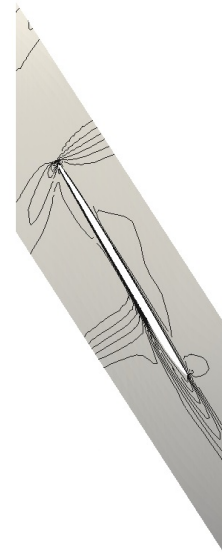
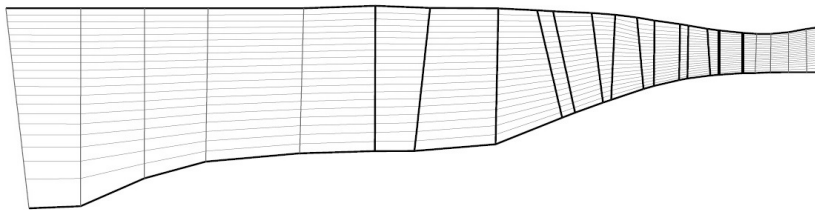


CHALMERS



Preliminary Compressor Design Method Development

Development of an S1-S2 calculation system for axial flow compressors

Master's thesis in Engineering Mathematics and Computational Science

DANIEL LINDBLAD

Department of Applied Mechanics

Division of Fluid Dynamics

CHALMERS UNIVERSITY OF TECHNOLOGY

Göteborg, Sweden 2014

Master's thesis 2014:38

MASTER'S THESIS IN ENGINEERING MATHEMATICS AND COMPUTATIONAL SCIENCE

Preliminary Compressor Design Method Development

Development of an S1-S2 calculation system for axial flow compressors

DANIEL LINDBLAD

Department of Applied Mechanics
Division of Fluid Dynamics
CHALMERS UNIVERSITY OF TECHNOLOGY
Göteborg, Sweden 2014

Preliminary Compressor Design Method Development
Development of an S1-S2 calculation system for axial flow compressors
DANIEL LINDBLAD

© DANIEL LINDBLAD, 2014

Master's thesis 2014:38
ISSN 1652-8557
Department of Applied Mechanics
Division of Fluid Dynamics
Chalmers University of Technology
SE-412 96 Göteborg
Sweden
Telephone: +46 (0)31-772 1000

Cover:

Left: Streamlines passing through a three-stage transonic compressor, computed by a streamline curvature method.

Right: Mach contours around a transonic rotor blade, computed by a quasi-three-dimensional blade-to-blade method.

Chalmers Reproservice
Göteborg, Sweden 2014

Preliminary Compressor Design Method Development
Development of an S1-S2 calculation system for axial flow compressors
Master's thesis in Engineering Mathematics and Computational Science
DANIEL LINDBLAD
Department of Applied Mechanics
Division of Fluid Dynamics
Chalmers University of Technology

ABSTRACT

The design of modern, transonic, axial flow compressors for applications within aero engines is a very complex process that is divided into many stages. It starts with fairly primitive methods to lay out the overall design, and ends with sophisticated 3D simulations using Computational Fluid Dynamics (CFD). In between these stages, throughflow methods are applied to design the annular geometry and spanwise variations of blade shapes. These methods are dependent on correlations, which often have problems in predicting the performance of modern blade designs. This makes the step between the throughflow method and the CFD method large, since the design predicted by the throughflow method often turn out insufficient when reality is approached in 3D CFD.

In this work, a possible remedy to this problem is investigated by coupling the streamline curvature (SLC) throughflow code SC90C with a Quasi-Three-Dimensional (Q3D) blade-to-blade method. The blade-to-blade method is used to correct the correlations used in SC90C in order to get better predictions for the performance of arbitrary blade designs. The coupling is done in the Python 3 programming language to obtain a fully automated S1-S2 calculation system.

In the SLC method, the inviscid momentum equations, together with the continuity and energy equations, are rewritten in a form suitable for the geometry of the compressor annulus. These are solved in conjunction with correlations on a mesh laid out between the hub and shroud, using a finite difference scheme. The blade-to-blade flow is modeled using the Favre averaged Navier-Stokes equations and the standard $k - \varepsilon$ turbulence model. These are solved using a finite volume discretization method on a mesh having the shape of a streamtube passing over the blade. A special source term is also used to model the pressure gradient normal to the flow. This removes the necessity of resolving it, resulting in a smaller mesh size and less time consuming simulations.

The S1-S2 system is used to predict the performance of a three-stage transonic compressor and the results are compared to 3D CFD. The results are promising, but also identifies several restrictions in the approach currently employed. These will have to be investigated further if the method should be applied in the future.

Keywords: Axial Flow Compressor, Compressible Flow, Compressor Performance, Computational Fluid Dynamics, CFD, Finite Volume Method, FVM, Quasi-Three-Dimensional Blade-To-Blade Calculations, Q3D, S1-S2 Calculation System, Streamline Curvature Method, SLC, Streamtube Source Term, Turbulence Modeling, Unsteady Favre averaged Navier-Stokes Equations

ACKNOWLEDGEMENTS

First and foremost, I would like to thank my supervisor Martin Olausson at GKN Aerospace for the help, support and many fruitful discussions he has offered throughout this project. Without his excellent knowledge in the field, this project would never have reached as far as it did.

I would also like to thank my examiner Tomas Grönstedt at Chalmers for all his support and interest in this project.

I would further like to thank all my colleagues at GKN Aerospace for contributing to a fun and creative atmosphere to work in. I would especially like to thank Pieter Groth, for showing great interest and belief in my work and for the many interesting discussions we have had over the last months.

I would finally like to thank family and friends, for the great support and friendship that they have offered during my five years of engineering studies, including the work towards this masters thesis.

NOMENCLATURE

Roman symbols

a	Speed of sound	P_k	Production of turbulent kinetic energy
b	Blockage	Pr	Prandtl number
c_p	Specific heat at constant pressure	Pr_t	Turbulent Prandtl number
c_v	Specific heat at constant volume	q	Coordinate along QO
C_f	Pressure loss correction factor	q_j	Heat flux vector
$C_{\varepsilon 1}$	Constant in $k - \varepsilon$ turbulence model	Q	Heat
$C_{\varepsilon 2}$	Constant in $k - \varepsilon$ turbulence model	QO	Quasi-orthogonal
C_μ	Constant in $k - \varepsilon$ turbulence model	\mathcal{Q}	State vector for flow equations in conservative form
e	Internal energy per unit mass	\mathbf{Q}	Volume average state vector for flow equations in conservative form
E	Internal energy	r	Radial coordinate
f_p	Average flux of momentum	R	Specific gas constant
f_e	Average flux of energy	s	Entropy per unit mass, Space
f_k	Average flux of turbulent kinetic energy	S	Entropy
f_ε	Average flux of dissipation of turbulent kinetic energy	S_j	Cartesian component of wall normal area vector
F_i	Force in streamtube source term	S_{ij}	Strain rate tensor
\mathcal{F}_j	Flux vector for flow equations in conservative form	t	Time
g	Gravitational acceleration	T	Temperature
h	Enthalpy per unit mass	u_i	Cartesian velocity component
H	Enthalpy	u_x	Axial velocity
\mathcal{H}	Source vector for flow equations in conservative form	u_r	Radial velocity
\mathbf{H}	Volume average source vector for flow equations in conservative form	u_θ	Tangential velocity
i	Incidence	u_m	Meridional velocity
I	Rothalpy	U	Local blade speed
k	Heat conductivity, Turbulent kinetic energy	v	Volume per unit mass
l	Chord length	V	Volume
L	Angular momentum	w_x	Axial velocity, relative frame of reference
m	Mass	w_r	Radial velocity, relative frame of reference
M	Mach number	w_θ	Tangential velocity, relative frame of reference
n_j	Cartesian component of wall normal vector	W	Work
p, P	Pressure	x	Axial coordinate
		Y_p	Pressure loss coefficient

Greek symbols

α	Swirl angle, Under-relaxation factor	μ_t	Turbulent viscosity
α'	Blade angle	ξ	Stagger angle
β	Swirl angle, relative frame of reference	ρ	Density
γ	Ratio of specific heats	σ	Solidity
δ	Deviation	σ_k	Constant in $k - \varepsilon$ turbulence model
δ_{ij}	Kronecker delta	σ_ε	Constant in $k - \varepsilon$ turbulence model
Δ_δ	Deviation correction	σ_{ij}	Viscous stress tensor
ε	Dissipation of turbulent kinetic energy, Deflection	τ	Torque
η_c	Isentropic efficiency	τ_{ij}	Complete (viscous + turbulent) stress tensor
η_p	Polytropic efficiency	ϕ	Sweep angle
θ	Angle	φ	Inclination angle
μ	Dynamics viscosity	Φ	Flow coefficient
		Ω	Rotational speed, Control volume

Subscripts

0	Stagnation/Total property	rel	Relative frame of reference
1	Inlet condition	rev	Reversible process
2	Outlet condition	s	State after isentropic process
irr	Irreversible process	S	Stator
m	Meridional component	t	Turbulent quantity
r	Radial component	θ	Tangential component
R	Rotor	x	Axial component

Superscripts

$\hat{\phi}$	Flux equivalent property		
$\bar{\phi}$	Time average		
$\tilde{\phi}$	Favre average	ϕ''	Turbulent fluctuation for Favre averaged quantity
$\dot{\phi}$	Rate of change		
ϕ'	Turbulent fluctuation for time averaged quantity	ϕ^*	Effective throttle area

Abbreviations

CFD	Computational Fluid Dynamics
DCA	Double Circular Arc
FVM	Finite Volume Method
IGV	Inlet Guide Vane
Q3D	Quasi-Three-Dimensional
SLC	Streamline Curvature

CONTENTS

Abstract	i
Acknowledgements	iii
Nomenclature	v
Contents	vii
1 Introduction	1
1.1 Context	1
1.2 Background	1
1.3 Purpose	1
1.4 Limitations	1
2 Theory	2
2.1 Axial Flow Compressor	2
2.1.1 Coordinate System and Velocity Triangles	2
2.1.2 Blade Row Geometry	3
2.1.3 Streamtube Concept	5
2.1.4 Losses in a Compressor	6
2.2 Thermodynamic Properties of Air	7
2.2.1 Equation of state	7
2.2.2 Internal Energy and Enthalpy	7
2.3 First Law of Thermodynamics	8
2.3.1 The first law	8
2.3.2 Energy	8
2.3.3 Transfer of energy	9
2.3.4 Steady state energy balance	10
2.4 Second Law of Thermodynamics	10
2.4.1 The Second Law	11
2.4.2 Clausius-Gibbs Equations	11
2.4.3 Entropy generation in Irreversible Processes	12
2.4.4 Isentropic Process Relation	12
2.5 Compressible Flow Relations	12
2.5.1 Stagnation Properties	13
2.5.2 Stagnation Property Relations	13
2.6 Compressor Performance	13
2.6.1 Lost work	14
2.6.2 Efficiency	14
2.6.3 Pressure Loss	15
2.6.4 Performance Characteristics	16
2.7 Euler Work Equation	17
2.7.1 Angular Momentum	17
2.7.2 Change of Angular Momentum	17
2.7.3 Steady State Angular Momentum Balance	18
2.7.4 Euler Work Equation	18
2.8 Streamline Curvature Equations	19
2.8.1 Assumptions and Coordinate System	19
2.8.2 Governing Equations	19
2.9 Favre Averaged Navier Stokes Equations	21
2.9.1 Governing Equations	21
2.9.2 Favre Averaging	22
2.9.3 Modeling and assumptions	24

2.9.4	Turbulence model	24
2.9.5	Final Equations	25
2.9.6	Rotating Frame of Reference	26
3	Method	27
3.1	Streamline Curvature Method	27
3.1.1	Computational Domain	27
3.1.2	Numerical Method	27
3.1.3	Correlations and Physical Models	29
3.2	Computational Fluid Dynamics	30
3.2.1	Computational Domain	31
3.2.2	Numerical Method	32
3.2.3	Streamtube Source Term	35
3.2.4	Flux Equivalent Flow Variables	36
3.3	S1-S2 Calculation System	36
3.3.1	Program Structure	37
3.3.2	Start Program	37
3.3.3	Read Data from SC90C	37
3.3.4	Set Boundary Conditions	37
3.3.5	Calculate Streamtube Geometry	39
3.3.6	Set up Mesh Files	39
3.3.7	Set up CFD Files	40
3.3.8	Create Mesh and Run CFD	41
3.3.9	Read Data from CFD	41
3.3.10	Set up SC90C Files	42
3.3.11	Run SC90C	43
4	Results	45
4.1	Simulation Results	45
4.1.1	Characteristic Map	45
4.1.2	Performance of individual components	46
4.1.3	Blade To Blade Calculations	53
4.2	Convergence of S1-S2 iterations	54
4.2.1	Deviation Correction	54
4.2.2	Pressure loss Correction	55
5	Discussion	56
5.1	Streamline Curvature Method	56
5.1.1	SLC Method implemented in SC90C	56
5.1.2	Setup and usage within S1-S2 system	57
5.2	Computational Fluid Dynamics	57
5.2.1	Modeling and CFD software	58
5.2.2	Setup and use within S1-S2 system	58
5.3	S1-S2 Calculation System	58
5.3.1	General	58
5.3.2	Implementation	59
5.3.3	Results	59
	References	61
A	Flux Equivalent Flow Variables	I
A.1	Average Fluxes	I
A.2	Flux Equivalent Properties	I

1 Introduction

1.1 Context

Turbofan and jet engines that power both civil and military aircraft are common machines in which axial flow compressors are found. With increased air travel, the demand for efficient engines, including the compressors, is also increasing in order to minimize emissions and environmental impact. The design of new compressors is to a large extent performed using computer simulations. The design process is therefore dependent on fast and accurate computer programs that can exploit a large design space in the shortest time possible.

1.2 Background

Several numerical approaches have been developed since the application of numerical methods to turbomachinery emerged in the 1940s, Denton and Dawes 1999. The backbone of the design process is the throughflow calculation, Casey and Robinson 2010. Several different throughflow methods have been developed over the years, and among these the streamline curvature (SLC) method has become the most common one, Denton and Dawes 1999. The SLC method has several important merits, it is fast, easy to use and can handle both subsonic and supersonic flows within the compressor. Also, provided that accurate correlations or good empirical input is provided for loss and work generated by the blades, the SLC method can give very accurate results, Denton and Dawes 1999. To obtain these input data, quasi-three-dimensional blade-to-blade calculations can be performed using Computational Fluid Dynamics (CFD). These methods can handle arbitrary blade shapes and enable the detailed flow pattern past the blade to be studied, Calvert and Ginder 1999.

For even more detailed analysis, fully three-dimensional CFD calculations of entire compressors are today possible to perform. These are however very computationally demanding, and are therefore not suited to replace the SLC method as the main tool in the design process.

For design purposes, continued development of the SLC method and how it can be coupled with a blade-to-blade method for blade performance analysis is therefore still important. This approach is less computationally demanding than three-dimensional CFD and have been shown to give good results, Calvert and Stapleton 1994.

1.3 Purpose

The purpose of this thesis is to investigate how a commercial SLC software, *SC90C* 2011, can be coupled with an in-house blade-to-blade software based on the work by Eriksson 1995 and Ellbrant and Eriksson 2014. The aim is to build a fully automated system, known as a S1-S2 calculation system, capable of predicting the performance of a transonic axial flow compressor.

1.4 Limitations

The project was limited to half a year of work for one masters thesis student. The project included an extensive literature review on the subjects of axial flow compressors, the SLC method and the blade-to-blade method. The project was limited to developing the system and comparing it to three-dimensional CFD results for an existing three-stage transonic compressor. It did not include any extensive validation or application of the system within development of new compressors.

2 Theory

2.1 Axial Flow Compressor

A compressor is a machine whose primary purpose is to transfer energy to a continuously moving fluid, thereby increasing the energy and pressure of it. The work is transferred from a shaft to the fluid, through aerodynamic forces generated by rotating blades attached to the shaft. In an axial flow compressor, the fluid moves roughly parallel to the axis of rotation and the velocity is continuously decreased. An important feature of an axial compressor is that the flow always moves against a pressure gradient. This favors boundary layer growth and separation from the blades, which complicates the design, Dixon and Hall 2013.

The general outline of a three-stage low pressure compressor is schematically depicted in Figure 2.1.

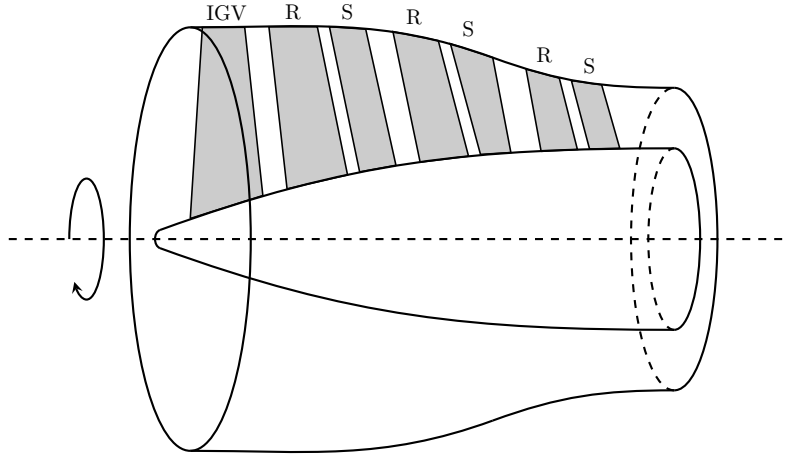


Figure 2.1: Outline of three-stage low pressure compressor.

The flow enters to the left, passes a set of compressor stages and then leaves to the right. A compressor stage is defined as a rotating blade row followed by a stationary blade row. The rotating blades are abbreviated rotors and are fixed to the inner casing, often denoted the hub. The stationary blades are abbreviated stators and are fixed to the outer casing, often denoted the shroud. Before the first stage, an inlet guide vane (IGV) is also depicted. The main role of this component is to accelerate and direct the flow so that it enters the first rotor with a suitable speed and angle.

2.1.1 Coordinate System and Velocity Triangles

Coordinate system

It is common to describe the flow in a cylindrical coordinate system, as depicted in Figure 2.2. Referring to this figure, a stream surface is defined such that the mean flow at all points is parallel to the surface, Dixon and Hall 2013. The figure depicts a stream surface that does not change radius in the circumferential direction. This is however generally not the case, as they tend to twist, Denton and Dawes 1999. Furthermore, the average of flow properties in the circumferential direction are usually considered. This will be assumed for the properties presented in the rest of this section.

Velocity triangles

Referring once again to Figure 2.2, the flow has velocity components along the x , r and θ axis. These are referred to as the axial, radial and swirl (or tangential) velocity respectively. The velocity along the stream surface is further denoted the meridional velocity

$$u_m = \sqrt{u_x^2 + u_r^2}. \quad (2.1)$$

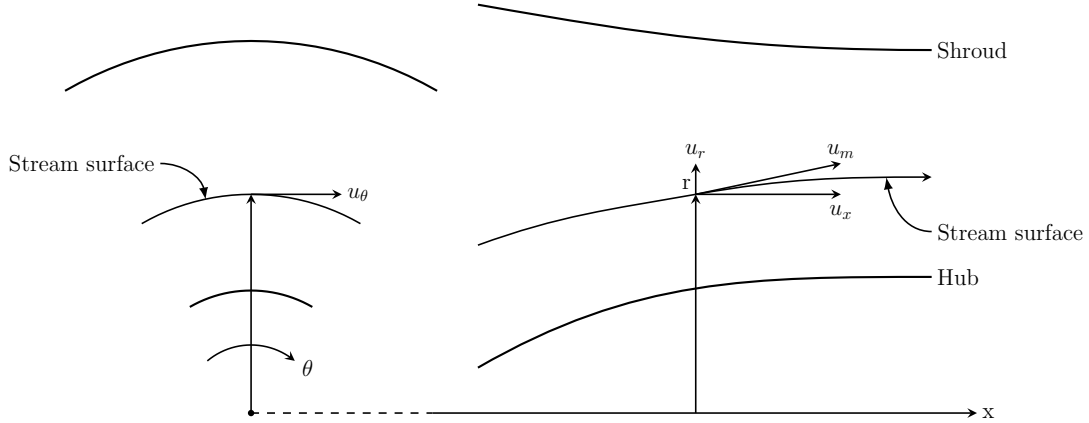


Figure 2.2: *Coordinate system for an axial flow compressor.*

The magnitude of the velocity is given by

$$u = \sqrt{u_m^2 + u_\theta^2}. \quad (2.2)$$

The swirl angle, α , is defined as a measure of how much the fluid rotates in the machine according to

$$\alpha = \arctan\left(\frac{u_\theta}{u_m}\right). \quad (2.3)$$

When analyzing the flow past a rotor, the flow is usually considered in a relative frame of reference moving with the blade. The blade speed in the circumferential direction at a certain location along the stream surface is denoted by U . The velocity relative to the blade, w , is obtained as the vector subtraction of U from u . This gives the following components of w

$$w_x = u_x, \quad (2.4)$$

$$w_r = u_r, \quad (2.5)$$

$$w_\theta = u_\theta - U. \quad (2.6)$$

The relative swirl angle, β , is defined as

$$\beta = \arctan\left(\frac{w_\theta}{u_m}\right). \quad (2.7)$$

The velocity of the fluid along a stream surface passing through a compressor stage can also be represented in terms of velocity triangles, as depicted in Figure 2.3.

Different conventions for defining positive swirl velocities, and consequently flow angles, exist. The convention adopted throughout this work, unless otherwise stated, is to take the velocities and flow angles in Figure 2.3 as positive. This means that the absolute and relative swirl velocities are defined as positive if they are in the same and opposite direction as the rotation of the blade respectively.

2.1.2 Blade Row Geometry

In addition to the flow between the blade rows, the flow relative the blades as well as the blade geometry itself are important parameters in compressor design and analysis. These are usually evaluated along a stream surface passing over the compressor blade row, as depicted in Figure 2.4.

The camber line together with the thickness distribution are sufficient to describe the shape of the blade. However, in order to describe the complete compressor blade row, a few more are needed, among the most common are listed in Table 2.1, Dixon and Hall 2013.

The flow past the blades is also described through a set of parameters, which are listed in Table 2.2, Dixon and Hall 2013.

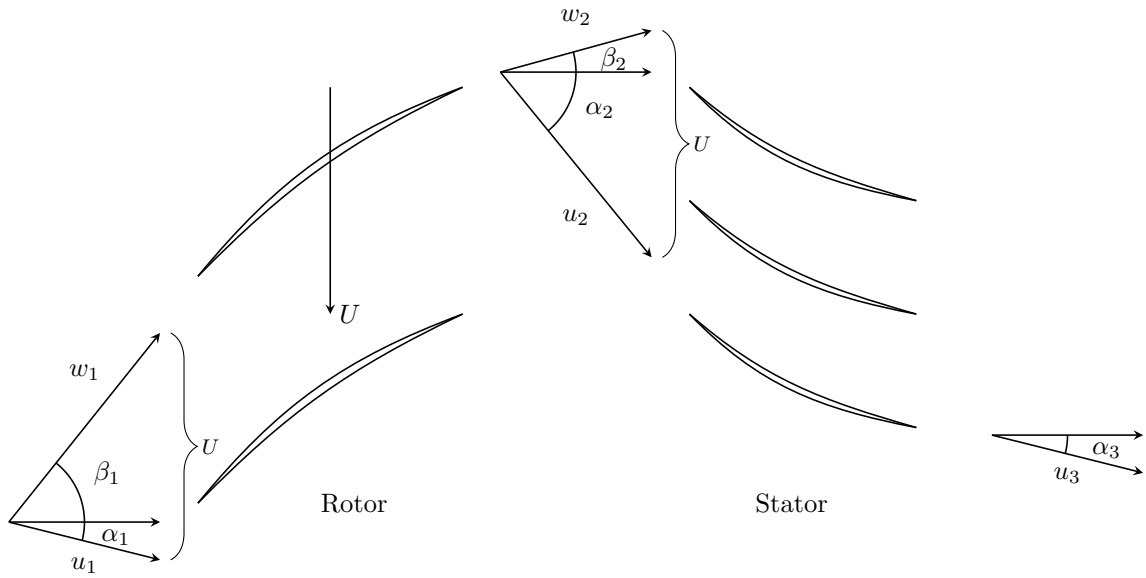


Figure 2.3: Velocity triangles for a compressor stage.

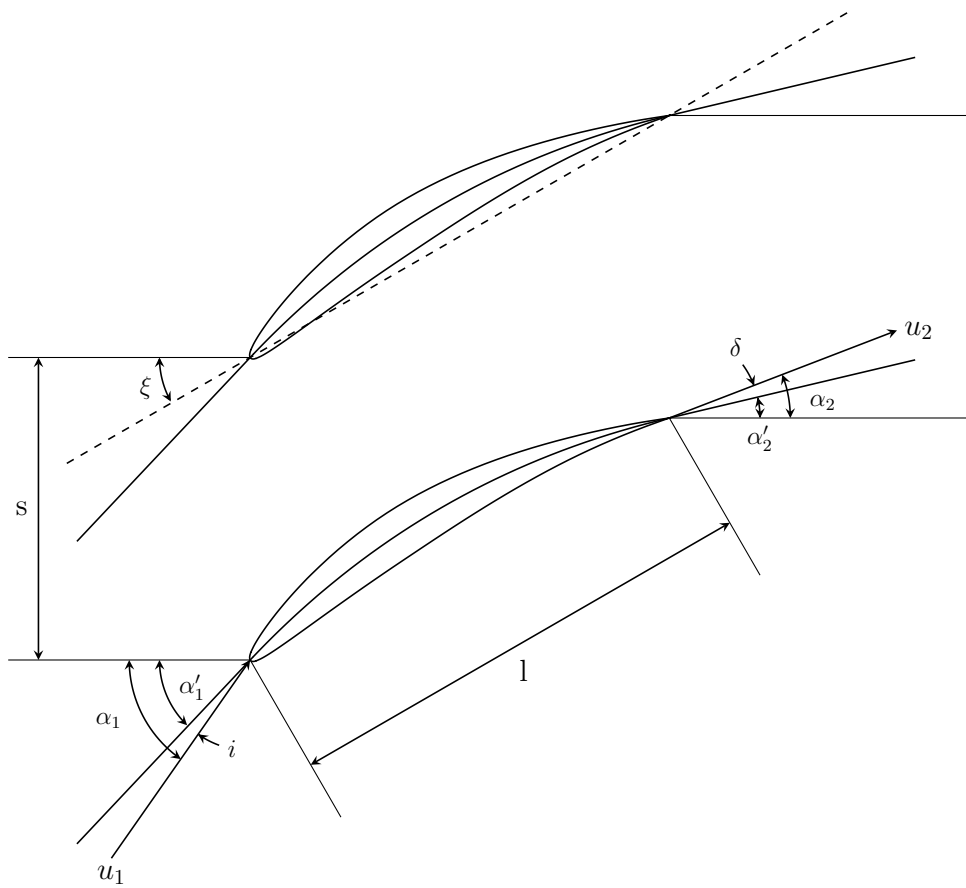


Figure 2.4: Blade row geometry with blade notation ¹.

¹Airfoil profile obtained from UIUC Airfoil Coordinates Database: http://www.ae.uiuc.edu/m-selig/ads/coord_database.html. Data is released under the GNU General Public Licence. See <http://www.ae.uiuc.edu/m-selig/pd/gpl.html> for more details.

Table 2.1: Blade row parameters.

Name	Symbol	Description
Chord	l	Length of the blade between the leading and trailing edge
Space	s	Distance between the blades, varies with number of blades in the blade row as well as radius
Stagger angle	ξ	Angle between the chord line (dashed in figure) and the axial direction
Inlet blade angle	α'_1	Angle between the camber line and the meridional direction at the leading edge
Outlet blade angle	α'_2	Angle between the camber line and the meridional direction at the trailing edge
Camber angle	$\theta = \alpha'_1 - \alpha'_2$	Change in blade angle between leading and trailing edge (not in figure)
Maximum thickness	t_{\max}	Maximal thickness of the blade (not in figure)
Solidity	$\sigma = l/s$	Ratio between spacing and chord

Table 2.2: Flow parameters.

Name	Symbol	Description
Inlet swirl angle	α_1, β_1	Absolute and relative swirl angle
Outlet swirl angle	α_2, β_2	Absolute and relative swirl angle
Incidence	$i = \alpha_1 - \alpha'_1$	Difference between the inlet swirl and blade angles
Deviation	$\delta = \alpha_2 - \alpha'_2$	Difference between the exit swirl and blade angles
Deflection	$\varepsilon = \alpha_1 - \alpha_2$	Change in swirl angle between leading and trailing edge (not in figure)

These parameters are often related, both alone and in combination, to the performance of the the compressor blade row.

2.1.3 Streamtube Concept

As depicted in Figure 2.5, a streamtube is defined as the region enclosed by two stream surfaces, Denton and Xu 1999.

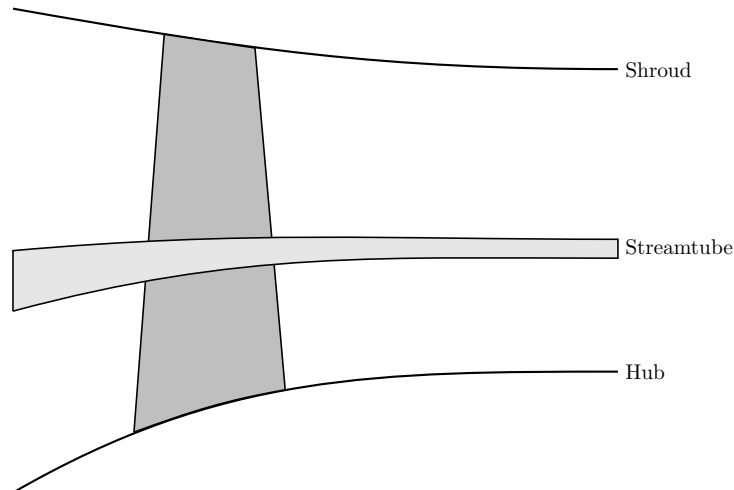


Figure 2.5: *Streamtube enclosed by two stream surfaces.*

Due to this definition, the mean mass flow within a streamtube is constant throughout the compressor. In general, a streamtube can change both thickness and radius as well as twist as it passes through the compressor, Denton and Xu 1999. It is important to realize that the streamtube is a concept, which only is valid for the steady flow field. Also, even though mass is not transferred between streamtubes, entropy as well as angular momentum and energy generally are due to turbulent mixing, Gallimore 1986, Casey and Robinson 2010.

The streamtube concept is broadly applied in the design and analysis of turbomachinery. In these applications,

which include performing CFD on streamtubes as well using throughflow methods, additional assumptions are often introduced. One assumption when applying CFD to streamtubes is to assume that they do not twist, Denton and Xu 1999. Another assumption, common in throughflow methods, is that there is negligible turbulent mixing between them, Casey and Robinson 2010.

2.1.4 Losses in a Compressor

The process of increasing the pressure of a fluid in a compressor is never ideal. This means that some of the work put in never transfers into increased pressure of the fluid, but instead into entropy. The mechanisms that cause these losses are often categorized into two and three dimensional, dependent on their nature, Dixon and Hall 2013. The possible 2D and 3D losses are outlined in Table 2.3.

Table 2.3: Compressor loss sources

2D		3D	
(i)	Blade boundary layer	(i)	End wall loss
(ii)	Mixing of trailing edge wake	(ii)	Tip leakage loss
(iii)	Flow separation from blade		
(iv)	Shock waves		

In this section, these losses and their underlying mechanisms will be discussed briefly. The connection between generated entropy and lost pressure will be presented later. It should be noted that even though some losses are categorized as 2D, their underlying mechanisms often include some three dimensional effects, Miller and Denton 2012. For example, a shock wave between two blades, as a result of the decreased flow area between the blades, is also strongly influenced by the amount of contraction of the channel due to changing radius of the hub and shroud. 2D losses should hence rather be viewed as quasi-three-dimensional effects taking place along stream surfaces, or in streamtubes.

Blade boundary layers

Since a compressor is designed to increase the pressure of the fluid, the flow will almost always move towards higher pressure. This adverse pressure gradient flow favors the build up of boundary layers on the blades, Dixon and Hall 2013. Within the boundary layers, entropy is generated through viscous friction due to shearing of the fluid. In general, the losses are greatest in the suction surface boundary layers because of the higher velocities present in them, Miller and Denton 2012.

Mixing of trailing edge wake

When the boundary layer leaves the blade, it will form a wake behind it, Dixon and Hall 2013. This wake will eventually mix out with the mean flow, a process in which viscous friction causes entropy generation. In this process, the kinetic energy in the turbulent eddies will also dissipate and generate heat. Since heat transfer through temperature gradients generate entropy, this will also be a contributing factor to the total entropy production in the wake, Miller and Denton 2012.

Flow separation from blade

Flow separation, in which the flow detaches from the suction surface of the blade, is an undesirable effect that should not be present in a compressor at design operating conditions, Dixon and Hall 2013. When the flow separates, the amount of work the compressor blade can perform is reduced, mainly because the flow is not turned as much. Also, work is lost due to entropy creation through viscous effects, as previously discussed.

Shock waves

In modern transonic compressors, the relative velocity at entrance to the rotors is close the the speed of sound. If the inlet flow is subsonic, the compression and subsequent expansion of the fluid that occurs when the flow passes through the blade row can cause a shock wave. In cases where the inlet flow already is supersonic, the shock may instead be detached in front of the leading edge. In either case, a shock waves is a source of entropy and hence lost work. The shock wave also generates a compression, which will favor thickening of the boundary

layers behind the shock and thus contribute to more losses indirectly, Dixon and Hall 2013. Despite this, it can be shown that under certain conditions, a shock wave is a very efficient compression process, which is one reason to why transonic compressors still are being employed. Another reason is that transonic compressors can be made very compact, allowing for the design of smaller and more lightweight engines.

End wall loss

Boundary layers will build up at the hub and shroud throughout the compressor, Dixon and Hall 2013. These boundary layers does not form an isolated loss source, but instead interact with the boundary layers formed at the blades to form a complex and highly three dimensional flow field. Entropy is then generated through viscous friction in the boundary layers, as well as when the vortices formed are mixed out, Dixon and Hall 2013.

Tip leakage loss

There is often a tip clearance gap between rotor and shroud as well as between stator and hub in a compressor. These gaps causes loss of work in two ways. First, since the rotor does not cover the entire span between the hub and shroud, it can not do work on all the fluid passing through. Secondly, loss will arise due to entropy generation. This entropy is generated through both viscous shear in the tip gap as well as through mixing out of vortices formed when this flow interacts with the main stream flow, Dixon and Hall 2013.

2.2 Thermodynamic Properties of Air

In this section, some of the thermodynamic properties and relations used to describe the fluid considered in this work will be presented.

2.2.1 Equation of state

The fluid is assumed to be an ideal gas, meaning that intermolecular forces are neglected. This means that the gas can be assumed to obey the ideal gas law Sonntag, Borgnakke, and Van Wylen 1998

$$P = \rho RT, \quad (2.8)$$

where R is the specific gas constant, P the static pressure and T the static temperature of the fluid. This is a good model for air in the temperature range $160 - 2100K$, Dixon and Hall 2013.

2.2.2 Internal Energy and Enthalpy

The internal energy of a fluid constitutes of all molecular energies, such as molecular potential, kinetic, rotational and chemical energy, Sonntag, Borgnakke, and Van Wylen 1998. The internal energy and the internal energy per unit mass are here denoted E and e respectively. The enthalpy and enthalpy per unit mass are then defined as, Sonntag, Borgnakke, and Van Wylen 1998

$$H = E + PV, \quad (2.9)$$

$$h = e + Pv. \quad (2.10)$$

The volume and volume per unit mass of the fluid are here denoted V and v respectively. The specific heats of the gas at constant pressure and volume are defined as, Sonntag, Borgnakke, and Van Wylen 1998

$$c_p = \left(\frac{\partial h}{\partial T} \right)_P, \quad (2.11)$$

$$c_v = \left(\frac{\partial e}{\partial T} \right)_v. \quad (2.12)$$

The gas is assumed to be calorically perfect, meaning that the specific heats are assumed to be constant. In this case, the internal energy and enthalpy per unit mass can be written as, Andersson 2004

$$e = c_v T, \quad (2.13)$$

$$h = c_p T. \quad (2.14)$$

For a calorically perfect gas that obeys the ideal gas law, the following relations are also valid, Andersson 2004

$$R = c_p - c_v, \quad (2.15)$$

$$c_p = \frac{\gamma R}{\gamma - 1}, \quad (2.16)$$

$$c_v = \frac{R}{\gamma - 1}, \quad (2.17)$$

where $\gamma = c_p/c_v$ is the ratio of specific heats. The values of the various constants are listed in Table 2.4.

Table 2.4: Gas constants for air

γ	R [J/(kg K)]	c_p [J/(kg K)]	c_v [J/(kg K)]
1.4	287	1004.5	717.5

2.3 First Law of Thermodynamics

In this section, the first law of thermodynamics will be presented and used to derive the steady state energy balance for an open system. The concepts presented are important in understanding the flow through an axial flow compressor.

2.3.1 The first law

The first law of thermodynamics states that for a closed system that is taken through a complete cycle, the net sum of heat and work supplied to the system is zero, Sonntag, Borgnakke, and Van Wylen 1998

$$\oint d(Q + W) = 0. \quad (2.18)$$

Here, Q and W represent heat and work transfer respectively. If the system undergoes a change along some arbitrary path between state 1 and 2, there is a unique change in the energy, E_0 , of the system

$$E_{0,2} - E_{0,1} = \int_1^2 d(Q + W). \quad (2.19)$$

The first law can also be written in terms of the rate of change of energy, in which case it reads, Sonntag, Borgnakke, and Van Wylen 1998

$$\frac{dE_0}{dt} = \dot{Q} + \dot{W}. \quad (2.20)$$

Here, the dot represent rate of change with time.

2.3.2 Energy

In the first law, the energy considered is the macroscopic energy dependent on the mass of the system. The corresponding energy per unit mass is denoted e_0 . In either case, the macroscopic energy can be divided into internal energy, kinetic energy and potential energy. The kinetic and potential energy of the system represents energy due to macroscopic movement and displacement of the system, Sonntag, Borgnakke, and Van Wylen 1998. Using this division, the energy may be written as

$$E_0 = E + \frac{mu^2}{2} + mgz, \quad (2.21)$$

$$e_0 = e + \frac{u^2}{2} + gz, \quad (2.22)$$

where u is the magnitude of the velocity, g the gravitational acceleration, z the displacement normal to the earth surface and m the mass of the system.

2.3.3 Transfer of energy

The first law of thermodynamics is formulated for a closed system, in which mass is not exchanged with the surroundings. For such a system, heat and work exchange are the only two ways through which the energy in the system can be changed. The goal is to develop a balance of energy for an open system, in which mass can also enter and leave the system, as depicted in Figure 2.6. To do this, also the energy exchange due to flow over the system boundaries must be included. Below, all the different mechanisms are outlined.

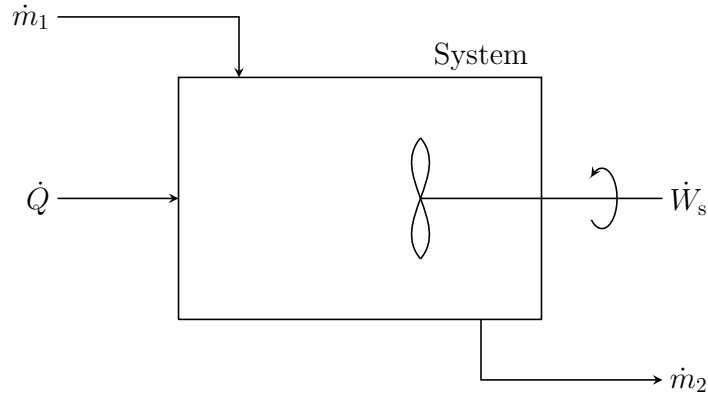


Figure 2.6: *Energy balance for open system.*

Work

Considering the system depicted in Figure 2.6, two types of work can be performed on it. The first is shaft work, which is due to the rotation of an impeller device inside the system. The rate of work done by this device is denoted \dot{W}_s .

The second type is flow work, which is work performed at the system boundaries by the fluid entering or leaving it. According to classical mechanics, work equals force multiplied by distance. For a one dimensional fluid flow, entering the system at velocity u_1 , the rate of work done on the system at the inlet is therefore given by, Sonntag, Borgnakke, and Van Wylen 1998

$$\dot{W}_{\text{flow, in}} = F_1 u_1. \quad (2.23)$$

If the flow enters through the inlet area A_{in} with a static pressure P_1 , the force is given by $P_1 A_{\text{in}}$ and thus the above expression may be rewritten as

$$\begin{aligned} \dot{W}_{\text{flow, in}} &= P_1 A_{\text{in}} u_1 \\ &= P_1 v_1 \dot{m}_1, \end{aligned} \quad (2.24)$$

where \dot{m}_1 and $v_1 = 1/\rho_1$ are the mass flow rate and volume per unit mass of the fluid entering the system respectively. The fluid leaving the system instead performs work on the surroundings, so the work done on the system at the outlet changes sign. Therefore, the net rate of flow work done on the system can be written as

$$\dot{W}_{\text{flow}} = \dot{m}_1 [Pv]_1 - \dot{m}_2 [Pv]_2. \quad (2.25)$$

Heat transfer

Heat transfer to or from a system can only change the internal energy of it. There are many types of heat transfer, such as convection, conduction and radiation. The individual mechanisms will not be considered here, but instead net rate of heat transfer due to all sources will be used, which is denoted \dot{Q} .

Energy convection

The fluid flow entering and leaving the system does not only perform work on it, it also carries energy across the system boundaries. If the fluid enters the system at the mass flow rate \dot{m}_1 , with an energy per unit mass e_0 , then the rate of energy addition to the system becomes

$$\dot{E}_{0,\text{in}} = \dot{m}_1 e_{0,1}. \quad (2.26)$$

Similarly, the fluid leaving the system carries energy out of the system. Therefore, the net rate of energy transfer to the system due to fluid flow becomes

$$\dot{E}_{0,\text{flow}} = \dot{m}_1 e_{0,1} - \dot{m}_2 e_{0,2}. \quad (2.27)$$

2.3.4 Steady state energy balance

The first law essentially states that energy can not be created nor destroyed. Thus it can be argued that the only ways for the energy to change within the system depicted in Figure 2.6 is through the mechanisms discussed above. By including these in (2.20), the extension of the first law for the open system becomes, Sonntag, Borgnakke, and Van Wylen 1998

$$\frac{dE_0}{dt} = \dot{Q} + \dot{W}_s + \dot{W}_{\text{flow}} + \dot{E}_{0,\text{flow}}. \quad (2.28)$$

The flow is assumed to be at steady state, meaning that the rate of change of both mass and energy at every point inside the system is zero. This implies that the mass flow in equals the mass flow out of the system, $\dot{m}_1 = \dot{m}_2 = \dot{m}$, and that the left hand side of (2.28) is zero. Under the steady state assumption, the extension of the first law thereby simplifies to

$$0 = \dot{Q} + \dot{W}_s + \dot{m} [Pv]_1 - \dot{m} [Pv]_2 + \dot{m} \left[e + \frac{u^2}{2} + gz \right]_1 - \dot{m} \left[e + \frac{u^2}{2} + gz \right]_2. \quad (2.29)$$

Introducing the definition of enthalpy, (2.10), and rearranging (2.29) slightly gives

$$\dot{Q} + \dot{W}_s = \dot{m} \left[(h_2 - h_1) + \left(\frac{u_2^2}{2} - \frac{u_1^2}{2} \right) + g(z_2 - z_1) \right]. \quad (2.30)$$

This is usually referred to as the steady state energy balance for an open system. When this energy balance is applied to an axial flow compressor, the change in potential energy is negligible compared to other terms. Furthermore a compressor is close to adiabatic, meaning that heat addition to the fluid is small, Dixon and Hall 2013. The sum of the enthalpy and the kinetic energy is further defined as the stagnation enthalpy

$$h_0 = h + \frac{u^2}{2}. \quad (2.31)$$

Using these simplifications and additional definitions, the final form of the steady state energy balance applied to a compressor becomes

$$\dot{W}_s = \dot{m}(h_{0,2} - h_{0,1}). \quad (2.32)$$

2.4 Second Law of Thermodynamics

In this section, the second law of thermodynamics is briefly presented. The consequences of this law are examined in order to define the concepts of entropy, reversible and irreversible processes.

2.4.1 The Second Law

The second law of thermodynamics postulates which types of thermodynamic cycles that can and can not occur. For example, it forbids the occurrence of a cyclic process that continuously transfers heat from a cold to a hot body, without the addition of work to the cycle. The exact formulations of the second law and the implications that they have on thermodynamic cycles will be omitted here. Instead, the main results of the second law will be presented.

From the formulation of the second law, it is possible to prove the 'Inequality of Clausius'. It states that for a closed system that passes through a complete cycle, involving heat and work exchange with the surroundings, the following inequality holds, Sonntag, Borgnakke, and Van Wylen 1998

$$\oint \frac{dQ}{T} \leq 0. \quad (2.33)$$

For a cycle that is performed reversibly, meaning that it is done in such a way that both the system and its surroundings will return to their respective initial state, it is also possible to prove that equality holds

$$\oint \left(\frac{dQ}{T} \right)_{\text{rev}} = 0. \quad (2.34)$$

If the system undergoes a process, reversible or irreversible, along some arbitrary path between state 1 and 2, there will be a unique change of a property called entropy, S . The change in entropy can be uniquely defined in terms of a reversible process between the two states according to

$$S_2 - S_1 = \int_1^2 \left(\frac{dQ}{T} \right)_{\text{rev}}. \quad (2.35)$$

This can also be written in differential form as

$$dS = \left(\frac{dQ}{T} \right)_{\text{rev}}. \quad (2.36)$$

It should be noted that the entropy change in the system between two states is independent on if the process is reversible or not. The change in entropy is however given by some reversible process between the states, according to (2.35), Sonntag, Borgnakke, and Van Wylen 1998. The entropy is here written as an extensive property dependent on the mass of the system, whereas the entropy per unit mass is denoted s .

2.4.2 Clausius-Gibbs Equations

Two important equations can be derived by combining the first and second law, known as the Clausius-Gibbs equations. Start by considering a system undergoing a reversible process that does not involve any change of potential or kinetic energy as well as any shaft work. For this system, the first law can be written in differential form as

$$dE = dQ + dW. \quad (2.37)$$

The system can only experience work through expansion or contraction

$$dW = -PdV. \quad (2.38)$$

Using this equation together with the definition of entropy, (2.36), equation (2.37) becomes

$$TdS = dE + PdV. \quad (2.39)$$

This is the first of the two equations. To derive the second one, start by differentiating the definition of enthalpy, (2.9), to obtain

$$dH = dE + PdV + VdP. \quad (2.40)$$

Inserting this expression into (2.39) gives the second equation sought

$$TdS = dH - VdP. \quad (2.41)$$

The Clausius-Gibbs equations may also be written in terms of properties per unit mass

$$Tds = de + Pdv, \quad (2.42)$$

$$Tds = dh - v dP. \quad (2.43)$$

It should be noted that the Clausius-Gibbs equations are written in terms of state properties. The change of these properties are independent on the path, reversible or irreversible, between two states. This means that the Clausius-Gibbs equations can be used to relate properties between two states of any process, as long as they are integrated along a reversible path between them, Sonntag, Borgnakke, and Van Wylen 1998.

2.4.3 Entropy generation in Irreversible Processes

For a system undergoing a change in state, (2.35) can be used to calculate the change in entropy. For an arbitrary, and possibly irreversible, process between the same two states it furthermore holds that, Sonntag, Borgnakke, and Van Wylen 1998

$$S_2 - S_1 \geq \int_1^2 \frac{dQ}{T}. \quad (2.44)$$

This inequality becomes strict if some part of the process is irreversible. The inequality can also be expressed in differential form according to

$$dS \geq \frac{dQ}{T}. \quad (2.45)$$

From this inequality it follows that if the same amount of heat dQ is supplied at the same absolute temperature T in a reversible and irreversible process respectively, then the entropy change in the irreversible process is greater, Sonntag, Borgnakke, and Van Wylen 1998. It also means that since the entropy change between two states is independent on the path, the entropy generation due to supplied heat is smaller in the irreversible case. Instead, entropy is generated through other mechanisms, which can be expressed as

$$dS = \frac{dQ}{T} + dS_{\text{irr}}. \quad (2.46)$$

The term dS_{irr} represents entropy generated due to irreversible effects such as friction, heat transfer through temperature gradients etc, Sonntag, Borgnakke, and Van Wylen 1998. From this equation it also follows that if the process is both adiabatic and reversible, there will be no entropy change. This type of process is denoted an isentropic process.

2.4.4 Isentropic Process Relation

For an isentropic process, the assumption of calorically perfect gas (2.11), ideal gas law (2.8) and Clausius-Gibbs equation (2.43) can be used to show that

$$\frac{P_2}{P_1} = \left(\frac{T_2}{T_1} \right)^{\gamma/(\gamma-1)}. \quad (2.47)$$

This equation can be used to relate the temperature and pressure between two states in an isentropic process.

2.5 Compressible Flow Relations

In this section, the concept stagnation property is defined and a set of relations for stagnation properties in a compressible flow field are presented.

2.5.1 Stagnation Properties

The properties of a fluid at the isentropic stagnation state are called stagnation, or total, properties. The isentropic stagnation state is further defined as the state the fluid would attain if it would undergo a reversible and adiabatic, i.e. isentropic, deceleration to zero velocity, Sonntag, Borgnakke, and Van Wylen 1998. The name total properties are sometimes used to better distinguish the isentropic stagnation state from the actual stagnation state that arise during a possibly irreversible deceleration to zero velocity. Both names are however used to denote the isentropic stagnation state in this work.

The stagnation properties can also be defined in a relative, or moving, frame of reference. The isentropic stagnation state is defined such that the velocity is zero in the relative frame of reference in this case.

2.5.2 Stagnation Property Relations

Two important equations that relate the stagnation pressure and temperature to the static pressure and temperature can be derived for a compressible flow field. To begin with, the local Mach number of the gas is defined as the ratio between the magnitude of the velocity and the local speed of sound, Andersson 2004

$$M = \frac{u}{a}. \quad (2.48)$$

The speed of sound for a calorically perfect gas that obeys the ideal gas law can further be calculated as, Andersson 2004

$$a = \sqrt{\gamma RT}. \quad (2.49)$$

If a calorically perfect gas is brought isentropically to rest, in the absence of work addition or change in vertical distance z , the first law (2.30) becomes

$$c_p T_0 = c_p T + \frac{u^2}{2}. \quad (2.50)$$

Here, the stagnation temperature, $T_0 = h_0/c_p$, has been introduced. Dividing both sides by $c_p T$ and using equations (2.16) and (2.49) yields

$$\begin{aligned} \frac{T_0}{T} &= 1 + \frac{u^2}{2c_p T} \\ &= 1 + \frac{(\gamma - 1)u^2}{2\gamma RT} \\ &= 1 + \frac{\gamma - 1}{2} \frac{u^2}{a^2}. \end{aligned} \quad (2.51)$$

By the definition of Mach number, this equation finally becomes

$$\frac{T_0}{T} = 1 + \frac{\gamma - 1}{2} M^2. \quad (2.52)$$

This relation can be used to relate the stagnation to the static temperature as long as the local Mach number and ratio of specific heats are known.

To relate the total and the static pressure, (2.47) can be combined with (2.52) to obtain

$$\frac{P_0}{P} = \left(1 + \frac{\gamma - 1}{2} M^2\right)^{\gamma/(\gamma-1)}. \quad (2.53)$$

2.6 Compressor Performance

The connection between entropy generation and lost work in a compressor is presented in this section. These effects are then quantified in terms of pressure loss and efficiency coefficients. Finally, methods of graphically presenting the performance of a compressor is presented.

2.6.1 Lost work

A compressor is close to adiabatic ($dQ \approx 0$) and hence the entropy generated within it almost exclusively originate from irreversible effects. The connection between entropy generation and lost work can be illustrated through the following example, taken from Dixon and Hall 2013.

Suppose that there exist two compressors that achieve the same pressure ratio when operating with the same inlet conditions. The first one does this reversibly and the second irreversibly. This means that the entropy change of the gas per unit mass over the first compressor is 0, and over the second one it is denoted Δs . Let further the stagnation enthalpy at the inlet to both compressors be denoted by $h_{0,1}$, and at the outlet $h_{0,2s}$ and $h_{0,2}$ for the first and second compressor respectively. The work transferred to the fluid in the two compressors is then given by

$$\Delta W_{\text{rev}} = h_{0,2s} - h_{0,1}, \quad (2.54)$$

$$\Delta W_{\text{irr}} = h_{0,2} - h_{0,1}. \quad (2.55)$$

Since both compressors achieve the same exit pressure, the Clausius-Gibbs equation (2.43) can be integrated along a constant pressure path ($dP = 0$) between the two states 2 and $2s$. By approximating the temperature as constant, the following is obtained

$$h_{0,2s} - h_{0,2} \approx -T_{0,2}\Delta s. \quad (2.56)$$

Using this result, the difference in work input to the two compressors can be approximated as

$$\begin{aligned} \Delta W_{\text{irr}} - \Delta W_{\text{rev}} &= h_{0,2} - h_{0,2s} \\ &\approx T_{0,2}\Delta s. \end{aligned} \quad (2.57)$$

This shows that the work needed to achieve the same exit pressure for an irreversible process is higher compared to a reversible one, due to the generation of entropy. Hence, some of the work put into the irreversible machine is lost in the sense that it goes into increased entropy instead of pressure.

2.6.2 Efficiency

Two types of efficiencies applicable to compressors will be presented in this part, namely the isentropic and polytropic efficiency.

Isentropic Efficiency

The ratio between the minimum and the actual work needed to reach a certain total pressure is defined as the isentropic efficiency. For a compressor, which is close to adiabatic, the minimum work input is represented by an isentropic process. Denoting the state of the fluid at the inlet and outlet 1 and 2 respectively, the following equation for the isentropic efficiency is obtained, Dixon and Hall 2013

$$\eta_c = \frac{h_{0,2s} - h_{0,1}}{h_{0,2} - h_{0,1}}. \quad (2.58)$$

This equation needs to be rewritten slightly to evaluate the efficiency for a given compressor, since the isentropic stagnation enthalpy at outlet is unknown. First, the enthalpy is rewritten using (2.14), which yields

$$\eta_c = \frac{T_{0,2s} - T_{0,1}}{T_{0,2} - T_{0,1}}. \quad (2.59)$$

The isentropic stagnation temperature can be found by noting that the isentropic process should reach the same stagnation pressure as the real one. Therefore, (2.47) can be inverted to give an equation for the isentropic stagnation temperature as follows

$$T_{0,2s} = T_{0,1} \left(\frac{P_{0,2}}{P_{0,1}} \right)^{(\gamma-1)/\gamma}. \quad (2.60)$$

By inserting (2.60) into (2.59) and rewriting it slightly, the following expression for the isentropic efficiency can finally be obtained

$$\eta_c = \frac{\left(\frac{P_{0,2}}{P_{0,1}}\right)^{(\gamma-1)/\gamma} - 1}{\frac{T_{0,2}}{T_{0,1}} - 1}. \quad (2.61)$$

Polytropic Efficiency

The isentropic efficiency was defined in terms of comparing the compressor to a single, isentropic, compression of the fluid to the same stagnation pressure. Another efficiency can be defined by regarding the compressor as made up of a set of finite compression processes. The polytropic efficiency is defined as the ratio between the work needed to perform an infinitesimal, isentropic, compression and the corresponding work needed for the real compression, Dixon and Hall 2013

$$\eta_p = \frac{dh_{0,s}}{dh_0}. \quad (2.62)$$

For an isentropic process, the Clausius-Gibbs equation (2.43) gives that $dh_{0,s} = v dP_0$. Furthermore, from (2.14) it also holds that $dh_0 = c_p dT_0$. Hence, the polytropic efficiency can be rewritten as

$$\eta_p = \frac{v dP_0}{c_p dT_0}. \quad (2.63)$$

The volume per unit mass and the specific heat may be rewritten using (2.8) and (2.16) respectively to obtain

$$\frac{dT_0}{T_0} = \frac{\gamma - 1}{\eta_p \gamma} \frac{dP_0}{P_0}. \quad (2.64)$$

By assuming that each infinitesimal compression process has the same efficiency, (2.64) may be integrated between the inlet and outlet states of the compressor. The resulting equation can then be rearranged to obtain the following expression for the polytropic efficiency

$$\eta_p = \frac{\gamma - 1}{\gamma} \frac{\ln\left(\frac{P_{0,2}}{P_{0,1}}\right)}{\ln\left(\frac{T_{0,2}}{T_{0,1}}\right)}. \quad (2.65)$$

The difference between isentropic and polytropic efficiency can be illustrated by considering two compressors with equal polytropic efficiencies that attain different pressure ratios. It can be argued that both compressors are equally efficient, since each small compression is done equally efficient and the only difference is how much the fluid is compressed. However, it can also be shown that the isentropic efficiency is lower for the compressor with the higher pressure ratio, Dixon and Hall 2013. The polytropic efficiency is therefore considered a better way of comparing compressors of different pressure ratio than the isentropic efficiency.

2.6.3 Pressure Loss

The concept of pressure loss is often used in turbomachinery to quantify lost total pressure over the blade rows due to irreversible effects. The pressure loss is defined as the difference in total pressure after the blade row between a reversible and the real process, both attaining the same stagnation enthalpy. The pressure loss is quantified through the pressure loss coefficient, Y_p , which in words is defined as, Dixon and Hall 2013

$$Y_p = \frac{\text{Loss in total pressure}}{\text{Reference dynamic pressure}}. \quad (2.66)$$

For rotors, it is common to evaluate the stagnation properties in a relative frame of reference. The reference dynamic pressure is taken at the inlet to the blade row, as the difference between the total and the static pressure.

Pressure loss coefficient for a rotor

The states of the fluid before and after the blade row are denoted with subscripts 1 and 2 respectively. Using the definition above, the pressure loss coefficient for a rotor can be written as

$$Y_{p,R} = \frac{P_{0,2s,rel} - P_{0,2,rel}}{P_{0,1,rel} - P_1}. \quad (2.67)$$

The subscript 'rel' is used to indicate that the stagnation properties are evaluated in a relative frame of reference. To calculate the pressure loss coefficient, the static temperature and pressure as well as the magnitude of the velocity must be known at inlet and outlet. First, the relative Mach number is calculated as

$$M_{i,rel} = \frac{w_i}{a}. \quad (2.68)$$

Here, i is used to denote either inlet or outlet. The speed of sound is known through (2.49) since the static temperature is known. By using the relative Mach number at inlet and outlet, the relative stagnation temperature at inlet and outlet can be calculated using (2.52) according to

$$T_{0,i,rel} = T_i \left(1 + \frac{\gamma - 1}{2} M_{i,rel}^2 \right). \quad (2.69)$$

The relative total pressure at inlet and outlet can further be obtained using (2.53)

$$P_{0,i,rel} = P_i \left(1 + \frac{\gamma - 1}{2} M_{i,rel}^2 \right)^{\gamma/(\gamma-1)}. \quad (2.70)$$

The reversible reference state $2s$ after the blade row will attain the same stagnation temperature as the actual state 2, since both attain the same stagnation enthalpy. This means that the reversible reference pressure can be calculated using (2.47) according to

$$P_{0,2s,rel} = P_{0,1,rel} \left(\frac{T_{0,2,rel}}{T_{0,1,rel}} \right)^{\gamma/(\gamma-1)}. \quad (2.71)$$

Inserting the results into (2.67) gives the pressure loss coefficient.

Pressure Loss Coefficient for a Stator

The pressure loss coefficient for a stator is defined in an absolute frame of reference as

$$Y_{p,S} = \frac{P_{0,2s} - P_{0,2}}{P_{0,1} - P_1}. \quad (2.72)$$

The evaluation of the pressure loss coefficient for a stator proceeds in the same manner as for a rotor. The only difference is that all stagnation properties are taken in an absolute frame of reference instead.

2.6.4 Performance Characteristics

The performance of a compressor is usually presented in the form of a characteristic map, Dixon and Hall 2013. A typical characteristic map for a transonic compressor is presented in Figure 2.7, where subscript 1 and 2 are used to denote inlet and outlet conditions to the compressor.

In a characteristic map, the stagnation pressure ratio over the entire machine is plotted as a function of the corrected mass flow, $\dot{m}\sqrt{T_{0,1}}/P_{0,1}$, for a set of fixed corrected rotational speeds $\Omega/\sqrt{T_{0,1}}$. Each such plot is called a speedline and represent how the pressure ratio depends on the mass flow and inlet conditions to the compressor.

If the pressure ratio is increased while the rotational speed is kept constant, the compressor will eventually reach the surge line. Beyond this line, the operation of the compressor becomes unstable due to surge or stall, Dixon and Hall 2013. Stall means that the flow over at least some of the blades have stalled, which results in lost capability to build up pressure. Surge on the other hand represent a complete breakdown of the compressor, in which the blades can no longer withstand the back pressure, resulting in that the axial flow speed starts oscillating or even in some cases that the flow runs backwards out of the compressor.

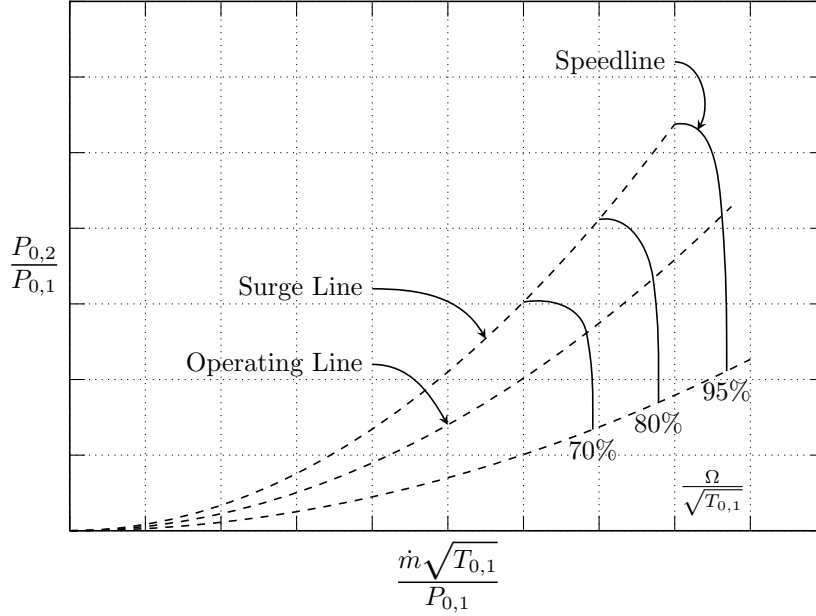


Figure 2.7: *Characteristic map for a transsonic compressor.*

If the pressure ratio on the other hand is decreased, the mass flow will increase and eventually reach an upper limit, which is seen by the more and more vertical shape of the speedline. This represents a case in which some passage of the machine is choked ($M = 1$) and hence can not pass any more mass flow, Dixon and Hall 2013.

When a compressor is installed into an engine, it is restricted to operate along an operating line. This line is set by the flow area downstream of the compressor and fixes the pressure ratio and mass flow through the compressor for a given rotational speed, Dixon and Hall 2013.

2.7 Euler Work Equation

By combining the law of conservation of angular momentum with the steady state energy balance, an important equation relating changes in stagnation enthalpy and angular velocity along stream surfaces in a compressor can be obtained. This equation is known as the Euler work equation and will be presented below.

2.7.1 Angular Momentum

The angular momentum of a fluid particle relative to some fixed axis in space is given by

$$L = mru_{\theta}, \quad (2.73)$$

where m is the mass of the particle, r is the distance measured perpendicular to the axis and u_{θ} is the angular velocity of the particle around the axis.

2.7.2 Change of Angular Momentum

Consider a system in the form of an axisymmetric streamtube passing over a rotor. The angular momentum within this system can change in either of two ways. First, it can change due to the transfer of fluid carrying angular momentum over the system boundaries. Secondly, it can change due to the torque that the rotor applies to the fluid. These mechanisms will be outlined below.

Transfer through convection

Due to the definition of a streamtube, fluid flow can only enter and leave it at the beginning and end of it. Let the tangential velocity of the fluid at the inlet be denoted $u_{\theta,1}$ and suppose that it enters at a radius r_1 . The

rate of angular momentum entering the system is then given by

$$\dot{L}_{\text{flow, in}} = \dot{m}_1 r_1 u_{\theta,1}. \quad (2.74)$$

The fluid that leaves the system carries angular momentum out of the system, whereas the corresponding term at the outlet becomes negative. The net rate of change of angular momentum in the system due to fluid flow therefore becomes

$$\dot{L}_{\text{flow}} = \dot{m}_1 r_1 u_{\theta,1} - \dot{m}_2 r_2 u_{\theta,2}. \quad (2.75)$$

Transfer through torque

The rate at which angular momentum is transferred to the fluid by the rotor blade can be shown to be equal to the torque of the blade, Dixon and Hall 2013

$$\dot{L}_{\text{rotor}} = \tau_R. \quad (2.76)$$

2.7.3 Steady State Angular Momentum Balance

To balance the angular momentum over a streamtube, it will be assumed that the system is at steady state. Hence the rate of change of both mass and angular momentum at every point inside the system is zero. This means that the angular momentum balance reads

$$0 = \dot{L}_{\text{flow}} + \dot{L}_{\text{rotor}}. \quad (2.77)$$

Inserting the formulas for the rate of change due to mass flow and rotor torque and using the fact that the mass flow in and out of the system is equal yields, Dixon and Hall 2013

$$\tau_R = \dot{m}(r_2 u_{\theta,2} - r_1 u_{\theta,1}). \quad (2.78)$$

2.7.4 Euler Work Equation

The rate of work that the rotor performs on the fluid inside the streamtube is given by, Dixon and Hall 2013

$$\dot{W}_s = \Omega \tau_R, \quad (2.79)$$

where Ω is the angular velocity of the blade. Inserting (2.78) into this expression further gives

$$\begin{aligned} \dot{W}_s &= \Omega \dot{m}(r_2 u_{\theta,2} - r_1 u_{\theta,1}) \\ &= \dot{m}(U_2 u_{\theta,2} - U_1 u_{\theta,1}). \end{aligned} \quad (2.80)$$

Here, the blade speed $U = \Omega r$ was also introduced. By applying the steady state energy balance (2.32) to the streamtube, and substituting the shaft work for (2.80), the following is obtained

$$\dot{m}(h_{02} - h_{01}) = \dot{m}(U_2 u_{\theta,2} - U_1 u_{\theta,1}). \quad (2.81)$$

Dividing by the mass flow rate, this equation may be rewritten as

$$\Delta h_0 = \Delta(U u_{\theta}). \quad (2.82)$$

This equation is referred to as the Euler work equation and it can be used to relate the changes in stagnation enthalpy and angular velocity along stream surfaces as long as the flow does not involve heat transfer, Dixon and Hall 2013. Rearranging the Euler work equation, it can be seen that the property

$$I = h_0 - U u_{\theta}, \quad (2.83)$$

is conserved along streamlines. This property is usually denoted rothalpy, Dixon and Hall 2013. It should be noted that in the absence of a rotating blade ($U = 0$), the conservation of rothalpy is equivalent to the conservation of stagnation enthalpy, which is consistent with (2.32).

2.8 Streamline Curvature Equations

The governing equations for the SLC method are derived in this section. These equations can be written in a variety of forms, see for example Denton 1978, Pachidis et al. 2007, Hu et al. 2011a and Hu et al. 2011b. The derivation here will result in the same equations as those given by Denton 1978, Korpela 2011 and Pullan 2012. The documentation on the SLC software SC90C also indicates that this formulation is the one implemented, even though the exact details are not given, *SC90C* 2011.

2.8.1 Assumptions and Coordinate System

To begin with, the flow is assumed to be steady, inviscid and axisymmetric, meaning that flow properties does not vary in the circumferential direction. The axisymmetry can be obtained by regarding all flow properties as circumferentially averaged, Denton 1978.

Since the flow is assumed to be axisymmetric, stream surfaces are assumed not to twist and are therefore usually called streamlines instead. This further means that the flow can be represented in two dimensions in what is known as the meridional plane, depicted in Figure 2.8.

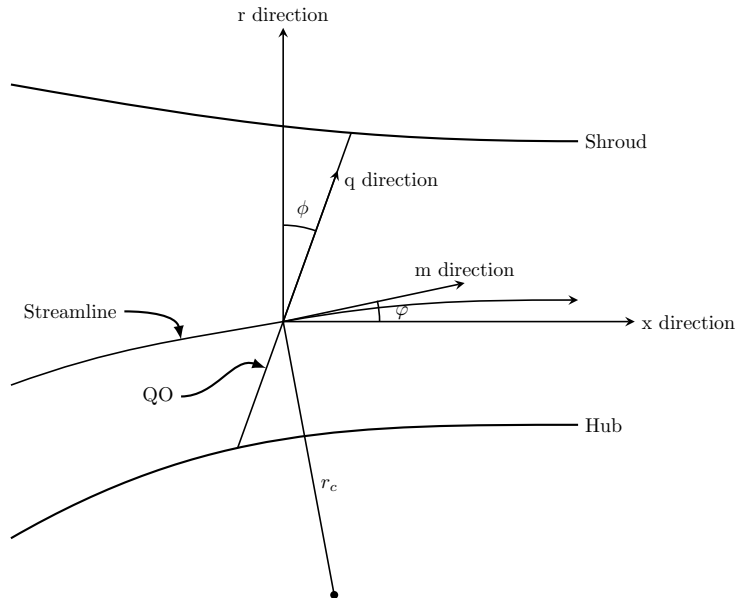


Figure 2.8: *Meridional plane with quasi-orthogonal calculation line.*

The momentum equations and the continuity equation are rewritten and solved in the meridional plane along lines that are roughly perpendicular to the streamlines, abbreviated quasi-orthogonals (QO's), see Figure 2.8. These QO's must be placed along leading and trailing edges of the rotors and stators, but may also be placed between components as well as inside blade rows, Denton 1978.

2.8.2 Governing Equations

The derivation starts with the Euler equations, describing the balance of momentum for an inviscid fluid. In cylindrical coordinates, non conservative and steady form, they read

$$u_r \frac{\partial u_r}{\partial r} + \frac{u_\theta}{r} \frac{\partial u_r}{\partial \theta} + u_x \frac{\partial u_r}{\partial x} - \frac{u_\theta^2}{r} = -\frac{1}{\rho} \frac{\partial P}{\partial r} + F_r, \quad (2.84)$$

$$u_r \frac{\partial u_\theta}{\partial r} + \frac{u_\theta}{r} \frac{\partial u_\theta}{\partial \theta} + u_x \frac{\partial u_\theta}{\partial x} + \frac{u_r u_\theta}{r} = -\frac{1}{\rho} \frac{\partial P}{r \partial \theta} + F_\theta, \quad (2.85)$$

$$u_r \frac{\partial u_x}{\partial r} + \frac{u_\theta}{r} \frac{\partial u_x}{\partial \theta} + u_x \frac{\partial u_x}{\partial x} = -\frac{1}{\rho} \frac{\partial P}{\partial x} + F_x. \quad (2.86)$$

Here, gravitational forces have been neglected and F_r , F_θ and F_x are the blade forces per unit mass of fluid in the radial, tangential and axial direction respectively.

The angles φ and ϕ in Figure 2.8 are denoted the inclination and sweep angle respectively. The inclination angle is taken as positive and the sweep angle as negative in this figure. The meridional velocity of the fluid along a streamline is denoted u_m . Referring to Figure 2.8, the axial and radial velocity can then be expressed as

$$u_r = u_m \sin(\varphi), \quad (2.87)$$

$$u_x = u_m \cos(\varphi). \quad (2.88)$$

Furthermore, the directional derivatives in the meridional direction and along the QO are given by

$$\frac{\partial}{\partial m} = \sin(\varphi) \frac{\partial}{\partial r} + \cos(\varphi) \frac{\partial}{\partial x}, \quad (2.89)$$

$$\frac{\partial}{\partial q} = \cos(\phi) \frac{\partial}{\partial r} - \sin(\phi) \frac{\partial}{\partial x}. \quad (2.90)$$

By inserting (2.87) and (2.88) into (2.84), expanding the derivatives and using the fact that all derivatives with respect to θ are zero, the following is obtained.

$$\begin{aligned} & u_m \sin(\varphi) \left[\frac{\partial u_m}{\partial r} \sin(\varphi) + u_m \cos(\varphi) \frac{\partial \varphi}{\partial r} \right] \\ + & u_m \cos(\varphi) \left[\frac{\partial u_m}{\partial x} \sin(\varphi) + u_m \cos(\varphi) \frac{\partial \varphi}{\partial x} \right] - \frac{u_\theta^2}{r} = -\frac{1}{\rho} \frac{\partial P}{\partial r} + F_r. \end{aligned} \quad (2.91)$$

Rearranging this equation yields

$$\begin{aligned} & u_m \sin(\varphi) \left[\sin(\varphi) \frac{\partial u_m}{\partial r} + \cos(\varphi) \frac{\partial u_m}{\partial x} \right] \\ + & u_m^2 \cos(\varphi) \left[\sin(\varphi) \frac{\partial \varphi}{\partial r} + \cos(\varphi) \frac{\partial \varphi}{\partial x} \right] - \frac{u_\theta^2}{r} = -\frac{1}{\rho} \frac{\partial P}{\partial r} + F_r. \end{aligned} \quad (2.92)$$

The terms within the brackets may be rewritten using (2.89) to obtain

$$u_m \sin(\varphi) \frac{\partial u_m}{\partial m} + u_m^2 \cos(\varphi) \frac{\partial \varphi}{\partial m} - \frac{u_\theta^2}{r} = -\frac{1}{\rho} \frac{\partial P}{\partial r} + F_r. \quad (2.93)$$

In a similar manner, (2.86) may be transformed into

$$u_m \cos(\varphi) \frac{\partial u_m}{\partial m} - u_m^2 \sin(\varphi) \frac{\partial \varphi}{\partial m} = -\frac{1}{\rho} \frac{\partial P}{\partial x} + F_x. \quad (2.94)$$

By multiplying (2.93) by $\cos(\phi)$ and (2.94) by $-\sin(\phi)$, the following may be obtained by adding the results together and applying some trigonometry together with the definition of directional derivative (2.90)

$$u_m \sin(\varphi - \phi) \frac{\partial u_m}{\partial m} + u_m^2 \cos(\varphi - \phi) \frac{\partial \varphi}{\partial m} = -\frac{1}{\rho} \frac{\partial P}{\partial q} + \frac{u_\theta^2}{r} \cos(\phi) + F_q. \quad (2.95)$$

Here it was also used that the component of blade force along the QO may be expressed as $F_q = \cos(\phi)F_r - \sin(\phi)F_x$. In the Streamline Curvature Method, the gradient of the pressure along a QO is rewritten in terms of gradients of enthalpy and entropy using the Clausius-Gibbs equation (2.43) according to

$$-\frac{1}{\rho} \frac{\partial P}{\partial q} = T \frac{\partial s}{\partial q} - \frac{\partial h}{\partial q}. \quad (2.96)$$

Further, using the definition of stagnation enthalpy, $h_0 = h + 1/2(u_m^2 + u_\theta^2)$, the Clausius-Gibbs equation becomes

$$-\frac{1}{\rho} \frac{\partial P}{\partial q} = T \frac{\partial s}{\partial q} - \frac{\partial h_0}{\partial q} + \frac{1}{2} \frac{\partial u_m^2}{\partial q} + \frac{1}{2} \frac{\partial u_\theta^2}{\partial q}. \quad (2.97)$$

Inserting this result into (2.95) and rearranging gives

$$\frac{1}{2} \frac{\partial u_m^2}{\partial q} = \frac{\partial h_0}{\partial q} - T \frac{\partial s}{\partial q} + u_m \sin(\varphi - \phi) \frac{\partial u_m}{\partial m} + u_m^2 \cos(\varphi - \phi) \frac{\partial \varphi}{\partial m} - \frac{u_\theta^2}{r} \cos(\phi) - \frac{1}{2} \frac{\partial u_\theta^2}{\partial q} - F_q \quad (2.98)$$

The rate of change of inclination angle in the meridional direction, $\frac{\partial \varphi}{\partial m}$, represents the amount of curvature of the streamline. It can be rewritten by locally representing the streamline by a circular arc of radius r_c , see Figure 2.8, which gives

$$\frac{\partial \varphi}{\partial m} = \frac{1}{r_c}. \quad (2.99)$$

Here, r_c is taken as positive if the streamline bends away from the axis of rotation, and negative if it bends towards it (as depicted in Figure 2.8). Referring to Figure 2.8, it can also be seen that $\frac{\partial r}{\partial q} = \cos(\phi)$. This identity can be used to show that

$$\frac{1}{2r^2} \frac{\partial (ru_\theta)^2}{\partial q} = \frac{1}{2} \frac{\partial u_\theta^2}{\partial q} + \frac{u_\theta^2}{r} \cos(\phi). \quad (2.100)$$

Inserting the results of (2.99) and (2.100) into (2.98) gives the final meridional streamline curvature equation

$$\frac{1}{2} \frac{\partial u_m^2}{\partial q} = \frac{\partial h_0}{\partial q} - T \frac{\partial s}{\partial q} - \frac{1}{2r^2} \frac{\partial (ru_\theta)^2}{\partial q} - F_q + \sin(\varphi - \phi) u_m \frac{\partial u_m}{\partial m} + \cos(\varphi - \phi) \frac{u_m^2}{r_c}. \quad (2.101)$$

This equation describes the gradient of meridional velocity along a QO, but does not account for the magnitude of it. To do this, continuity must be ensured by requiring that the mass flow past each QO is constant. Since the flow is assumed axisymmetric, the mass flow can be evaluated as, Denton 1978

$$\dot{m} = \int_{QO} 2\pi r \rho u_m \cos(\varphi - \phi) (1 - b) dq. \quad (2.102)$$

The integral is taken along a QO between the hub and shroud of the compressor. The parameter b describes the fraction of the passage that is blocked due to the thickness of the blades and boundary layers, in cases the QO is situated inside a blade row.

2.9 Favre Averaged Navier Stokes Equations

Modeling of fluid flow through Computational Fluid Dynamics (CFD) is nowadays an important and common tool in the design and analysis of turbomachinery. If applied correctly, CFD can give detailed information about blade pressure distribution, shock wave patterns, boundary layer development etc., for arbitrary turbomachinery designs, Calvert and Ginder 1999, Denton and Dawes 1999. In this section, the Favre averaged Navier-Stokes equations are derived and the closure models needed to model turbulence are presented.

2.9.1 Governing Equations

The flow is considered to follow the compressible form of the continuity, momentum and energy equations. These are often referred to as the Navier-Stokes equations, which in conservative form read, Wilcox 1998

$$\frac{\partial \rho}{\partial t} + \frac{\partial (\rho u_j)}{\partial x_j} = 0, \quad (2.103)$$

$$\frac{\partial (\rho u_i)}{\partial t} + \frac{\partial (\rho u_i u_j)}{\partial x_j} = -\frac{\partial p}{\partial x_i} + \frac{\partial \sigma_{ij}}{\partial x_j}, \quad (2.104)$$

$$\frac{\partial (\rho e_0)}{\partial t} + \frac{\partial (\rho e_0 u_j)}{\partial x_j} = -\frac{\partial (p u_j)}{\partial x_j} - \frac{\partial q_j}{\partial x_j} + \frac{\partial (u_i \sigma_{ij})}{\partial x_j}. \quad (2.105)$$

In equations (2.104) and (2.105), σ_{ij} is the viscous stress tensor, which is modeled through Newton's viscosity law according to

$$\sigma_{ij} = 2\mu \left(S_{ij} - \frac{1}{3} S_{kk} \delta_{ij} \right). \quad (2.106)$$

The term S_{ij} is the strain-rate tensor, which is defined as

$$S_{ij} = \frac{1}{2} \left(\frac{\partial u_i}{\partial x_j} + \frac{\partial u_j}{\partial x_i} \right). \quad (2.107)$$

The heat flux vector, q_j , in (2.105) is modeled through Fourier's law as

$$q_j = -k \frac{\partial T}{\partial x_j} = -c_p \frac{\mu}{Pr} \frac{\partial T}{\partial x_j}, \quad (2.108)$$

where k is the constant of heat conductivity, μ the dynamic viscosity and Pr the laminar Prandtl number

$$Pr = \frac{c_p \mu}{k}. \quad (2.109)$$

The specific heat, dynamic viscosity and constant of heat conductivity are assumed to be constants. The energy equation is written in terms of the energy per unit mass, e_0 . The potential energy is neglected, whereby it becomes the sum of internal and kinetic energy

$$e_0 = e + \frac{u_k u_k}{2}. \quad (2.110)$$

To close the system of equations, an equation of state for the fluid is also needed. As before, the gas is assumed to obey the ideal gas law

$$p = \rho RT. \quad (2.111)$$

Also, since the gas is assumed to be calorically perfect, the relations given in (2.13), (2.14) and (2.15) holds for the internal energy, enthalpy and gas constant respectively.

2.9.2 Favre Averaging

The flow within a transonic compressor is both turbulent and takes place at high Reynolds numbers. Under these conditions, it is too expensive to solve the governing equations (2.103) - (2.105) directly by resolving all turbulent scales. Instead, the concept of Favre averaging is introduced. The Favre, or density-weighted, average, of a certain flow field variable Ψ is defined as, Versteeg and Malalasekera 2007

$$\tilde{\Psi} = \frac{\overline{\rho \Psi}}{\bar{\rho}}. \quad (2.112)$$

Here, the overline denotes time averaging according to

$$\bar{\Phi}(t) = \frac{1}{2T} \int_{t-T}^{t+T} \Phi(\tau) d\tau. \quad (2.113)$$

The idea behind the averaging is to decompose flow field variables into an averaged part, describing the mean field, and a fluctuating part, containing the turbulent fluctuations. The mean field part can either be taken as the time average or the Favre average of the flow field variable, giving rise to the following two decompositions

$$\Phi = \bar{\Phi} + \Phi', \quad (2.114)$$

$$\Psi = \tilde{\Psi} + \Psi''. \quad (2.115)$$

This decomposition is based upon the assumption of scale separation. This means that in the time averaging, (2.113), the time T can be found such that it is larger than the largest time scale of the turbulent fluctuations, yet smaller than a representative time scale of the mean field. Under this assumption, it also holds true that

any time averaged quantity, and thereby Favre averaged quantity, can be moved outside the integral if it is being part of a time average, i.e.

$$\overline{\psi \overline{\Phi}} = \overline{\psi} \overline{\Phi}, \quad (2.116)$$

$$\overline{\psi \tilde{\Psi}} = \overline{\psi} \tilde{\Psi}. \quad (2.117)$$

This further can be used to show that

$$\overline{\overline{\Phi'}} = 0, \quad (2.118)$$

$$\overline{\rho \Psi''} = 0. \quad (2.119)$$

The Navier-Stokes equations can be rewritten by decomposing the velocity, u_i , the internal energy, e , and temperature, T , according to (2.115). The pressure is further decomposed according to (2.114). By time averaging the resulting equations and applying the relations presented above, the Favre averaged Navier-Stokes equations are obtained, Wilcox 1998

$$\frac{\partial \overline{p}}{\partial t} + \frac{\partial(\overline{p}\tilde{u}_j)}{\partial x_j} = 0, \quad (2.120)$$

$$\frac{\partial(\overline{p}\tilde{u}_i)}{\partial t} + \frac{\partial(\overline{p}\tilde{u}_i\tilde{u}_j)}{\partial x_j} = -\frac{\partial \overline{p}}{\partial x_i} + \frac{\partial}{\partial x_j} \left(\overline{\sigma_{ij}} - \overline{\rho u_i'' u_j''} \right), \quad (2.121)$$

$$\begin{aligned} \frac{\partial(\overline{p}\tilde{e}_0)}{\partial t} + \frac{\partial(\overline{p}\tilde{e}_0\tilde{u}_j)}{\partial x_j} &= -\frac{\partial(\overline{p}\tilde{u}_j)}{\partial x_j} - \frac{\partial}{\partial x_j} \left(\overline{\rho u_j'' e''} + \overline{p u_j''} \right) + \frac{\partial}{\partial x_j} \left(\tilde{u}_i \left(\overline{\sigma_{ij}} - \overline{\rho u_i'' u_j''} \right) \right) \\ &\quad - \frac{\partial \overline{q_j}}{\partial x_j} + \frac{\partial}{\partial x_j} \left(\overline{\sigma_{ij} u_i''} - \frac{1}{2} \overline{\rho u_i'' u_i'' u_j''} \right) \end{aligned} \quad (2.122)$$

Here, the Favre averaged energy is defined as the sum of the Favre averaged internal energy, mean kinetic energy and turbulent kinetic energy according to

$$\tilde{e}_0 = \tilde{e} + \frac{\tilde{u}_k \tilde{u}_k}{2} + \frac{\widetilde{u_k'' u_k''}}{2}. \quad (2.123)$$

Furthermore, the time average of the viscous stress tensor and heat flux vector are given by

$$\overline{\sigma_{ij}} = \underbrace{2\mu \left(\tilde{S}_{ij} - \frac{1}{3} \tilde{S}_{kk} \delta_{ij} \right)}_{\tilde{\sigma}_{ij}} + \underbrace{2\mu \left(\overline{S_{ij}''} - \frac{1}{3} \overline{S_{kk}''} \delta_{ij} \right)}_{\overline{\sigma_{ij}''}}, \quad (2.124)$$

$$\overline{q_j} = \underbrace{-c_p \frac{\mu}{Pr} \frac{\partial \tilde{T}}{\partial x_j}}_{\tilde{q}_j} - \underbrace{c_p \frac{\mu}{Pr} \frac{\partial \overline{T''}}{\partial x_j}}_{\overline{q_j''}}. \quad (2.125)$$

The Favre averaged strain rate tensor and the corresponding fluctuating part, \tilde{S}_{ij} and $\overline{S_{ij}''}$, are defined as in equation (2.107) but with the velocity being the Favre average and its corresponding fluctuating part respectively.

Applying the same procedure to the ideal gas law gives, Wilcox 1998

$$\overline{p} = \overline{\rho} R \tilde{T}. \quad (2.126)$$

In the equations for the internal energy and enthalpy, (2.13) and (2.14), the energy, enthalpy and temperature are decomposed according to (2.115). By multiplying the resulting equations by the density and time average, the following equations are obtained

$$\tilde{e} = c_v \tilde{T}, \quad (2.127)$$

$$\tilde{h} = c_p \tilde{T}. \quad (2.128)$$

The Favre averaged Navier stokes equations, (2.120) - (2.122), together with the equation of state (2.126) and the relations for internal energy and enthalpy, (2.127) and (2.128), does not form a closed system of equations. In order to close the system of equations, further models and assumptions must be introduced for the unknowns introduced in the averaging process.

2.9.3 Modeling and assumptions

Viscous stress and heat flux

Starting with the time averaged viscous stress tensor in (2.124), the term containing the contributions from turbulent fluctuations, $\overline{\sigma''_{ij}}$, is being neglected. The same approach is also taken for the time averaged heat flux vector in (2.125), where the term $\overline{q''_j}$ is being neglected.

Reynolds-stress tensor

The Reynolds-stress tensor, $\overline{\rho u''_i u''_j}$, present in (2.121) and (2.122) is modeled through a eddy viscosity approach using the Boussinesq assumption, Wilcox 1998

$$-\overline{\rho u''_i u''_j} = 2\mu_t \left(\tilde{S}_{ij} - \frac{1}{3} \tilde{S}_{kk} \delta_{ij} \right) - \frac{2}{3} \bar{\rho} k \delta_{ij}, \quad (2.129)$$

where μ_t and k are the turbulent viscosity and turbulent kinetic energy respectively. These properties are calculated using a turbulence model, as will be presented later.

Turbulent Heat-Flux Vector

The heat flux due to turbulent fluctuations, $\overline{\rho u''_j e''} + \overline{p u''_j}$, in (2.122) is modeled through a temperature gradient approach to resemble its laminar counterpart. This gives rise to the following model, Wilcox 1998

$$\overline{\rho u''_j e''} + \overline{p u''_j} = -c_p \frac{\mu_t}{Pr_t} \frac{\partial \tilde{T}}{\partial x_j}, \quad (2.130)$$

where Pr_t is the turbulent Prandtl number.

Molecular Diffusion and Turbulent Transport

The terms $\overline{\sigma_{ij} u''_i}$ and $1/2 \overline{\rho u''_i u''_i u''_j}$ in (2.122) represent transport by molecular diffusion and turbulent fluctuations. These terms can be ignored for flows up to and around the sonic regime ($M \approx 1$) but must be considered for hypersonic speeds, Wilcox 1998. The flow in a transsonic compressor typically lies in the sonic regime but is never close to being hypersonic. These terms are therefore being neglected.

2.9.4 Turbulence model

To close the system of equations, a turbulence model needs to be introduced in order to compute the turbulent viscosity, μ_t , and the turbulent kinetic energy, k . In this work, the standard $k - \varepsilon$ model with a reliability constraint has been used. In this model, two transport equations for the Favre averaged turbulent kinetic energy and its corresponding dissipation rate are solved. They read as follows, Olausson 2011

$$\frac{\partial(\bar{\rho}k)}{\partial t} + \frac{\partial(\bar{\rho} \tilde{u}_j k)}{\partial x_j} = P_k + \frac{\partial}{\partial x_j} \left(\left(\mu + \frac{\mu_t}{\sigma_k} \right) \frac{\partial k}{\partial x_j} \right) - \bar{\rho} \varepsilon, \quad (2.131)$$

$$\frac{\partial(\bar{\rho} \varepsilon)}{\partial t} + \frac{\partial(\bar{\rho} \tilde{u}_j \varepsilon)}{\partial x_j} = C_{\varepsilon 1} \frac{\varepsilon}{k} P_k + \frac{\partial}{\partial x_j} \left(\left(\mu + \frac{\mu_t}{\sigma_\varepsilon} \right) \frac{\partial \varepsilon}{\partial x_j} \right) - C_{\varepsilon 2} \bar{\rho} \frac{\varepsilon^2}{k}. \quad (2.132)$$

The production of turbulent kinetic energy is further given by

$$P_k = \left(2\mu_t \left(\tilde{S}_{ij} - \frac{1}{3} \tilde{S}_{kk} \delta_{ij} \right) - \frac{2}{3} \bar{\rho} k \delta_{ij} \right) \frac{\partial \tilde{u}_i}{\partial x_j}. \quad (2.133)$$

The turbulent viscosity is calculated using a realizability constraint according to, Olausson 2011

$$\mu_t = \min \left(C_\mu \bar{\rho} \frac{k^2}{\varepsilon}, \frac{0.4 \bar{\rho} k}{\sqrt{\tilde{S}_{ij} \tilde{S}_{ij}}} \right). \quad (2.134)$$

The various constants used in the turbulence model as well as in the Navier-stokes equations are listed in Table 2.5.

Table 2.5: Model constants.

C_μ	$C_{\varepsilon 1}$	$C_{\varepsilon 2}$	σ_k	σ_ε	Pr_t	Pr	μ [Pa s]
0.09	1.44	1.92	1.0	1.3	0.9	0.72	$1.7 \cdot 10^{-5}$

2.9.5 Final Equations

By substituting the models into the Favre averaged Navier-Stokes equations as well as omitting the neglected terms, the modeled Favre averaged Navier-Stokes equations can be written in compact form as

$$\frac{\partial \mathcal{Q}}{\partial t} + \frac{\partial \mathcal{F}_j}{\partial x_j} = \mathcal{H}. \quad (2.135)$$

The state vector \mathcal{Q} , which includes the conservative variables, is given by

$$\mathcal{Q} = \begin{bmatrix} \bar{\rho} \\ \bar{\rho} \tilde{u}_i \\ \bar{\rho} \tilde{e}_0 \\ \bar{\rho} k \\ \bar{\rho} \varepsilon \end{bmatrix} \quad (2.136)$$

The flux vector \mathcal{F}_j is furthermore given by

$$\mathcal{F}_j = \begin{bmatrix} \bar{\rho} \tilde{u}_j \\ \bar{\rho} \tilde{u}_i \tilde{u}_j + \bar{p} \delta_{ij} - \tau_{ij} \\ \bar{\rho} \tilde{e}_0 \tilde{u}_j + \bar{p} \tilde{u}_j - c_p \left(\frac{\mu}{Pr} + \frac{\mu_t}{Pr_t} \right) \frac{\partial \tilde{T}}{\partial x_j} - \tilde{u}_i \tau_{ij} \\ \bar{\rho} \tilde{u}_j k - \left(\mu + \frac{\mu_t}{\sigma_k} \right) \frac{\partial k}{\partial x_j} \\ \bar{\rho} \tilde{u}_j \varepsilon - \left(\mu + \frac{\mu_t}{\sigma_\varepsilon} \right) \frac{\partial \varepsilon}{\partial x_j} \end{bmatrix} \quad (2.137)$$

The complete stress tensor, τ_{ij} , containing both viscous and turbulent effects, is given by

$$\tau_{ij} = 2(\mu + \mu_t) \left(\tilde{S}_{ij} - \frac{1}{3} \tilde{S}_{kk} \delta_{ij} \right) - \frac{2}{3} \bar{\rho} k \delta_{ij}. \quad (2.138)$$

Finally the source vector \mathcal{H} is given by

$$\mathcal{H} = \begin{bmatrix} 0 \\ 0 \\ 0 \\ P_k - \bar{\rho} \varepsilon \\ C_{\varepsilon 1} \frac{\varepsilon}{k} P_k - C_{\varepsilon 2} \bar{\rho} \frac{\varepsilon^2}{k} \end{bmatrix} \quad (2.139)$$

These equations, together with (2.123), (2.126), (2.127) and (2.128) form a closed system of equations.

2.9.6 Rotating Frame of Reference

When CFD is applied to rotors, a rotating frame of reference is applied. In this case, the Favre averaged Navier-Stokes equations are reformulated in terms of the relative velocity instead. Additional source terms must then be added to the equations to include the fictive coriolis and centrifugal force. If the x axis is aligned with the shaft of the compressor, the source term in the y and z momentum equations become

$$S_{y,R} = 2\Omega\bar{\rho}\tilde{u}_z + \Omega^2\bar{\rho}x_y, \quad (2.140)$$

$$S_{z,R} = -2\Omega\bar{\rho}\tilde{u}_y + \Omega^2\bar{\rho}x_z. \quad (2.141)$$

Here, the first and second terms on the right hand side represent the coriolis and centrifugal effects respectively.

A source term must also be added to the energy equation, since the fictive acceleration gives rise to extra work. This source term can be shown to be

$$S_{e,R} = \Omega^2\bar{\rho}(\tilde{u}_y x_y + \tilde{u}_z x_z). \quad (2.142)$$

3 Method

3.1 Streamline Curvature Method

The streamline curvature method is based upon solving the meridional streamline curvature equation (2.101) and the continuity equation (2.102) together with a suitable form of the energy equation, e.g. the Euler work equation (2.82), and an equation of state, Templalexis et al. 2011. Additional correlations and physical models are also needed if no empirical data is provided. The correlations are used to determine the losses and turning of the flow over the blades and are functions of the blade geometry. The physical models are used to model effects such as mixing of entropy, energy and angular momentum in the spanwise direction, Gallimore 1986.

The streamline curvature software SC90C, which is developed and distributed by PCA Engineers Ltd, is used in this project. The source code to SC90C is closed and the documentation on the implementation is sparse. However, literature on most of the correlations and physical models employed in SC90C is available in the open literature. Also, good references are available on how the general numerical algorithm in streamline curvature codes works.

The setup of SC90C is described in this section. This includes the computational domain, boundary conditions as well as choice of correlations and physical models. A general description of how the numerical algorithm works is also presented.

3.1.1 Computational Domain

The discretization of the meridional plane is done by introducing a mesh consisting of a set of QO's and streamlines. The grid points, in which all data is stored, is defined as the intersection between the QO's and the streamlines, Templalexis et al. 2011.

The computational domain was set up without QO's inside blade rows, since the available version of SC90C does not feature this option, *SC90C* 2011. The compressor that was analyzed consist of three stages and an inlet guide vane (IGV) before the first stage. In total, 24 QO's was used, 5 was placed in front of the IGV in the inlet duct, one QO was placed at every leading and trailing edge of the following components (total = 14) and finally 5 QO's was placed after the last stator. No QO's were placed in between the components, since they are quite closely stacked and SLC methods become more unstable the more closely the QO's are placed, Denton 1978. Due to restrictions in the available version of SC90C, the QO's can only be straight lines. This means that the exact position of curved leading and trailing edges of swept blades can not be captured. The computational grid is depicted in Figure 3.1.

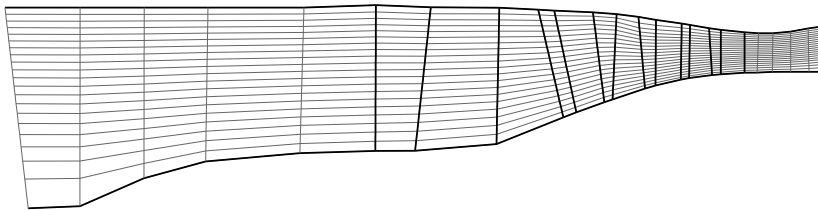


Figure 3.1: *Computational grid in the meridional plane.*

The positions of the streamlines are kept fixed at the trailing edge of the first rotor, but are allowed to vary along the other QO's as the program converges. The movement of the streamlines is done to ensure that the mass flow in each streamtube, between two streamlines, is constant throughout the compressor.

3.1.2 Numerical Method

Boundary Conditions

The following boundary conditions must be specified at the inlet to the compressor in the SLC method.

- Spanwise variation of total pressure, P_0 .
- Spanwise variation of total temperature, T_0 .
- Spanwise variation of swirl angle, α .
- Total mass flow through compressor.

The spanwise variation in total pressure and temperature are set based on 3D CFD data available on the compressor. Further, the swirl angle is set to a uniform distribution of 0 and the mass flow is varied to achieve a desired pressure ratio. Finally, the rotational speed must also be specified.

Numerical Algorithm

Below, the general numerical algorithm in the SLC method is presented, as given by Pullan 2012. The exact implementation in SC90C is not available, but where literature relevant for SC90C has been found, additional information has been added to the description below.

1. Initialization of the solution
 - a) Initialize the location of the streamlines
 - b) Initialize the velocity distribution along each QO
2. By using a curve fit of the streamlines through each grid point, compute the following
 - a) Radius of curvature, r_c
 - b) Inclination angle, φ
3. Starting with the specified inlet conditions, march along each streamline, from inlet to outlet, and determine the following at the intersection with each QO
 - a) Tangential velocity, u_θ .
 At the inlet it is known through the meridional velocity and the specified swirl angle through (2.3). Between blade rows, it can be found through the conservation of angular momentum, ru_θ . Within blade rows, the tangential velocity can be obtained from the meridional velocity together with the flow angles imposed by the blade geometry. Finally at the exit of blade rows, it can be obtained from the meridional velocity together with specified flow exit angles, obtained from empirical input or correlations. In cases the blade is a rotor, the tangential velocity due to rotation, $r\Omega$, must also be added. In SC90C, angular momentum is also assumed to be able to transfer in the spanwise direction through turbulent mixing. Therefore, the exact conservation of angular momentum along a streamline is not valid, as will be described later.
 - b) Stagnation enthalpy, h_0 .
 Along each streamline, the rothalpy, (2.83), is conserved. Since u_θ is known, the conservation of rothalpy along each streamline can be used to calculate the stagnation enthalpy along each streamline. In SC90C, the stagnation enthalpy, like the angular momentum, is also assumed to be able to transfer between streamlines in the spanwise direction as a result of turbulent mixing. As for the angular momentum, this means that the rothalpy is not exactly conserved, which will be described later.
 - c) Entropy, s .
 At the inlet, the entropy can be obtained from an equation of state using the other specified quantities. Between blade rows, the entropy is assumed to be conserved. Across blade rows, the changes can be found through loss coefficients, obtained from correlations or empirical input. As for both the angular momentum and stagnation enthalpy, SC90C allows for spanwise transport of entropy through turbulent mixing. This means that additional entropy change along each streamline also occurs throughout the machine, which will be described later.

4. Integrate the streamline curvature equation, (2.101), along each QO using a finite difference scheme. The iteration typically starts with the velocity at the mid streamline and proceeds outwards towards hub and shroud to obtain a new velocity profile.
5. Evaluate the continuity equation, (2.102). The density can be obtained through an equation of state for the fluid, since the thermodynamics properties along each streamline have been obtained in the previous steps. If the mass flow does not coincide with the specified mass flow, update the mid streamline velocity accordingly and return to step 4.
6. Update the streamline positions to make sure that each streamtube passes the same mass flow throughout the compressor.
7. Return to step 2.

The models used in SC90C for flow exit angles, losses and spanwise mixing will be described next.

3.1.3 Correlations and Physical Models

Deviation

The swirl angle is necessary to have to compute the tangential velocity at exit to the blades. Referring to Figure 2.4, the swirl angle can be calculated as the sum of the blade exit angle and the deviation according to

$$\alpha_2 = \alpha'_2 + \delta. \quad (3.1)$$

It should be noted that for rotors, the outlet swirl angle is the relative swirl angle, β_2 . In SC90C, the blade angles are specified across the span and the correlations of Wright and Miller 1991 are used to calculate the deviation.

Pressure loss

The entropy generation over the blades is calculated based on correlations for the pressure loss coefficient, Y_p , given in (2.67) and (2.72). The correlations used are those of Wright and Miller 1991. The model computes the total pressure loss based on individual correlations for the profile loss, shock loss and secondary losses according to

$$Y_{p, \text{ tot}} = Y_{p, \text{ prof}} + Y_{p, \text{ shock}} + Y_{p, \text{ sec}}. \quad (3.2)$$

The profile and shock loss includes losses generated in the boundary layers and shock waves respectively. The secondary loss includes three dimensional losses. These correlations were devised for rotors and stators but does not apply to inlet guide vanes. In cases where an IGV is used, SC90C instead uses a constant pressure loss coefficient of 0.02 across the span, *SC90C* 2011.

It should be noted that the Wright and Miller correlations for both deviation and loss were devised for Double Circular Arc (DCA) blade profiles. These profiles are rarely used in modern compressors, but instead more sophisticated blade profiles tailored by CFD are employed to minimize losses. For this purpose, SC90C allows correction factors for both the deviation and the individual loss coefficients to be specified across the span.

The pressure loss coefficient can also be used to calculate the stagnation pressure after the blade row, once the stagnation temperature before and after the blade row are known. By the definition of the pressure loss coefficient, (2.67) and (2.72), and the relation for the isentropic stagnation pressure after the blade row, (2.71), the stagnation pressure after the blade row becomes

$$P_{0,2} = P_{0,1} \left(\frac{T_{0,2}}{T_{0,1}} \right)^{\gamma/(\gamma-1)} - Y_{p, \text{ tot}} (P_{0,1} - P_1). \quad (3.3)$$

The stagnation properties are evaluated in a relative and absolute frame of reference for a rotor and stator respectively.

Annulus Wall Boundary Layers

Correlations developed by Wright and Miller 1991 for predicting the blockage of the channel due to boundary layers at the hub and shroud are also implemented in SC90C. The effect of the boundary layers are assumed to be that they compress the inviscid part of the flow. This is accounted for by calculating a blockage factor that is introduced into the continuity equation, (2.102). This results in that the blockage affects every streamtube across the span equally much, which is nonphysical. The experience from previous use of blockage factors at GKN Aerospace is also that the results are not satisfactory. Therefore, the boundary layer calculation was not used in this work.

Spanwise Mixing

In conventional SLC codes, no transport of stagnation enthalpy, entropy or angular momentum is assumed to take place between streamlines. This is not a good assumption for multistage axial flow compressors, in which especially mixing due to turbulent diffusion has been found to have an important effect on the spanwise distribution of stagnation enthalpy, entropy and angular momentum, Gallimore 1986, Howard and Gallimore 1993. Below follows a short description of how spanwise mixing is accounted for in SC90C.

Starting with the stagnation enthalpy, the Euler work equation, (2.82), states that in the absence of a rotating blade, it is constant along a streamline. This is not generally true since the equation was derived under the assumption that there is no heat transfer and shear forces between adjacent streamtubes. In a compressor, there is almost always a temperature gradient in the spanwise direction, meaning that in reality, there is a heat flux in the spanwise direction. Furthermore, the temperature can rise in a streamtube due to the dissipation of turbulence. Finally, if velocity gradients exist in the spanwise direction, turbulent shear stress will cause the velocity in a streamtube to change as well.

The angular momentum should also be conserved along a streamline in the absence of blade forces, according to (2.78). However, this equation was derived by assuming that no forces acted on the top and bottom of the streamtube. If in fact velocity gradients exist in the spanwise direction, turbulent shear stress will give rise to tangential forces, which thereby can change the angular momentum in a streamtube.

Finally, it was mentioned in section 2.4.3 that heat transfer through temperature gradients and dissipation of turbulence due to viscous friction generates entropy. Therefore, in the presence of turbulence and spanwise temperature gradients, the entropy is no longer conserved along a streamline.

Several improvements have been observed on SLC solutions when spanwise mixing is included, Gallimore 1986. First, it has been found that very different spanwise loss distributions must be specified in order to achieve the same velocity profiles dependent if spanwise mixing is used or not. This affects the design of a compressor, in which a false distribution of loss can give the desired performance. Secondly, it has been found that accurate stagnation temperature profiles are very hard to achieve when spanwise mixing is not used, independent on the input of loss distributions. Finally, it has been found that if realistic (high) losses at the hub and shroud are specified, the use of spanwise mixing is essential for preventing unrealistic temperature rise in these regions.

The spanwise mixing model of Gallimore 1986 is implemented in SC90C and have been employed in this work. The exact equations describing the change of the properties along streamlines will not be given here. In general however, they can be written as

$$\frac{\partial\psi}{\partial m} = \Phi_{\text{mix}} + \Phi_{\text{blade}}, \quad (3.4)$$

where ψ is a certain property. Furthermore, Φ_{mix} and Φ_{blade} are the rate of change due to spanwise mixing and blade effects respectively.

On a final note, the meridional streamline curvature equation (2.101) can be left intact even when turbulent effects are being considered, as long as the QO's and streamlines are close to orthogonal. This is because the shear stresses in the meridional direction then have negligibly small components, Gallimore 1986.

3.2 Computational Fluid Dynamics

The flow in axisymmetrical streamtubes passing over the blades have been computed using Computational Fluid Dynamics (CFD) to analyze the flow past them. These types of calculations are usually referred to as Quasi-three-dimensional (Q3D) blade-to-blade calculations, Denton and Xu 1999. The abbreviation Q3D comes

from that the two dimensional features of the flow are resolved, while the three dimensional effects associated with changes in thickness and radius of the streamtube are still accounted for.

The code used in this work belongs to the family of G3D finite-volume codes developed by Eriksson 1995. It solves the compressible Navier-Stokes equations in conservative form on a structured, boundary-fitted, curve-linear, non-orthogonal, multiblock mesh using the finite volume method (FVM). To enable efficient Q3D simulations on streamtubes, the code also includes the source term developed by Ellbrant and Eriksson 2014.

3.2.1 Computational Domain

For each blade, a set of blade-to-blade calculations are performed in axisymmetric streamtubes at different spanwise locations. This is accomplished by constructing a three dimensional mesh that has the shape of a streamtube, as depicted by the dark shaded region in Figure 3.2.

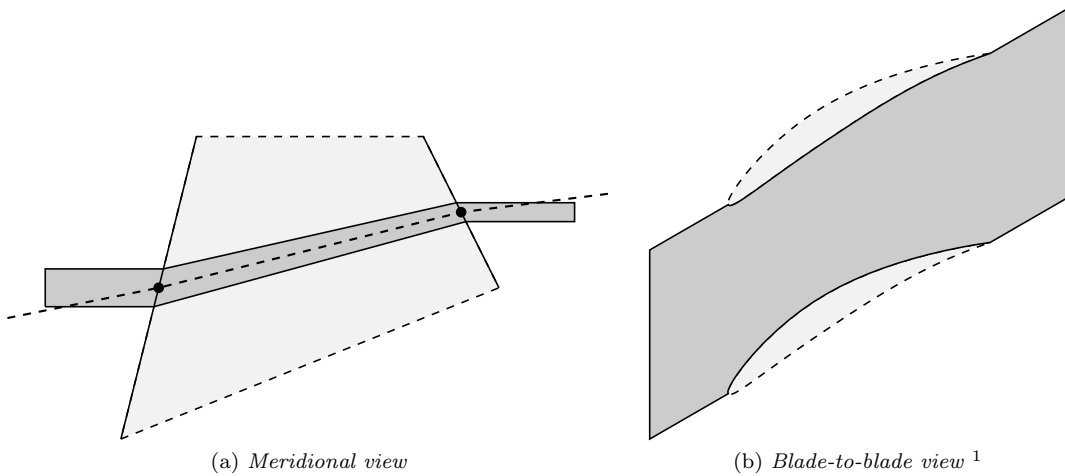


Figure 3.2: *Schematic representation of the computational domain.*

The mesh is three dimensional in the sense that it changes both radius and thickness over the blade, as depicted in Figure 3.2 (a). The effects associated with changing radius and thickness of the streamtube can then be accounted for, since the three dimensional governing equations are solved on the mesh. Accurately accounting for these two effects is very important in order to obtain good results from blade-to-blade calculations, Denton and Dawes 1999. It should also be noted that the mesh is only one cell thick in the radial direction. This is possible by the use of an extra source term, as will be described later.

The mesh is constructed based on data obtained from the SLC method. First of all it is wrapped around a selected streamline that the SLC method has calculated, see Figure 3.2 (a). As presented in Figure 3.2, it was also chosen to extend the domain to include an inlet region and outlet region before and after the blade passage respectively. The extension of the domain gives rise to a problem, since the SLC data will be used as boundary conditions for the blade-to-blade calculation. This is because the SLC data is only available at the leading and trailing edge, but they should be applied at the inlet and outlet of the domain, which lies in front and behind the leading and trailing edge respectively. To account for the problem, it was decided to extend the domain with constant radius and thickness, as seen in Figure 3.2 (a). In doing so, most properties will stay unchanged in the CFD solution between the inlet/outlet and leading/trailing edge. For example the conservation of angular momentum leads to the swirl velocity being unchanged.

The change in streamtube thickness is accounted for by letting the mesh linearly change thickness between the leading and trailing edge of the blade. The thickness at the leading and trailing edge is furthermore calculated based on the spanwise variation in mass flow obtained from the SLC solution.

An example of the computational domain for a rotor, including the block structure and final mesh topology is presented in Figure 3.3.

¹Airfoil profile obtained from UIUC Airfoil Coordinates Database: http://www.ae.uiuc.edu/m-selig/ads/coord_database.html. Data is released under the GNU General Public Licence. See <http://www.ae.uiuc.edu/m-selig/pd/gpl.html> for more details.

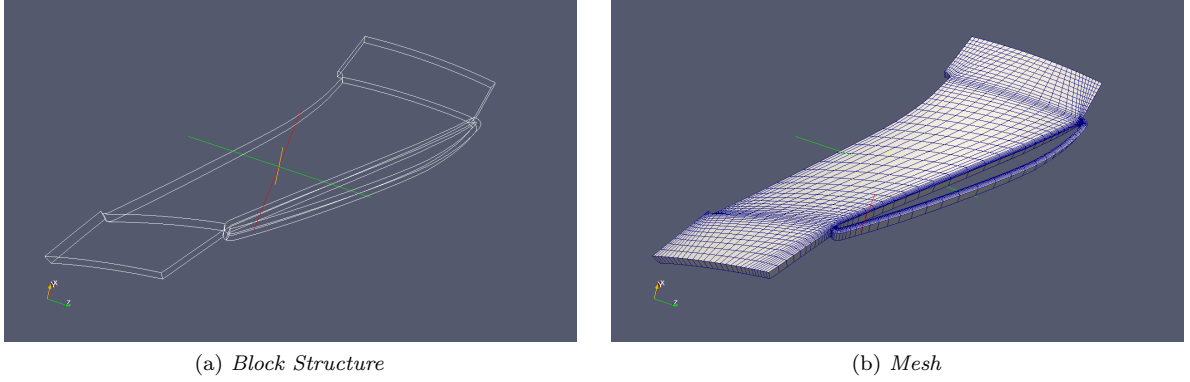


Figure 3.3: Example of a computational domain.

3.2.2 Numerical Method

Discretization of Governing Equations

The governing equations, written in conservative and compact form reads

$$\frac{\partial \mathcal{Q}}{\partial t} + \frac{\partial \mathcal{F}_j}{\partial x_j} = \mathcal{H}. \quad (3.5)$$

The state vector \mathcal{Q} , the flux vector \mathcal{F}_j and the source vector \mathcal{H} have been defined previously in (2.136), (2.137) and (2.139) respectively. Integrating (3.5) over an arbitrary control volume Ω yields

$$\int_{\Omega} \frac{\partial \mathcal{Q}}{\partial t} dV + \int_{\Omega} \frac{\partial \mathcal{F}_j}{\partial x_j} dV = \int_{\Omega} \mathcal{H} dV. \quad (3.6)$$

Let the volume average of \mathcal{Q} and \mathcal{H} be denoted \mathbf{Q} and \mathbf{H} respectively. Let further the volume of Ω be denoted V . By applying the Gauss Theorem to the second term in (3.6), the equation may be rewritten as

$$\frac{\partial \mathbf{Q}}{\partial t} V + \int_{\partial \Omega} \mathcal{F}_j \cdot dS_j = \mathbf{H}V. \quad (3.7)$$

Here it was also assumed that the control volume does not change in time. For the rectangular shaped control volumes employed in the finite volume discretization, the surface integral is approximated as

$$\int_{\partial \Omega} \mathcal{F}_j \cdot dS_j = \sum_{k=1}^{\text{All Faces}} [\mathcal{F}_j \cdot S_j]_k. \quad (3.8)$$

The area vector S_j can be rewritten as $n_j S$, where n_j and S denote the outwards facing normal and area of the face respectively. Substitution of (3.8) into (3.7) gives the following formulation of the governing equations

$$\frac{\partial \mathbf{Q}}{\partial t} V + \sum_{k=1}^{\text{All Faces}} [\mathcal{F}_j \cdot S_j]_k = \mathbf{H}V. \quad (3.9)$$

The volume averaged values of the conservative variables in the state vector \mathbf{Q} are regarded as the unknowns in the numerical solution. Furthermore, the volume averaged source vector is approximated using the volume averaged entities in \mathbf{Q} , i.e.

$$\mathbf{H} \approx \mathcal{H}(\mathbf{Q}). \quad (3.10)$$

The flux vector is reconstructed on the faces using different types of numerical schemes, as will be presented next.

Spatial Discretization

To reconstruct the flux vector on the cell faces, it is first divided into convective and diffusive fluxes according to

$$\mathcal{F}_j = \begin{bmatrix} \bar{\rho}\tilde{u}_j \\ \bar{\rho}\tilde{u}_i\tilde{u}_j + \bar{p}\delta_{ij} \\ \bar{\rho}\tilde{e}_0\tilde{u}_j + \bar{p}\tilde{u}_j \\ \bar{\rho}\tilde{u}_j k \\ \bar{\rho}\tilde{u}_j \varepsilon \end{bmatrix} + \begin{bmatrix} 0 \\ -\tau_{ij} \\ -c_p \left(\frac{\mu}{Pr} + \frac{\mu_t}{Pr_t} \right) \frac{\partial \tilde{T}}{\partial x_j} - \tilde{u}_i \tau_{ij} \\ - \left(\mu + \frac{\mu_t}{\sigma_k} \right) \frac{\partial k}{\partial x_j} \\ - \left(\mu + \frac{\mu_t}{\sigma_\varepsilon} \right) \frac{\partial \varepsilon}{\partial x_j} \end{bmatrix}. \quad (3.11)$$

The convective and diffusive fluxes are reconstructed using different numerical schemes, as will be briefly presented next. A more throughout description of the schemes are given by Andersson 2005 and Burak 2010.

Convective Fluxes The convective fluxes are reconstructed on the cell faces using a third-order upwind scheme. The upwinding is done on what is known as the characteristic variables, and the direction of upwinding is based upon the direction of propagation relative to the cell faces of these variables, known as the characteristic speeds. The characteristic variables and corresponding speeds can be shown to be functions of the primitive variables ($\bar{\rho}$, \tilde{u}_i , \bar{p} , k and ε). The primitive variables are in turn interpreted as the cell averages, and are computed directly from the state vector \mathbf{Q} . The characteristic variables linked to the density, velocities and pressure can be interpreted as one entropy wave, two vorticity waves and two acoustic waves. The turbulent quantities are their own characteristic variables, with characteristic speeds given by the velocity of the flow relative to the cell face.

The algorithm starts by calculating the characteristic speeds at the cell faces, based on the average value of the primitive variables in the two adjacent cells. The characteristic variables are then computed at the cell face based on upwinded values of the primitive variables at the cell face. The direction of upwinding for the primitive variables are based on the speed of the characteristic variable that is being calculated. The characteristic variables are finally transformed back into the primitive variables, which in turn are used to calculate the convective part of the flux vector (3.11) at the face.

Diffusive Fluxes The gradients and values of the primitive variables needs to be estimated at the cell faces to evaluate the diffusive fluxes. This is done using a compact, second order, centered difference scheme.

The algorithm starts by calculating the gradients of the primitive variables at each face in the computational space using a centered difference scheme. The computational space can be regarded as the space occupied by the corresponding unwrapped mesh with cells consisting of cubes with side 1. These gradients are then transformed into physical space, based on the topology of the mesh. To estimate the values of the primitive variables at the faces, the centered average of the values in the adjacent cells are used. Finally, the gradients and values of the primitive variables at the faces are used to calculate the diffusive part of the flux vector in (3.11).

Temporal Discretization

The governing equations are integrated explicitly in time using a three-stage, second order, Runge-Kutta algorithm. In this work, only steady state flow over the blades are studied. This means that it is assumed that the flow will eventually converge towards a steady state solution from the initial conditions set.

When the fluxes over the cell faces together with the source vector have been evaluated, (3.9) can be written as

$$\frac{\partial \mathbf{Q}^n}{\partial t} = \mathcal{R}^n, \quad (3.12)$$

where n and \mathcal{R} denotes the current time step and the sum of the fluxes and source terms respectively. The algorithm then computes the state vector \mathbf{Q} at time step $n + 1$ according to

$$\begin{aligned}
\mathbf{Q}^* &= \mathbf{Q}^n + \Delta t \mathcal{R}^n, \\
\mathbf{Q}^{**} &= \frac{1}{2} (\mathbf{Q}^n + \mathbf{Q}^* + \Delta t \mathcal{R}^*), \\
\mathbf{Q}^{n+1} &= \frac{1}{2} (\mathbf{Q}^n + \mathbf{Q}^* + \Delta t \mathcal{R}^{**}).
\end{aligned} \tag{3.13}$$

As can be seen, the algorithm depends on the flux and source vector to be recalculated twice using the intermediate values for the state vector \mathbf{Q} , which are denoted with asterix.

Boundary Conditions

The boundary conditions are applied at the cell faces by using two layers of ghost cells placed outside the boundary. The values in these cells are chosen so that the interpolated value at the boundary becomes the specified one. Using ghost cells has the advantage that the same numerics that is applied inside the domain also can be applied at the boundary. Furthermore, no boundary conditions are applied at the top and bottom of the domain. The effects of these boundaries are instead accounted for using a special source term, as will be described later.

Inlet At the inlet, the following boundary conditions are set

- Stagnation enthalpy, h_0 .
- Stagnation pressure, P_0 .
- Velocity components in axial, radial and circumferential direction, \tilde{u}_x , \tilde{u}_r and \tilde{u}_θ .
- Turbulent kinetic energy, k .
- Dissipation of turbulent kinetic energy, ε .

These properties are sufficient to completely specify the state of the fluid at a supersonic inlet. The velocity components are only used to set the direction of the flow, meaning that the magnitude of the velocity at inlet is allowed to vary. This is necessary since the flow at the throat between the blades may be choked ($M = 1$), in which case the mass flow is limited by the mass flow at the throat. The boundary conditions are obtained from the SLC solution, except for k and ε . These are instead set to the same constant values for every streamtube ($0.01 \text{ m}^2/\text{s}^2$ and $0.1 \text{ m}^2/\text{s}^3$ respectively).

Outlet Since the Navier-Stokes equations are solved for in time, transient waves may occur in the domain. To favor convergence towards a steady solution, a non-reflective boundary condition is therefore applied at outlet, which allows these waves to pass through. For a converged solution, the boundary condition effectively acts as a static pressure boundary condition.

Blade surface At the surface of the blade, the following boundary conditions are set

- Velocity \tilde{u}_i . Set in the first cell adjacent to wall using wall functions for tangential component and zero for normal component.
- Turbulent kinetic energy, k . Set in first cell adjacent to surface using wall functions.
- Dissipation of turbulent kinetic energy, ε . Set in first cell adjacent to wall using wall functions.
- Static pressure, p . Set as zero gradient normal to wall, representing no driving of the fluid flow through the wall.
- Adiabatic wall. Set as zero heat flux normal to the wall.

The use of wall functions is necessary for two reasons. Firstly, the mesh is too coarse close to the wall to resolve the viscous sublayer. Second, the turbulence model applied is a high-Reynolds number model, and is therefore not suited for resolving the viscous sublayer if not additional damping is used.

Periodic surfaces The flow is assumed to be rotationally periodic, meaning that the flows in two adjacent blade-to-blade domains are equivalent. The periodic surfaces are therefore connected by setting the values in the ghost cells outside one boundary to the values inside the connecting boundary.

3.2.3 Streamtube Source Term

In this work, a novel method developed by Ellbrant and Eriksson 2014 for performing Q3D blade-to-blade simulations is adopted. This method can account for changes in streamtube thickness and radius and assumes, like the SLC method, that the streamtubes does not twist over the blades. In conventional blade-to-blade methods, these effects are accounted for by transforming the governing equations and solving them on a purely two dimensional mesh. These effects are instead accounted for in this method by changing the radius and thickness of the mesh.

By the definition of a streamtube, there is no mass flow through the stream surfaces that bounds it. Therefore, the flow should at all places in the domain be parallel to the mesh. Since the three-dimensional Navier-Stokes equations are solved, there must therefore be a force in the radial direction to turn the flow along the streamtube. Normally, the radial pressure gradient does this, but since the mesh is only once cell thick, it can not be resolved. Instead, the effect of the pressure gradient is accounted for with an extra source term.

Consider a part of the mesh, as depicted in Figure 3.4 (a), where the flow enters to the left and leaves to the right and where \mathbf{n} denotes the outwards facing normal at the cell center.

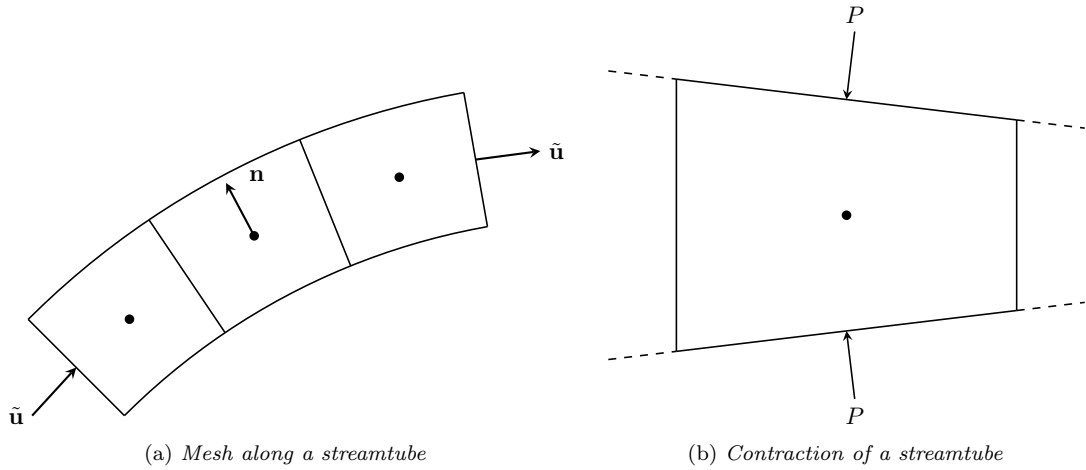


Figure 3.4: Illustration of Q3D mesh.

For a given cell, the source term is defined as a force per unit volume according to

$$\frac{\partial \sigma}{\partial t} = -C (\bar{\rho} \tilde{u}_i \cdot n_i), \quad (3.14)$$

$$F_i = \sigma \cdot n_i. \quad (3.15)$$

The force is introduced into the governing momentum and energy equation according to

$$\frac{\partial(\bar{\rho} \tilde{u}_i)}{\partial t} + \frac{\partial}{\partial x_j} (\bar{\rho} \tilde{u}_i \tilde{u}_j + \bar{p} \delta_{ij} - \tau_{ij}) = F_i, \quad (3.16)$$

$$\frac{\partial(\bar{\rho} \tilde{e}_0)}{\partial t} + \frac{\partial}{\partial x_j} \left(\bar{\rho} \tilde{e}_0 \tilde{u}_j + \bar{p} \tilde{u}_j - c_p \left(\frac{\mu}{Pr} + \frac{\mu_t}{Pr_t} \right) \frac{\partial \tilde{T}}{\partial x_j} - \tilde{u}_i \tau_{ij} \right) = F_i \cdot \tilde{u}_i. \quad (3.17)$$

The source term will not have any contribution to the energy equation for a converged solution, since the force is perpendicular to the velocity in this case.

As can be seen from the definition of the source, (3.14) - (3.15), it is updated during convergence of the solution to force the flow into following the mesh. To ensure stability, Ellbrant and Eriksson 2014 also derived

a stability criteria for the constant C when the three stage Runge-Kutta algorithm is used. In these cases, the criteria reads

$$C \leq \frac{2}{\Delta t^2}. \quad (3.18)$$

The pressure at the bounding stream surfaces will give rise to a force in the direction of the flow when the streamtube changes thickness, as illustrated in Figure 3.4 (b). The effects of endwall pressure must also be taken into account separately, since no boundary conditions are applied at these boundaries. Therefore, Ellbrant and Eriksson 2014 also derived an extra term, which is included when the pressure contribution to the flux vector is calculated.

3.2.4 Flux Equivalent Flow Variables

Before the results from the blade-to-blade simulation can be used as input to the SLC method, the flow properties before and after the blade needs to be averaged in the circumferential direction. This is done by first calculating the average flux of mass, momentum, energy, turbulent kinetic energy and dissipation of turbulent kinetic energy at the inlet and outlet. From the average fluxes, the flux equivalent values for the density, velocity, pressure, turbulent kinetic energy and dissipation of turbulent kinetic energy, here denoted $\hat{\rho}$, \hat{u}_i , \hat{p} , \hat{k} and $\hat{\epsilon}$ respectively, can be defined and calculated. The flux equivalent properties can be used to calculate other properties, such as the stagnation enthalpy, temperature and pressure using standard formulas. The properties obtained are regarded as the circumferentially averaged ones. The derivation of the flux equivalent properties are given in Appendix A.

3.3 S1-S2 Calculation System

An S1-S2 calculation system is referred to as a system that couples the flow on axisymmetric stream surfaces, denoted S1 surfaces, with the circumferentially averaged flow in the meridional plane, denoted the S2 surface, Calvert and Ginder 1999. The flow on the S1 surfaces are computed using a blade-to-blade method and the flow on the S2 surface is computed with a throughflow method, like the SLC method. The coupling of the two methods can be summarized as follows, Calvert and Ginder 1999

1. The blade-to-blade method calculates the flow on axisymmetric stream surfaces situated at a set of spanwise locations between the hub and shroud. This is done for each component in the compressor.
2. The throughflow method calculates the flow in the meridional plane, using input from the blade-to-blade method. The input from the blade-to-blade method reduces the need for correlations in the throughflow method.
3. A blade geometry routine calculates new intersections between the stream surfaces calculated in step 2. and a specified, three-dimensional, blade shape for each component. This, together with the solution from step 2., gives updated information on streamtube shape and boundary conditions for step 1.

This gives rise to an iterative procedure, in which the program alternates between calculating the flow on the S1 and S2 surfaces until the problem converges.

The main advantages of an S1-S2 calculation system is that the computational cost compared to a fully three dimensional CFD method is small. Furthermore, the blade shapes at the spanwise positions where blade-to-blade calculations are performed can be tailored individually, instead of having to design the entire three-dimensional blade at once, Calvert and Ginder 1999. The major drawback of the method is that three-dimensional effects on losses and deviation, as well as blockage of the annulus due to boundary layers, can not be predicted by the blade-to-blade method. Therefore, the method still relies on correlations or empirical input. Also, it can neither be used to design the blades to minimize these effects.

The S1-S2 system is not aimed at replacing either the throughflow method or the fully three-dimensional CFD method. It should instead be seen as a natural step in between the two methods in the design of a compressor.

The S1-S2 system developed in this work is based upon coupling the SLC program SC90C with the Q3D blade-to-blade CFD code described in section 3.2. The coupling of the two codes was done in the Python 3 programming language. The programming essentially follows the outline given by Calvert and Stapleton

1994 and Calvert and Ginder 1999. However, apart from the general outline given by these authors, there is little information available in the open literature on the details of implementing such a system. Therefore, the majority of the coding is based upon ideas developed by the persons involved in the project. It should also be noted that due to the closed source code of SC90C, certain restrictions on how much data that could be fed back from the blade-to-blade method appeared. This did to some extent limit the development of the system.

Below follows a description of the implementation. First, the general program structure is presented. After this, the individual steps in the program are presented and specific algorithms employed are described.

3.3.1 Program Structure

A flowchart of the S1-S2 calculation system is presented in Figure 3.5.

The read area denoted **Main Program** represents the body of the S1-S2 system. It essentially includes the steps described in the previous section in the order 3. → 1. → 2. The loop hence starts by reading the data from SC90C and uses these to set boundary conditions and the streamtube geometry for the blade-to-blade calculations. After this, the blade-to-blade method calculates the flow in the newly defined streamtubes. The results from the blade-to-blade calculations are used to calculate a set of correction factors. These are used by SC90C to correct the results obtained from the correlations used.

As can also be seen from the flowchart, the program uses one input and one output file, presented in the yellow area denoted **Input/Output**. These are used to set up the simulation and to print out various results, including the correction factors. Both the blade-to-blade software and SC90C uses a set of control files to specify boundary and running conditions. Some of these are created at run-time by the program, but others are stored as templates, which is indicated by the green area denoted **Program Files** in the flowchart.

Finally, the data from the blade-to-blade and SLC calculations are stored in a separate directory for each iteration. This is illustrated in the flowchart by the blue areas denoted **Iteration n-1** and **Iteration n**, for the previous and current iteration respectively.

Below, the different parts of the program are described in further detail.

3.3.2 Start Program

To begin with, the program sets up the simulation by reading the input file. The input file specifies all parameters needed for the simulation, but at this point only the following are set

- Number of iterations, N_{iter}
- Number of iteration directories that should be stored
- Correction factors used for SC90C, in case the program restarts from an old solution

The rest of the parameters in the input file are instead read in the loop when they are needed. This reduces the amount of data that have to be sent between different routines in the program.

3.3.3 Read Data from SC90C

In the first step of the loop, the SC90C solution from the previous iteration is being read. In the first iteration, it is therefore required that a SC90C solution has been prepared in advance so that the program have something to start from. This approach enables the user to control the starting point of the iteration. It also offers an intuitive way of continuing the design or analysis of a compressor where only SC90C has been used, to using the S1-S2 calculation system.

The data from SC90C is stored in the grid points, defined as the intersections between the streamlines and the QO's. Hence, for every component, the spanwise variation of data along the leading and trailing edges are available. This includes the velocity, total and static pressure, temperature and enthalpy together with Mach number and swirl angles.

3.3.4 Set Boundary Conditions

The next step of the iteration is to use the SC90C data to produce boundary conditions for the blade-to-blade calculations. In particular, the conditions at inlet and outlet to the streamtube domains are specified. This is done by using the data from SC90C to write two files for each component, describing the spanwise variation of

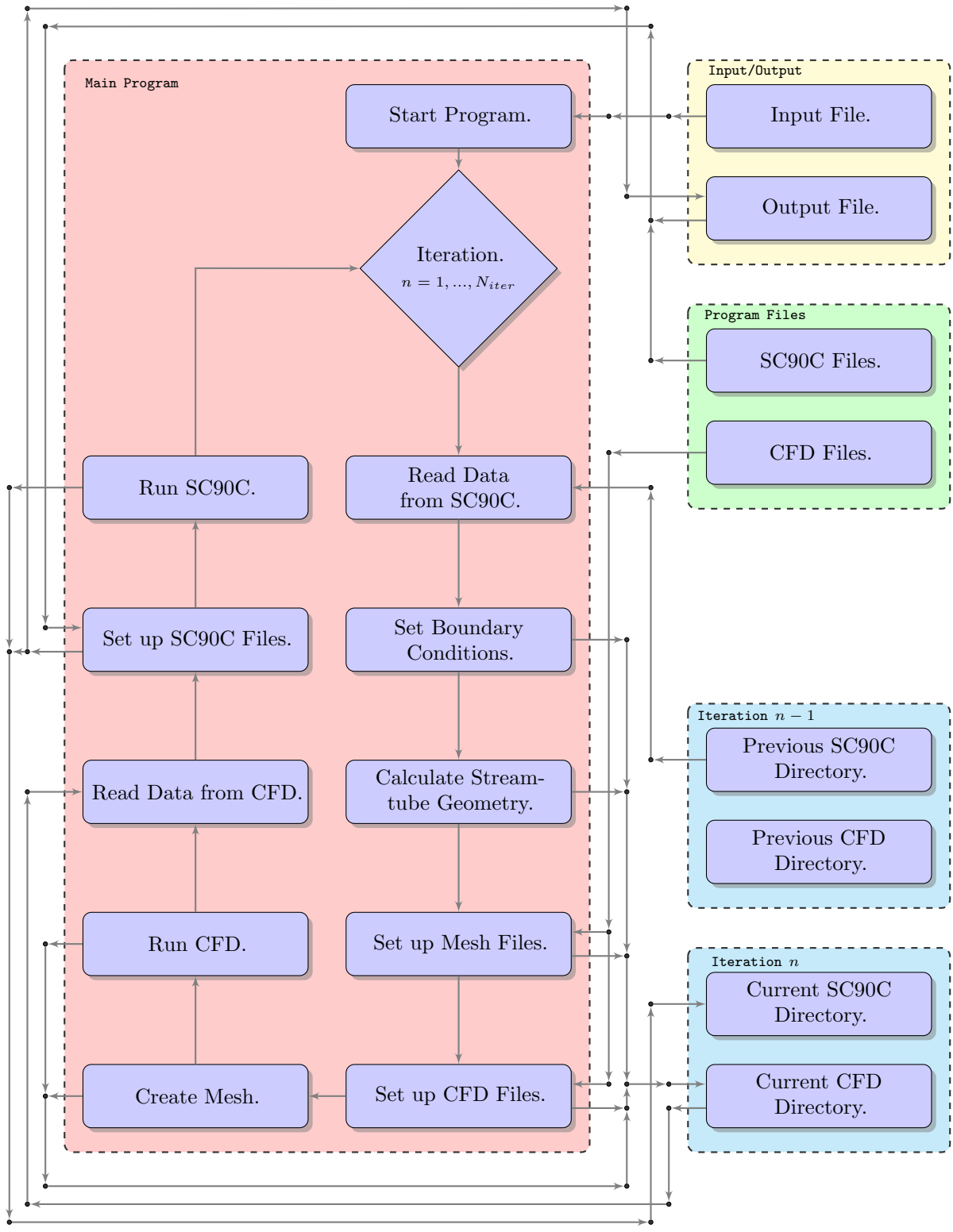


Figure 3.5: Flowchart for S1-S2 calculation system.

a set of properties along the leading and trailing edge. The blade-to-blade program will later interpolate in these lists to obtain data for the boundary conditions at the spanwise positions for which the blade-to-blade calculations are performed.

It should be noted that not all data will be used. Instead, dependent on which type of boundary conditions that are specified at the inlet and outlet, the solver will select the appropriate data from these files.

As indicated by the flowchart, these files are then written to the CFD directory situated within the current iteration directory.

3.3.5 Calculate Streamtube Geometry

The streamtubes that represent the domains for the blade-to-blade calculations are assumed axisymmetric. Also, the thickness is constant before the leading and after the trailing edge, and varies linearly in between. Therefore, it suffices to specify the coordinates of the upper and lower boundary at inlet, outlet as well as the intersections with the leading and trailing edge to completely specify the domain. The streamtubes are constructed by wrapping them around a set of selected streamlines calculated by SC90C. In this work, the blade-to-blade calculations was performed at 10, 20, 40, 60, 80 and 90% span for each component in the compressor. The coordinates of the upper and lower boundaries are written to two separate files for each component and stored in the current CFD directory.

Below follows a description of how these coordinates are calculated.

Streamtube thickness calculation

The program first calculates the coordinates where the upper and lower boundary of the streamtube intersects the leading and trailing edge. From SC90C, the cumulative mass flow, \dot{m}_c , as well as the axial and radial coordinates, denoted x_1 and x_2 , are available in each grid point: $j = 1, \dots, N_s$. The cumulative mass flow is defined as the total mass flow below a streamline going through a certain grid point. Further, denote the cumulative mass flow at the streamline around which the domain is wrapped by $\dot{m}_{c,s}$ and the specified mass flow in the streamtube $\dot{m}_{c,d}$. The cumulative mass flow at the upper and lower boundary, denoted $\dot{m}_{c,u}$ and $\dot{m}_{c,l}$ respectively, can then be calculated as

$$\dot{m}_{c,u} = \dot{m}_{c,s} + \frac{\dot{m}_{c,d}}{2}, \quad (3.19)$$

$$\dot{m}_{c,l} = \dot{m}_{c,s} - \frac{\dot{m}_{c,d}}{2}. \quad (3.20)$$

To find the corresponding axial and radial coordinates, interpolation is needed. Therefore, the coordinates are expressed as functions of the cumulative mass flow according to

$$x_i = f_i(\dot{m}_c), \quad (3.21)$$

where x_i denotes either the axial or radial coordinate. The values of the function f_i in between the nodes are obtained by adapting a cubic spline to the data set $(\dot{m}_{c,j}, (x_i)_j)$. The coordinates where the upper and lower boundary intersects either the leading or trailing edge can then be found according to

$$x_{i,u} = f_i(\dot{m}_{c,u}), \quad (3.22)$$

$$x_{i,l} = f_i(\dot{m}_{c,l}). \quad (3.23)$$

Finally, the coordinates at inlet and outlet are set with equal radius as those at the leading and trailing edge respectively.

3.3.6 Set up Mesh Files

The routine that creates the mesh needs a set of control files in addition to those described above. These files must be prepared in advance as templates and are at this point copied into the current CFD directory and completed. The information that already have been written to them include

- Orientation of blocks

- Number of cells within each block
- Definition of boundaries
- Definition of which type of boundary conditions that apply to each boundary

They are completed with the following information

- Name of files specifying the upper and lower boundary of the domain
- Number of blades in the blade row
- Name of file specifying the three dimensional blade shape

Hence, the mesh must be set up in advance as opposed to being specified at run-time. This approach was taken since it is both easier and more convenient to let the user manually set the mesh quality as opposed to automating the procedure.

3.3.7 Set up CFD Files

To run the CFD simulations, the solver needs a control file, which also must be prepared in advance as a template. This file is now copied into the current CFD directory and completed. The information that must be prepared in advance include

- Mesh topology
- Specification of numerical schemes, including coefficients for upwinding scheme
- Specification of gas properties
- Specification of turbulence model, including model constants

The file is completed with the following information

- Rotational speed, in case component is a rotor
- Number of time steps that should be taken, i.e. number of iterations
- CFL number to limit size of discrete time steps
- Name of the mesh file
- Number of CFD simulations per streamtube, including how much the boundary conditions will be varied between simulations

The option of running multiple CFD simulations with varying boundary conditions is described next

Performing multiple blade-to-blade simulations

There is a fundamental difference between the way boundary conditions are applied in SLC and CFD when analyzing compressors. In the SLC method, the mass flow is specified and the pressure ratio across a component becomes a function of it. In CFD the situation is reversed, since the pressure at inlet and outlet usually is specified and the mass flow becomes a function of this difference instead. As a result, it is usually the case that most properties, apart from those set as boundary conditions, obtained in the blade-to-blade calculation will differ from those obtained in SC90C. This can be interpreted as if the blade simulated in SC90C and CFD operate under different conditions. To overcome this problem, multiple CFD simulations are performed with varying boundary conditions. The results from these are interpolated to obtain data representing the same conditions as those in SC90C. This will be described in further detail later.

3.3.8 Create Mesh and Run CFD

The next step of the loop is to create the mesh for all streamtubes and run the CFD simulations. One CFD simulation, including meshing, takes about one minute to complete on a single CPU core with the current number of iterations and mesh size. For each component, 6 streamtubes are simulated and for each streamtube, 3 CFD simulations are performed with varying boundary conditions. The compressor analyzed in this work has 7 components, meaning that about $3 \cdot 6 \cdot 7 = 126$ minutes would be required to complete the blade-to-blade calculations on a single core. The meshing as well as the CFD simulations are therefore performed in parallel on a cluster instead, where each node on the cluster takes care of the meshing and blade-to-blade simulations of one streamtube.

The results from the simulations are flux averaged as described in section 3.2.4. The flux equivalent flow variables are written to two separate files and stored in the current CFD directory. The only difference, apart from the values, between these files and those used for boundary conditions, is that they only include one value of each property at the radial location of the streamtube inlet or outlet.

3.3.9 Read Data from CFD

The data available at the inlet and outlet from each blade-to-blade simulation are at this point read into the program. More than one value of each property is available as well if multiple simulations have been performed for a given streamtube. Before they can be used to calculate correction factors for SC90C, they must be interpolated into one set of values. Also, since the correction factors should be applied at the location of the SC90C streamlines, the values must be interpolated across the span to reach all SC90C streamlines. Finally, some additional properties not written out by the CFD solver are calculated.

Interpolation based on effective throttle area

The common denominator used to interpolate the values obtained from the multiple blade-to-blade simulations into one set of values consistent with those in SC90C is called the effective throttle area. Imagine that a throttle valve could be placed at the outlet of the streamtube used in the blade-to-blade simulation. The effective throttle area can then be thought of as the area this throttle would need to have in order to obtain the same flow as when the given pressure difference is used.

For each streamtube, the effective throttle area is calculated based on the data obtained from each blade-to-blade simulation. These will be denoted A_j^* . The effective throttle area is also calculated based on the SC90C data for the streamline around which the blade-to-blade domain was wrapped. This results will be denoted A_{SC90C}^* . Each property, y_i , calculated by the blade-to-blade simulation at either inlet or outlet is then expressed as a function of effective throttle area according to

$$y_i = g_i(A^*). \quad (3.24)$$

The shape of the function g_i is obtained by adapting a cubic spline curve to the data set $(A_j^*, (y_i)_j)$. Finally, the values of the properties at the same effective throttle area as calculated by SC90C is obtained according to

$$y_i^* = g_i(A_{\text{SC90C}}^*). \quad (3.25)$$

The idea behind this approach is to obtain data from the blade-to-blade simulation that operates towards the same external throttle as SC90C can be thought to do.

Interpolation across span

Blade-to-blade calculations are not performed for every streamline used in SC90C to reduce the computational cost. Instead, the results from the blade-to-blade calculations are interpolated across the span. This is done by expressing every property from the previous step as a function of the radius according to

$$y_i^* = h_i(r). \quad (3.26)$$

As before, the shape of the functions h_i are obtained by adapting a cubic spline curve to the data set $(r_j, (y_i^*)_j)$, where index j ranges over the blade-to-blade calculations that was done. The values of y_i^* at the location of the SC90C streamlines are obtained by inserting the radius of these streamlines into the function h_i .

Calculation of additional properties

At this point, values from the blade-to-blade method are available at every grid point along the leading and trailing edge. This data is used to calculate the performance of the blade in terms of the deviation and pressure loss coefficient. These results will later be used as a reference to specify correction factors for the Wright and Miller 1991 correlations employed by SC90C.

Deviation To calculate the deviation, the flow exit angle, α_2 for a stator and β_2 for a rotor, must first be calculated. This is done according to (2.3) or (2.7) for a stator and rotor respectively. After this, the deviation is calculated as the difference between the flow exit angle and the blade exit angle.

Pressure Loss Coefficient The calculation of the pressure loss coefficient proceeds as described in section 2.6.3. It should be noted at this point that the pressure loss obtained from the blade-to-blade calculations only can stem from losses defined as 2D in Section 2.1.4. This must be taken into account when correcting the pressure loss computed by SC90C, since it also includes 3D effects.

3.3.10 Set up SC90C Files

Before running SC90C, the control files must to be set up. These have, like the CFD files, been prepared in advance as templates and are now copied into the current SC90C directory and completed. The information left to be added to the files are

- Total mass flow in compressor
- Correction factors for deviation and 2D losses

At this point, only the correction factors are written to the files. The mass flow will instead be adjusted in the next step of the program. The correction factors can be specified at selected radial positions across the span, whereby SC90C will interpolate in this list to find the correction at the location of a given streamline. The correction factors are in this work calculated at the location of the streamlines computed in the previous SC90C solution, as will be described next.

Correction of deviation

The deviation used in SC90C is the sum of the deviation computed by the correlations developed by Wright and Miller 1991, δ_{corr} , and the deviation correction specified, Δ_δ , according to

$$\delta_{\text{SC90C}} = \delta_{\text{corr}} + \Delta_\delta. \quad (3.27)$$

From the previous SC90C solution, the value of δ_{SC90C} is available, denoted $\delta_{\text{SC90C}}^{n-1}$. At the previous iteration, the calculated deviation correction, Δ_δ^{n-1} , was also written to the output file, and it is at this point read back into the program. The new correction factor can then be calculated as the difference between the current deviation calculated by the blade-to-blade method and the previous correlation result calculated by SC90C according to

$$\Delta_\delta^n = \delta_{\text{CFD}} - (\delta_{\text{SC90C}}^{n-1} - \Delta_\delta^{n-1}). \quad (3.28)$$

If the deviation correction converges after some iterations, then the actual deviation used in SC90C will be the same as that computed by the blade-to-blade method. To favor convergence, the deviation correction is updated using under-relaxation. In this case, the new deviation correction will only partly be updated based on the blade-to-blade deviation according to

$$\begin{aligned} \Delta_\delta^n &= \alpha [\delta_{\text{CFD}} - (\delta_{\text{SC90C}}^{n-1} - \Delta_\delta^{n-1})] + (1 - \alpha)\Delta_\delta^{n-1} \\ &= \alpha [\delta_{\text{CFD}} - \delta_{\text{SC90C}}^{n-1}] + \Delta_\delta^{n-1}. \end{aligned} \quad (3.29)$$

Apart from being written to the control file, the new deviation correction is also written to the output file, as indicated by the flowchart.

Correction of pressure loss

As described in section 3.1.3, the pressure loss coefficient is calculated in SC90C as the sum of the losses due to 2D and 3D effects. Each individual pressure loss coefficient, $Y_{p,i}$, is further calculated as the pressure loss coefficient obtained by the correlation, $Y_{p, \text{corr},i}$, times a multiplying correction factor $C_{f,i}$ according to

$$Y_{p,i} = C_{f,i} \cdot Y_{p, \text{corr},i}. \quad (3.30)$$

Since the blade-to-blade method does not take three dimensional effects into account, correction factors are only specified for the profile and shock loss coefficients. The relative magnitude between the shock and profile loss coefficients is unimportant in SC90C, since it is their combined magnitude that is used to determine the entropy change. Therefore, they are corrected with the same correction factor C_f . The values of the pressure loss coefficients, $Y_{p,i}^{n-1}$, are available from the previous SC90C solution. Also, the correction factor used in the previous iteration, C_f^{n-1} , is available in the output file. A new correction factor can then be calculated as the fraction between the current pressure loss coefficient calculated by the blade-to-blade method and the combined pressure loss coefficient calculated by the SC90C correlations in the previous iteration according to

$$\begin{aligned} C_f^n &= \frac{Y_{p, \text{CFD}}}{Y_{p, \text{corr}, \text{prof}}^{n-1} + Y_{p, \text{corr}, \text{shock}}^{n-1}} \\ &= \frac{C_f^{n-1} \cdot Y_{p, \text{CFD}}}{Y_{p, \text{prof}}^{n-1} + Y_{p, \text{shock}}^{n-1}}. \end{aligned} \quad (3.31)$$

As in the case with the deviation correction, the total two dimensional loss used by SC90C will equal that computed by the blade-to-blade method if the correction factors converge. To ensure this, under-relaxation was also employed for the correction factor according to

$$\begin{aligned} C_f^n &= \alpha \frac{C_f^{n-1} \cdot Y_{p, \text{CFD}}}{Y_{p, \text{prof}}^{n-1} + Y_{p, \text{shock}}^{n-1}} + (1 - \alpha) C_f^{n-1} \\ &= \alpha \left[\frac{Y_{p, \text{CFD}}}{Y_{p, \text{prof}}^{n-1} + Y_{p, \text{shock}}^{n-1}} - 1 \right] C_f^{n-1} + C_f^{n-1}. \end{aligned} \quad (3.32)$$

As for the deviation correction, the pressure loss correction factor is written to both the control and output file.

3.3.11 Run SC90C

The final step of the iteration is to run SC90C using the updated corrections for the deviation and pressure loss. If the deviation and pressure loss correction has changed from the last iteration, then the performance of the compressor has changed as well. Referring to Figure 2.7, changing the performance of the compressor will change the location of the speedline. Due to the steep gradient of a speedline when the compressor operates close to choke, the pressure ratio can therefore change considerably compared to the last iteration if the same mass flow is used. This can lead to problem with convergence, since the pressure ratio is used for boundary conditions in the blade-to-blade method, which in turn is used to compute the deviation and loss corrections.

To overcome this problem, the mass flow in SC90C is adjusted to ensure that the compressor always lies on a specific operating line. This can be achieved by finding the intersection between the current speedline and the operating line, see Figure 2.7. Since the operating line is set by the conditions after the compressor, this approach represents that the program converges under a constant external condition. In each iteration, a new point along the operating line will be found due to changed correction factors. The program can then be considered converged when a stable point along the operating line has been found.

The operating line must be specified for each simulation, to set the conditions under which the compressor will operate. The shape of the speedline is however not known in advance. The intersection must therefore be found with an iterative procedure, as will be described next.

Algorithm for mass flow

To start with, the shape of the operating line must be specified. In this work, the shape is approximated as a second order polynomial according to

$$\text{PR} = a \dot{m}^2, \quad (3.33)$$

where \dot{m} and PR is the mass flow and pressure ratio across the compressor respectively. The coefficient a defines the slope of the operating line, a higher value will force the compressor to operate closer to stall and a lower value closer to choke. The aim of the algorithm is to find a mass flow such that the pressure ratio computed by SC90C equals the pressure ratio given by (3.33).

To begin with, the program sets the reference starting point for the search as the mass flow and pressure ratio from the previous iteration of the main program, denoted \dot{m}_0 and PR_0 respectively. It then sets the initial guess for the mass flow in SC90C, \dot{m}_1 , equal to \dot{m}_0 . The iteration to find the correct mass flow then proceeds as follows

1. Let SC90C calculate the pressure ratio, PR_i , given the mass flow set in the previous mass-iteration, \dot{m}_i .
2. Calculate the distance between the previous mass-iteration point and the current according to

$$d = \sqrt{(\dot{m}_i - \dot{m}_{i-1})^2 + (\text{PR}_i - \text{PR}_{i-1})^2}. \quad (3.34)$$

3. Find the point $(\dot{m}_{\text{OL}}, \text{PR}_{\text{OL}})$ on the operating line that is closest to the current mass-iteration point (\dot{m}_i, PR_i) . Since $\text{PR}_{\text{OL}} = a \dot{m}_{\text{OL}}^2$, this point can be found by minimizing the following function

$$f(\dot{m}_{\text{OL}}) = (\dot{m}_i - \dot{m}_{\text{OL}})^2 + (\text{PR}_i - a \dot{m}_{\text{OL}}^2)^2. \quad (3.35)$$

This is done by finding the real roots to the derivative $f'(\dot{m}_{\text{OL}})$, and selecting the one that gives the smallest value of $f(\dot{m}_{\text{OL}})$.

4. Update the mass flow for the next mass-iteration using under-relaxation according to

$$\dot{m}_{i+1} = \alpha \dot{m}_{\text{OL}} + (1 - \alpha) \dot{m}_i. \quad (3.36)$$

5. Check if the program has converged, it is considered converged if

$$d \leq d_{\text{max}}, \quad (3.37)$$

for some predefined largest step length d_{max} . If the program has not converged, use the newly updated mass flow and proceed to step 1.

When the algorithm has converged, the latest SC90C solution from the mass-iteration is considered to be on the operating line, and will therefore be used in the next iteration of the main program.

The representation of the operating line as a quadratic polynomial is only a rough approximation. This is however unimportant, since the only purpose of the operating line is to offer a controlled way for the program to converge. By varying the coefficient a , a complete speedline for the compressor can be obtained.

4 Results

4.1 Simulation Results

Various results from simulations of the three stage transsonic compressor are presented in this section. The compressor has only been analyzed under design conditions, and the behavior close to stall and choke has not been considered in any detail. The results are compared to 3D CFD data for the compressor, using a similar grid resolution as was employed in the blade-to-blade calculations.

4.1.1 Characteristic Map

To begin with, a complete speedline was computed with the S1-S2 system using a couple of different settings. The results are compared to 3D CFD in Figure 4.1, in which the operating line that represents standard operating conditions for the compressor is also included.

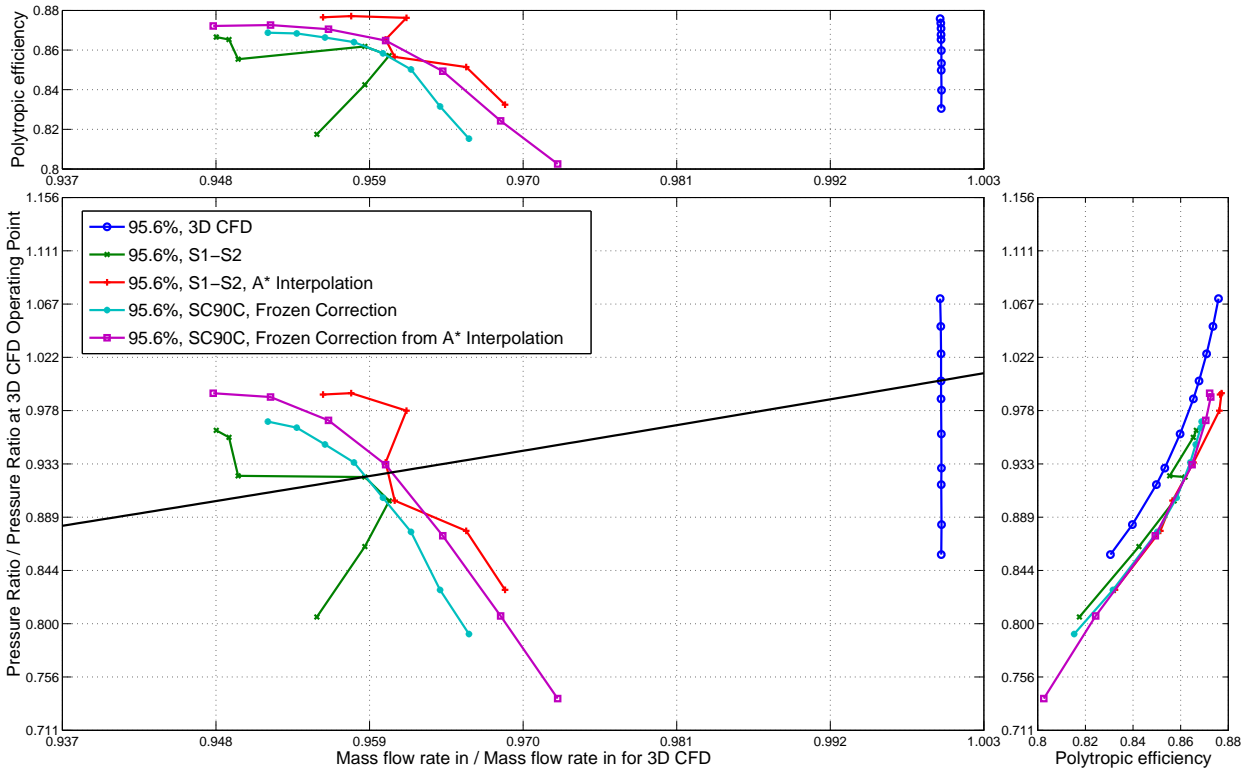


Figure 4.1: *Characteristic map for the three stage compressor at 95.6% of maximum rotational speed.*

Apart from the predicted speedline, the polytropic efficiency is also included as a function of the pressure ratio and mass flow, respectively. The results denoted 'S1-S2' was obtained using only one blade-to-blade calculation per iteration, and hence no interpolation based on effective throttle area was consequently performed. This was on the other hand done for the results denoted 'S1-S2, A* Interpolation', in which 3 blade-to-blade calculations was performed. In these simulations, the static pressure at the outlet was varied from the pressure predicted by SC90C with $\pm 5\%$. The two remaining results, denoted 'SC90C, Frozen Correction', was obtained by freezing the correction factors to those calculated at the operating point by the S1-S2 system. A complete speedline was then calculated by simply varying the mass flow.

The results show that the S1-S2 system predicts the operating point to lie lower down on the operating line compared to 3D CFD. This implies that the S1-S2 system predicts that the compressor transfers too little work to the fluid. By the Euler work equation, (2.82), this in turn implies that the system predicts too large deviation for the rotors. The lower pressure ratio could also imply that too large losses are predicted. However, since the polytropic efficiency agrees very well, this is not suspected to be the case.

Furthermore, it can be observed that the slope of the speedline is more flat than the slope computed by 3D CFD. This is much due to the SLC formulation, which is known to have problems predicting the steep slope of a speedline close to choke.

The speedlines computed by the S1-S2 system are also not as smooth as would be expected. This highlights that the system still have some problems in converging to a stable point along the operating line. Finally, the results indicate that the use of multiple blade-to-blade calculations improves the results.

4.1.2 Performance of individual components

In this part, the spanwise variation of a set of properties, predicted by the S1-S2 system and 3D CFD at the operating point, are presented for each component. Only the results from the best S1-S2 simulation, using multiple blade-to-blade calculations, is included to save space in the figures. An explanation of the different properties presented for rotors and stators/inlet guide vane are given in Tables 4.1 and 4.2 respectively.

Table 4.1: Properties presented for Rotors.

Abbreviation	Explanation	Symbol/Formula
PR	Stagnation Pressure Ratio	$P_{0,2}/P_{0,1}$
DTT	Stagnation Temperature Difference, normalized	$(T_{0,2} - T_{0,1})/T_{0,1}$
Loss Coef	Pressure Loss Coefficient	$Y_{p, R}$, see (2.67)
Incidence	Incidence	$i = \alpha_1 - \alpha'_1$
Swirl In	Relative Inlet Swirl Angle	α_1
Swirl out	Relative Outlet Swirl Angle	α_2
M in	Inlet Mach Number	$M_1 = u_1/a_1$
M out	Outlet Mach Number	$M_2 = u_2/a_1$
M-mer in	Inlet Meridional Mach Number	$M_{m,1} = u_{m,1}/a_1$
M-mer out	Outlet Meridional Mach Number	$M_{m,1} = u_{m,2}/a_2$
Vm/U in	Inlet Flow Coefficient	$\Phi_1 = u_{m,1}/U_1$
Vm/U out	Outlet Flow Coefficient	$\Phi_2 = u_{m,2}/U_2$
De Haller	De Haller Number	w_2/w_1
DF	Diffusion Factor	$\left(1 - \frac{w_2}{w_1}\right) + \left(\frac{w_{\theta,1} - w_{\theta,2}}{2w_1}\right) \frac{s}{l}$
DHU2	Stage Loading	$\psi = (h_{0,2} - h_{0,1})/U^2$
Deviation	Deviation	$\delta = \alpha_2 - \alpha'_2$

Table 4.2: Properties presented for Stators and Inlet Guide Vane.

Abbreviation	Explanation	Symbol/Formula
P0 in	Inlet Stagnation Pressure	$P_{0,1}$
P0 out	Outlet Stagnation Pressure	$P_{0,2}$
DPP	Stagnation Pressure Drop, normalized	$(P_{0,1} - P_{0,2})/P_{0,1}$
Incidence	Incidence	$i = \alpha_1 - \alpha'_1$
Swirl In	Inlet Swirl Angle	α_1
Swirl out	Outlet Swirl Angle	α_2
M in	Inlet Mach Number	$M_1 = u_1/a_1$
M out	Outlet Mach Number	$M_2 = u_2/a_2$
M-mer in	Inlet Meridional Mach Number	$M_{m,1} = u_{m,1}/a_1$
M-mer out	Outlet Meridional Mach Number	$M_{m,2} = u_{m,2}/a_2$
Mass flow in	Inlet Mass Flow to Streamtube	
Mass flow out	Outlet Mass Flow to Streamtube	
De Haller	De Haller Number	u_2/u_1
DF	Diffusion Factor	$\left(1 - \frac{u_2}{u_1}\right) + \left(\frac{u_{\theta,1} - u_{\theta,2}}{2u_1}\right) \frac{s}{l}$
DPD	Stagnation Pressure Drop, normalized (equivalent to pressure loss coefficient)	$(P_{0,1} - P_{0,2})/(P_{0,1} - P_1)$
Deviation	Deviation	$\delta = \alpha_2 - \alpha'_2$

Inlet Guide Vane

The results for the inlet guide vane are presented in Figure 4.2

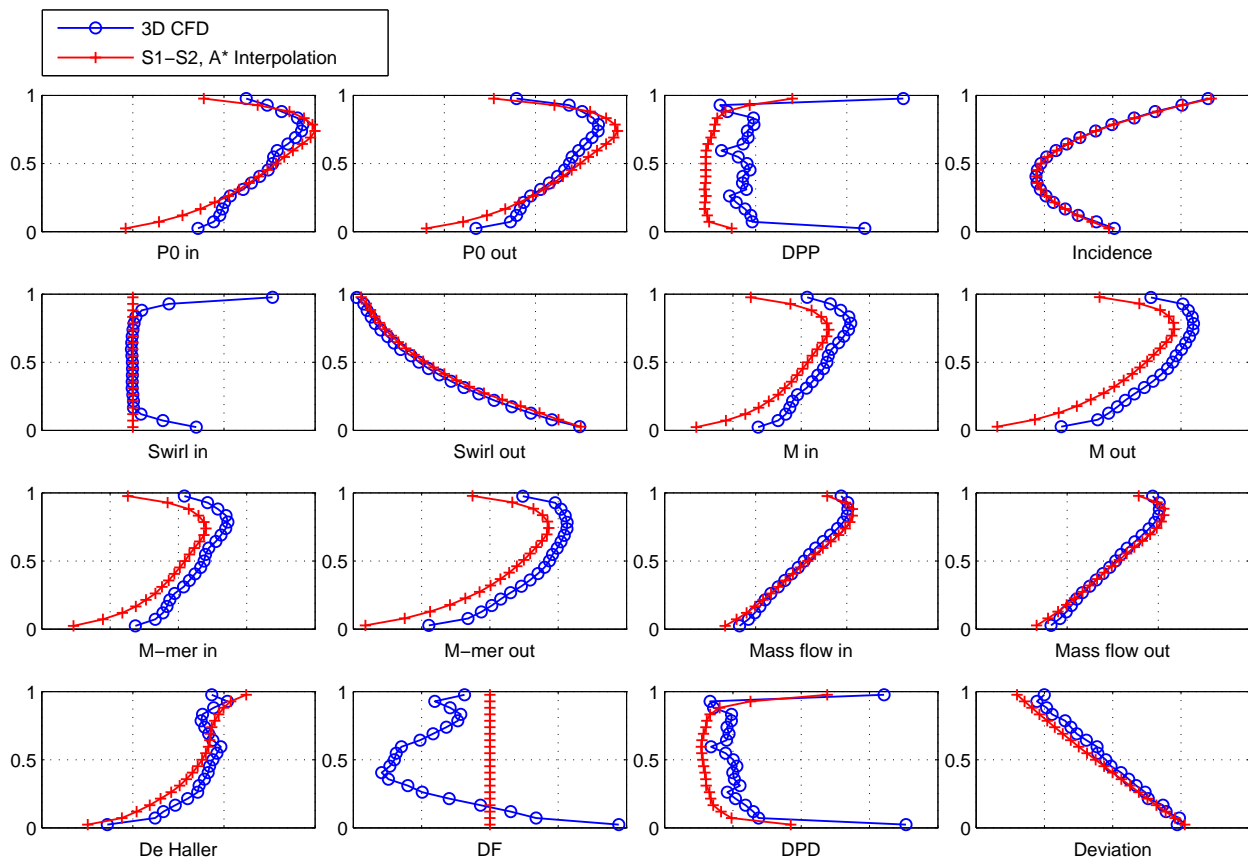


Figure 4.2: *Spanwise profiles for inlet guide vane.*

The overall agreement is good, and the profiles computed by the S1-S2 system shows the same trends as those computed by 3D CFD. It should be noted that no deviation correction was applied to the inlet guide vane, since a possible bug in SC90C caused deviation correction factors to be interpreted incorrectly for IGVs, prohibiting a consistent use of them.

The most apparent difference is that the velocity is lower across the span for the S1-S2 solution, seen from the lower Mach numbers. This can partly be attributed to the lower mass flow in the S1-S2 solution. Another reason is that the boundary layers at the hub and shroud are not taken into account, which otherwise causes lower velocity at the end walls and larger velocity in the bulk.

Rotor 1

The spanwise profiles calculated for the first rotor is presented in Figure 4.3

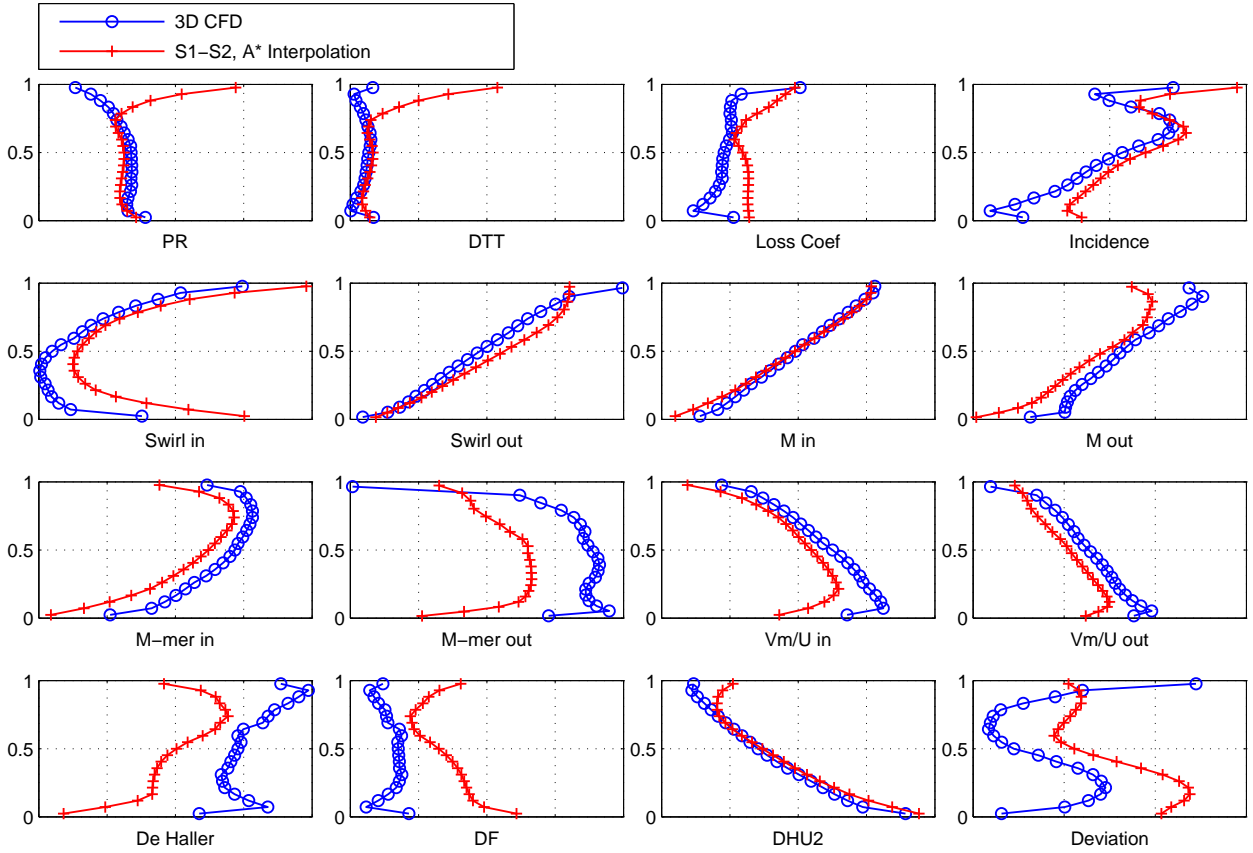


Figure 4.3: *Spanwise profiles for rotor 1.*

As for the IGV, the agreement with 3D CFD is reasonable and the spanwise profiles shows the same overall trends. The exception is the stagnation pressure and temperature ratios close to the shroud, which have been severely overpredicted by the S1-S2 system. The explanation is found when turning to the deviation, which has been under predicted close to the shroud. This means that the flow is turned too much here, resulting in a larger work transfer to the fluid by the Euler Work Equation, (2.82). The reason could be that the highly three dimensional flow field at the tip, caused by interactions between the blades and the boundary layer at the shroud, is neglected in the S1-S2 system. This flow field may have an important effect on the deviation from the blades.

The fact that the deviation otherwise is overpredicted across the span is hard to explain. The reason to why this does not affect the overall work input to the fluid is that the incidence also is overpredicted, causing the net turning of the flow to be little affected. Once again, the velocity is also consistently lower, by the same reasons as presented earlier.

The fact that the general trend of the profiles is captured well is an important result. It indicates that the use of 6 blade-to-blade calculations is sufficient to capture the majority of the spanwise variations present in the actual flow field.

Stator 1

The results for the first stator is presented in Figure 4.4

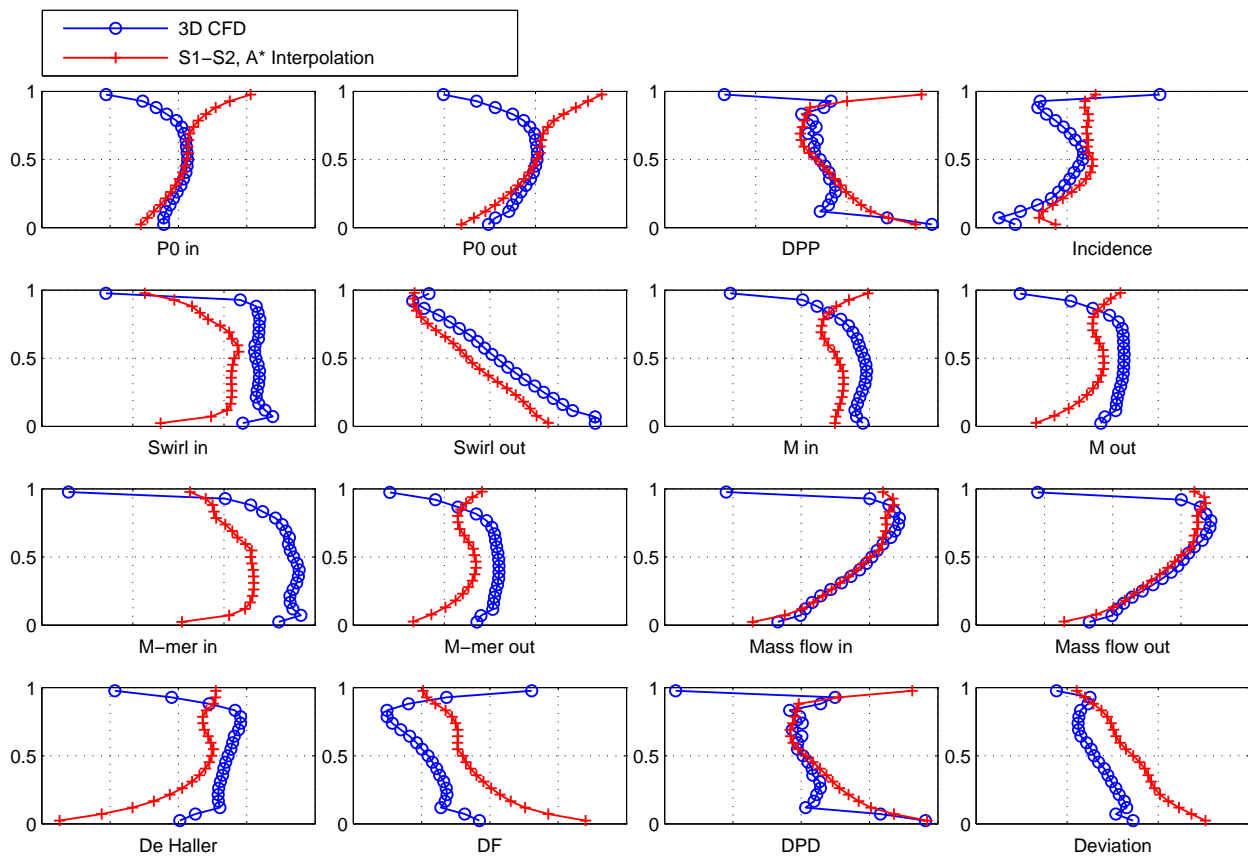


Figure 4.4: *Spanwise profiles for stator 1.*

Once again, the overall trends are predicted well by the S1-S2 system, but the absolute magnitude of most parameters differ.

To begin with, the total pressure in and out of the stator is higher close to the shroud. This is simply because of the the larger pressure computed by the first rotor in this region, which is mostly just convected across the stator. The small change in stagnation pressure across the stator due to losses is however well predicted.

The trend of overpredicting the deviation and the incidence is also present for this component, except for close to the shroud where boundary layer take effect in the 3D CFD solution.

Rotor 2

The results for the second rotor is presented in Figure 4.5

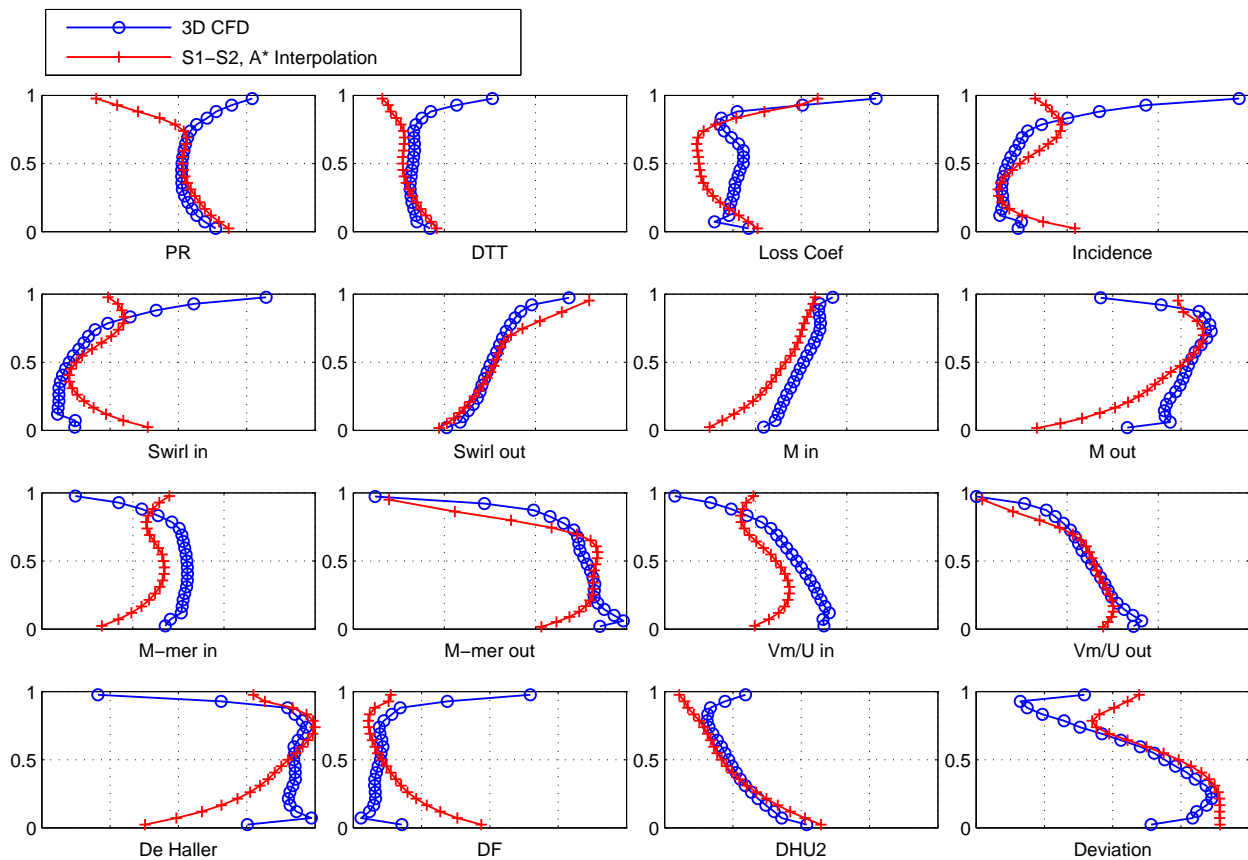


Figure 4.5: *Spanwise profiles for rotor 2.*

In terms of the total temperature and pressure ratio, the situation is reversed compared to the first rotor. In this case, the work transferred to the fluid is lower close to the shroud compared to 3D CFD. The explanation is once again found in the deviation, which has been overpredicted in this region by the S1-S2 system. This is also amplified by the under predicted incidence close to the shroud, which further decreases the net turning of the flow. It is hard to explain exactly why, but it is safe to assume that three dimensional flow field has a predominant effect on the velocity and deviation of the flow in this region.

Furthermore, the pressure loss coefficient can be seen to agree reasonably well.

Stator 2

The results computed for the second stator is presented in Figure 4.6

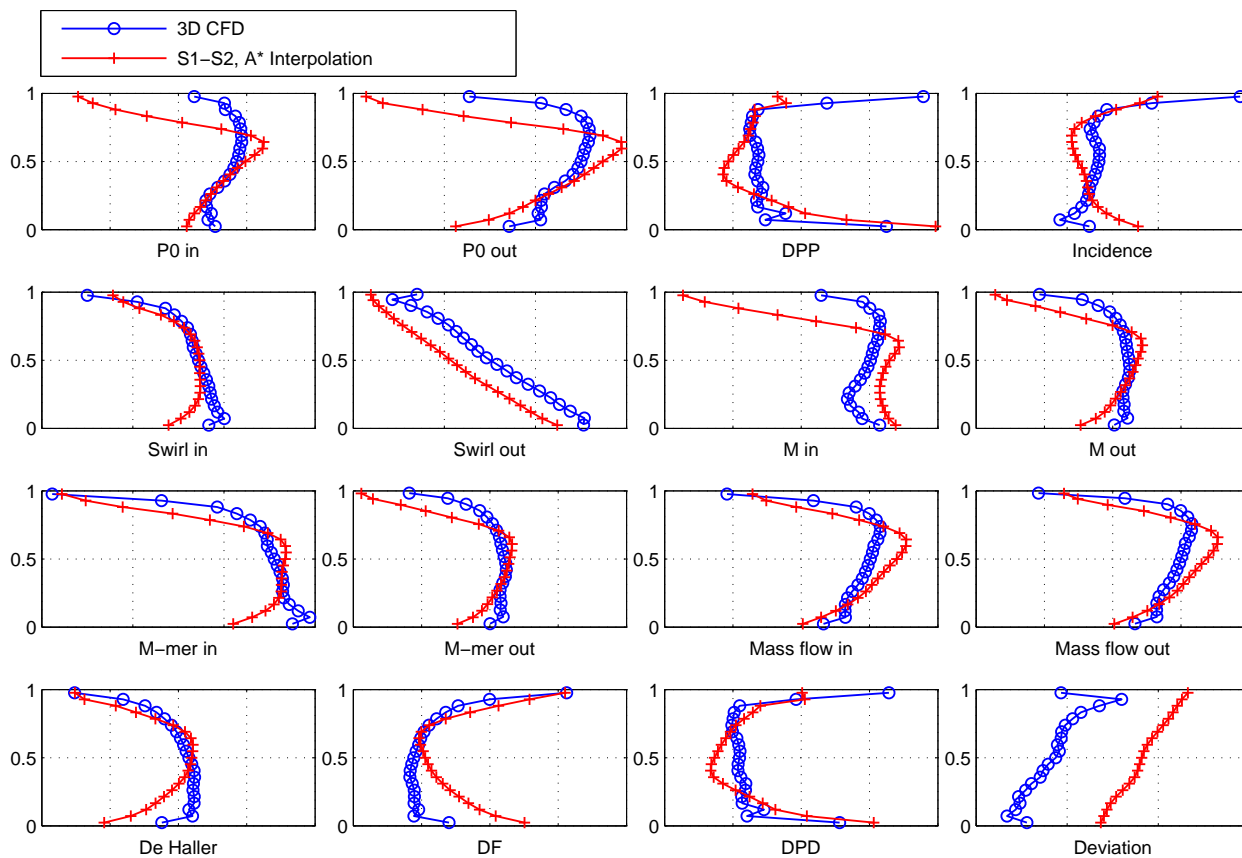


Figure 4.6: *Spanwise profiles for stator 2.*

The trends for this component is consistent with the previous stator. To begin with, the change in stagnation pressure across it is well predicted. The magnitude of the stagnation pressure in and out of the component is however quite different from 3D CFD. This is once again explained by the fact that the stator changes the pressure little, and that the stagnation pressure has been poorly predicted by the previous components.

The deviation is also overpredicted, like for the previous stator.

Rotor 3

Spanwise profiles computed for the third rotor is presented in Figure 4.7

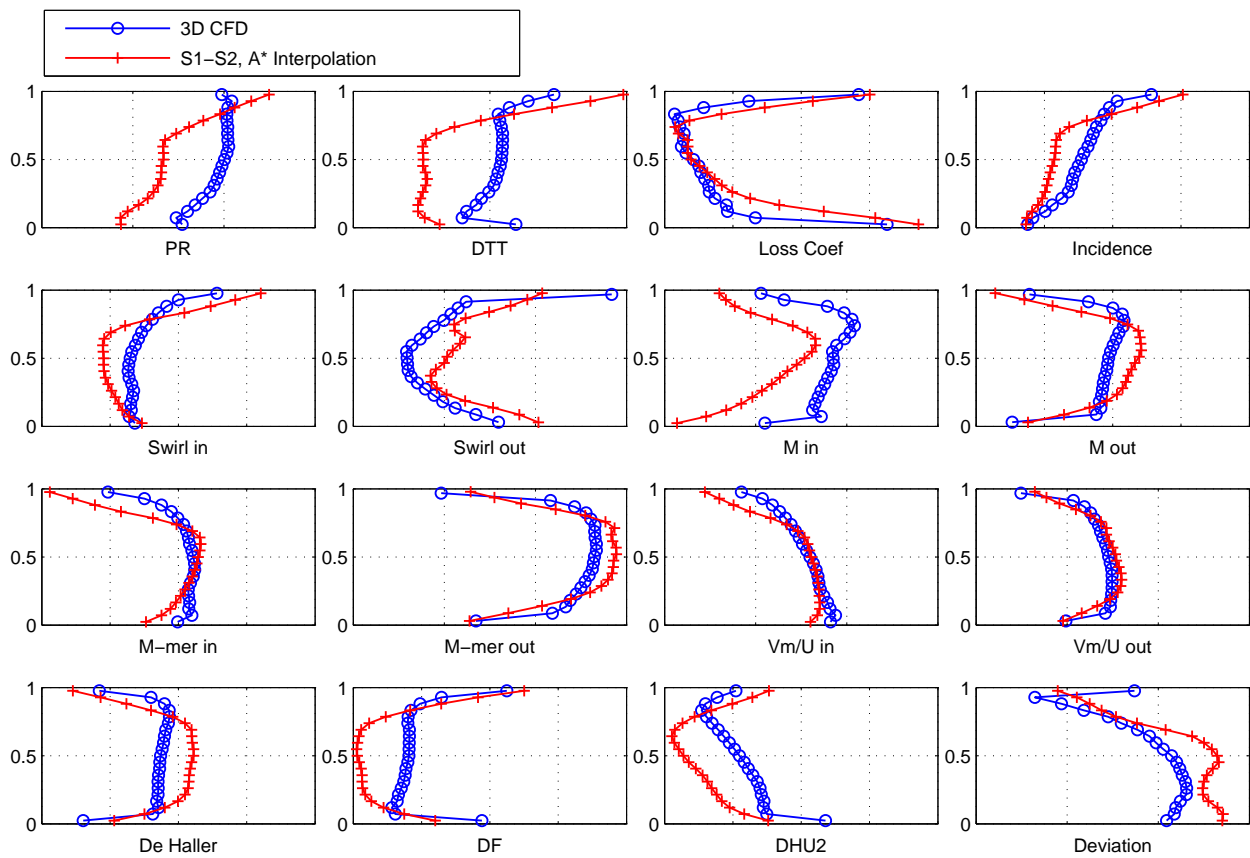


Figure 4.7: *Spanwise profiles for rotor 3.*

The stagnation pressure and temperature ratio is under-predicted across almost the entire span, which is reflected in the higher deviation present in the same region.

The remaining properties are fairly well predicted, including the pressure loss coefficient which shows good agreement both with respect to profile shape and magnitude.

Stator 3

Finally, the results from the third stator is presented in Figure 4.8

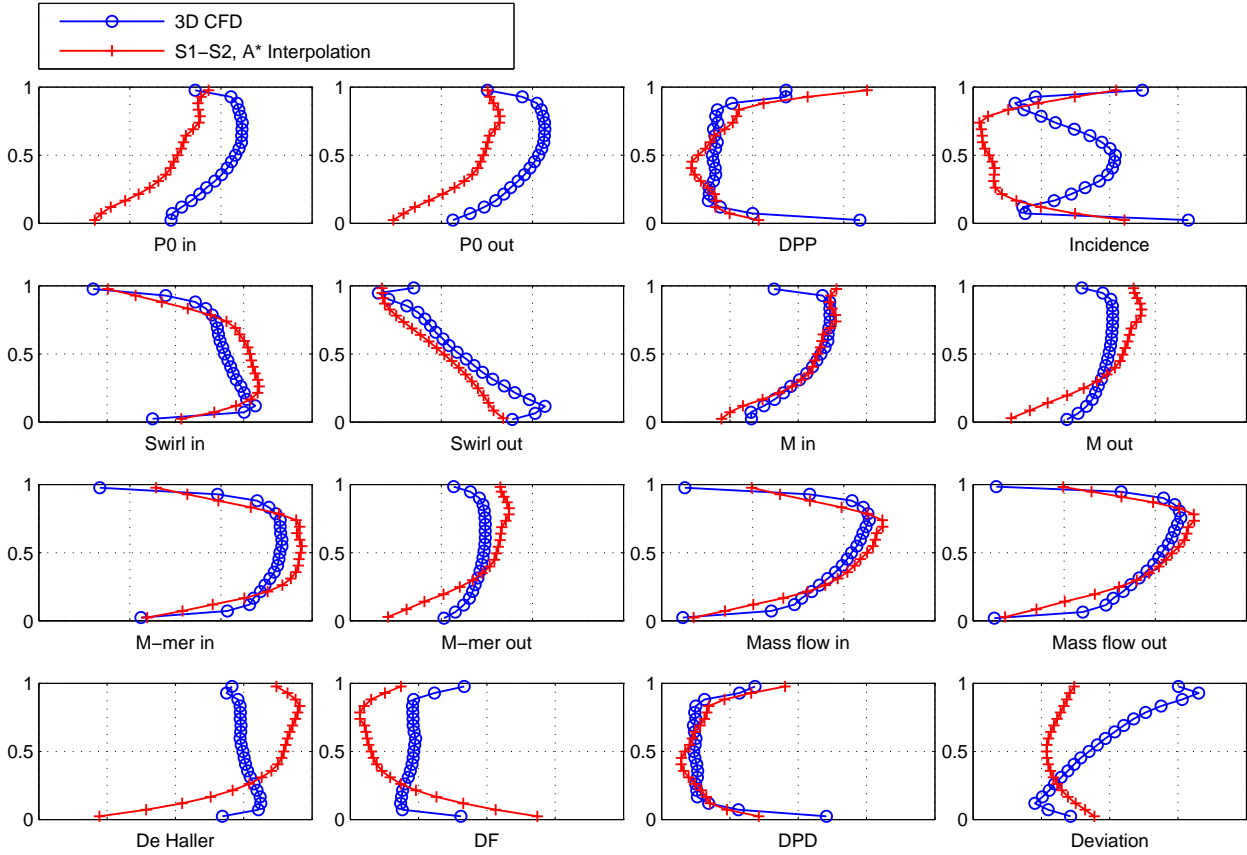


Figure 4.8: *Spanwise profiles for stator 3.*

Similar to the majority of the previous components, the profile shapes agree well with 3D CFD. A notable difference is the deviation, which has been wrongly predicted both in terms of shape and magnitude.

The stagnation pressure in and out from the component is lower than 3D CFD. This is expected, since the stagnation pressure ratio across the compressor at the operating point is under predicted by the S1-S2 system, as seen in Figure 4.1. Otherwise, the change in total pressure agrees very well also for this component, which results in the conclusion that the pressure loss consistently is well predicted by the S1-S2 system.

4.1.3 Blade To Blade Calculations

The relative Mach number contours for three blade-to-blade calculation at 90% span of the first rotor, in which the outlet pressure has been varied with $\pm 5\%$ from that of the converged S1-S2 solution, is presented in Figure 4.9.

First is should be mentioned that the contour plots show the values of every cell, and have not been interpolated. This is the reason for the spiky shapes of the contours.

It can be noted that the variation of the outlet pressure gives the expected response on the flow field. When the pressure is lowered, as depicted in Figure 4.9 (a), the blade is forced to operate close to choke. This can be seen from that the shock wave is swallowed by the blade passage. Increasing the pressure to that predicted by SC90C, as presented in Figure 4.9 (b), results in that the shock instead becomes attached to the leading edge. This is an indication that the blade operates close to maximum efficiency, Calvert and Ginder 1999. Finally, when the pressure is increased even further, the shock detaches from the leading edge, as seen in Figure 4.9 (c). The combination of a strong shock wave and the increased adverse pressure gradient also results in that the flow separates, indicating that the blade operates close to stall.

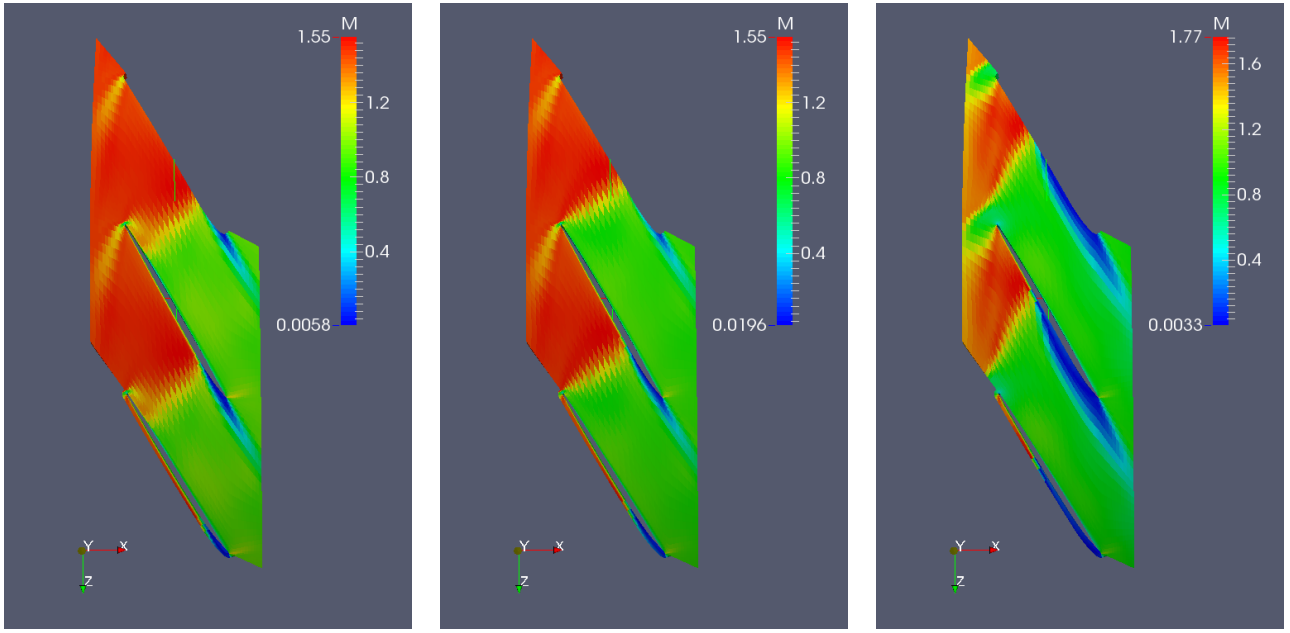


Figure 4.9: *Relative Mach number contours at different outlet pressures for rotor 1 at 90% span.*

4.2 Convergence of S1-S2 iterations

Arguably the most complicated task of building an S1-S2 calculation system is to find a way of simultaneously converging the SLC and blade-to-blade solutions. The system should be considered converged when a stable point along the operating has been found. This can only be achieved when the correction factors have converged, since only then will the same SLC solution be obtained in each iteration of the main program. In this section, this criteria is investigated.

4.2.1 Deviation Correction

The spanwise average of the deviation correction computed for each component in each iteration of the main program is presented in Figure 4.10.

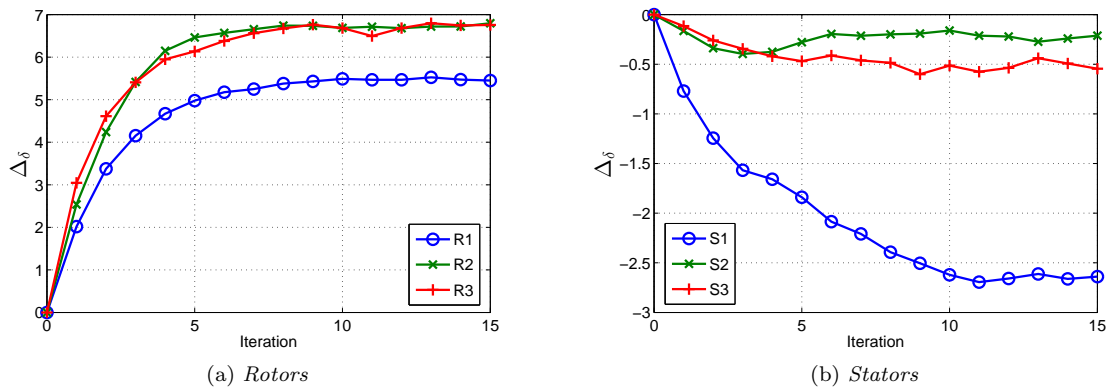


Figure 4.10: *Convergence of deviation correction, Δ_δ .*

The figures indicate that the deviation correction converges after about 10 iterations for all components except the first stator, for which about 12 iterations was needed.

It was found that when the program had found a stable point along the operating line, the solution still changed a little between each iteration, thereby making small oscillations around the stable point. These small oscillations causes a change in pressure ratio across the compressor, which in turn generally only affect the latter stages of the compressor. Therefore, the boundary conditions for the blade-to-blade method will still change slightly for the latter components between iterations. It is this that causes the small oscillations seen in the deviation correction for rotor 3 and stator 2 and 3.

4.2.2 Pressure loss Correction

The spanwise average of the pressure loss correction computed in each iteration of the main program is presented in Figure 4.11.

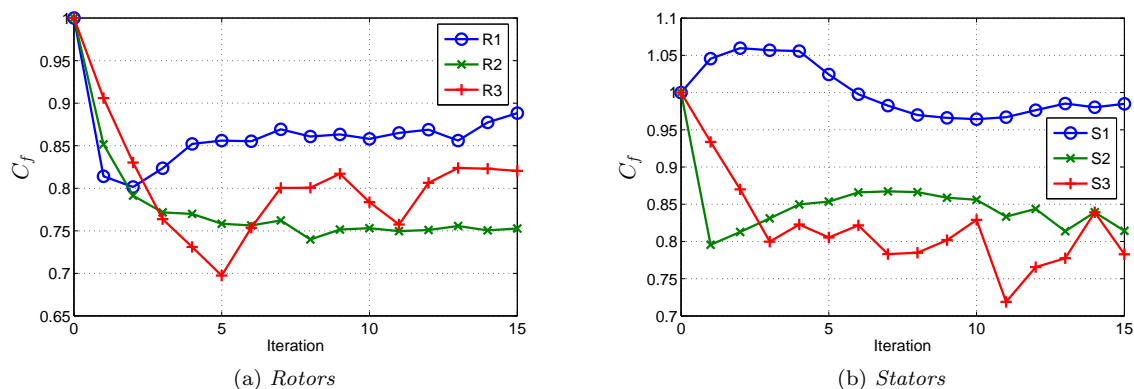


Figure 4.11: Convergence of pressure loss correction, C_f .

Apart from some oscillations, also the correction factors for the pressure loss have converged reasonably well. The oscillations are most probably due to the same reasons as for the deviation correction.

5 Discussion

5.1 Streamline Curvature Method

The SLC method will be discussed in this section. This will be done both with respect to the method and how it is implemented in SC90C, as well as its part of an S1-S2 calculation system.

5.1.1 SLC Method implemented in SC90C

The software SC90C is in the authors mind a very capable and well programmed software, which includes most of the features that has been developed over the years for SLC methods. Despite this, the experience at GKN Aerospace is that it does not predict the performance of a modern transonic compressor very well. This is one of the main reasons to why this thesis project was initiated. The question therefore arises to why it does not perform well, and what can be done to improve it.

The quick answer could be that the SLC method involves some very drastic assumptions, and therefore by default can not perform good results. This is however not the experience reported in the open literature, where several authors state that with good correlations/specifications for deviation, losses and endwall blockage, the SLC method can give very accurate predictions, Denton and Dawes 1999, Howard and Gallimore 1993. Instead, the author claims that the answer lies in the following three features

1. The Wright and Miller correlations for deviation, pressure loss and endwall blockage are outdated.
2. Placing calculating stations (QO's) inside blade rows is not possible.
3. Endwall effects on both blockage, wall shear stress and deviation is not taken into account in a proper way.

These aspects will be discussed in further detail below.

Correlations

The correlations by Wright and Miller 1991 were devised for DCA blades, which are rarely used in modern compressors. When these correlations are applied to modern compressor blades, they therefore give very different results compared to 3D CFD. The remedy to this problem is in the authors mind to use different, and more sophisticated, correlations. There are a variety of others implemented in SC90C, that have not been investigated in any detail yet. A quick solution to the problem with SC90C could therefore be to investigate these correlations in detail and asses their performance.

Calculation stations within blade rows

A feature that is not implemented in SC90C is the option of placing QO's within blade rows. This is a very severe restriction, since most other SLC codes presented in the open literature uses this option with good results, Denton 1978, Gallimore 1986, Casey and Robinson 2010.

This option comes at a cost however, since QO's placed inside blade rows requires that blade forces and blockage of the channel due to the thickness of the blades are specified as well. In SC90C, the blades are instead only accounted for by specifying the turning and losses that a blade causes.

Therefore, this option complicates the use of the SLC method, but should in turn give better results. This is because the blades are better accounted for, and the shape of the streamlines can in addition also be better resolved.

Endwall modeling

The effects of the endwalls on blockage, deviation and wall shear stress have not been accounted for in this work. The blockage could have been included through the use of blockage factors, but this approach was deemed unphysical and was therefore left out.

The effect of the endwalls on deviation is also not included in either the Wright and Miller correlations, or the blade-to-blade calculations. As was noted in the result chapter, this appears to be an important effect to

be accounted for, since the three-dimensional flow field close to hub and shroud can have a predominant effect on the flow angles. Other correlations for deviation available in SC90C can account for these effects, which further justifies the exploration of these.

Finally, the effect of wall shear stress at the hub and shroud can not be accounted for in SC90C. If these effects are accounted for, much more realistic velocity profiles in these regions can be captured with an SLC method, Howard and Gallimore 1993. This also excludes the need for blockage factors, since the reduced velocity close to hub and shroud will introduce the blockage explicitly.

5.1.2 Setup and usage within S1-S2 system

The setup of SC90C for the inclusion in the S1-S2 system was revised many times during the project. Almost all aspects of the setup, ranging from boundary conditions to mesh topology and use of physical models have been studied and considered. Despite this, there are still a set of parameters that are left for investigation and further improvement. The most important are briefly presented below.

Mesh

The most important feature of the mesh that could be improved is the number of QO's placed in the inlet and outlet ducts, as well as between components. As can be seen in Figure 3.1, very few QO's are placed in the inlet duct, and none in between components. The limited time of this project prohibited further investigation into how the number of QO's could affect the results and the stability of the code. Also, since QO's can not be placed within blade rows, the improvements on the blade-to-blade solutions could not be investigated. In general, it would probably be a great advantage, since the shape of the streamtubes is better predicted for the blade-to-blade method. This would result in that the drastic assumption of linear thickness variation between leading and trailing edge could be removed. Furthermore, the blade-to-blade method could be used to calculate blade forces for the SLC method in this case.

Correlations

The Wright and Miller correlations was adopted for a couple of reasons. First, because they were to be corrected, the actual results that they give are of little importance. Second, the correlations in themselves are relatively simple to use, with quite few input parameters for the blades having to be specified. In this work, only the 2D losses were corrected and the 3D losses were kept unchanged. This approach is not without its risks, since the correlations for different types of losses usually are developed together. Therefore, it might happen that the relative magnitude of the different losses are wrong, even though their combined magnitude is correct. This has not been investigated in this work, and hence could be a source of error.

Since the SLC method does not resolve the flow between the blades, it can not by default predict either stall or choke. Therefore, additional correlations are usually adopted to predict these effects, in order to limit the pressure ratio and mass flow. There is no information available in the documentation on which correlations that are implemented for this purpose in SC90C. In addition to this, it is not possible to correct them in any way either. Hence, the current S1-S2 system offers no improvement to predict these limits. At best, the flow conditions in the blade-to-blade solutions can be studied explicitly to see if the flow is close to either limit.

Physical Models

The use of spanwise mixing was included since it has been reported that it is vital for obtaining good results from SLC methods, Gallimore 1986. The exact effects of this feature have not been investigated in further detail however. Also, appropriate values for the mixing parameter used to determine the magnitude of the mixing has not been evaluated, but instead the default value suggested by the SC90C manual was used.

5.2 Computational Fluid Dynamics

In this section, the blade-to-blade calculations will be discussed. This will be done both with respect to the software and the physics being modeled, as well as the setup and use within the S1-S2 system.

5.2.1 Modeling and CFD software

The CFD solver used in this work, including all the numerics and how the governing equations are formulated, is very well validated. There is thus no reason to believe that any major source of error is introduced by the numerics. Therefore, the focus will be put on the turbulence modeling and the streamtube source term used instead.

Turbulence modeling

To date, no other turbulence model than the standard $k - \varepsilon$ model has been implemented into the blade-to-blade software. Consequently, comparisons between different models has not been possible. It can therefore not be stated that the choice of turbulence model is completely justified. All that can be said is that the $k - \varepsilon$ model has been used in 3D simulations on grids with similar wall normal resolution with good results.

Therefore, it is still possible that some errors are introduced in the turbulence modeling. However, due to the successful use of the $k - \varepsilon$ model in 3D, it is expected that the largest errors lie elsewhere.

Streamtube Source Term

The source term used in this work presents a novel method of performing Q3D blade-to-blade calculations. The most appealing feature about it is probably the simplicity of use compared to conventional blade-to-blade methods. This is because the same meshing algorithms that is used for 3D calculations can be used, the only difference is that the mesh only is made one cell thick.

Ellbrant [Ellbrant] have also validated the method and reported very good results. It is therefore not expected that the source term in itself have introduced any major errors into the solutions.

5.2.2 Setup and use within S1-S2 system

The largest source of error introduced by the blade-to-blade calculations is probably the setup of the computational domain, where several assumptions were made.

Computational domain

Several simplifications have been done when the computational domain is created. The most important are the assumptions of axisymmetric shape, linear thickness variation and extension of domain with constant radius.

The axisymmetry assumption is not expected to be the largest source of error. It is also an assumption that can not be taken away, since the SLC method that provides boundary conditions assumes the same thing.

The errors introduced by the thickness and overall shape of the streamtube are probably larger. It is well known that correct specification of streamtube thickness is critical for obtaining good results from blade-to-blade calculations, Denton and Xu 1999, Denton and Dawes 1999. This comes from that the thickness variation strongly affects the velocity and position of shock waves. Therefore, even though care was taken in the calculation of the thickness at the leading and trailing edge, the linear thickness variation is between is probably a too rough assumption in order to obtain good results.

5.3 S1-S2 Calculation System

The S1-S2 calculation system will be discussed in this section. This will be done both with respect to S1-S2 systems in general, as well as the implementation applied in this work.

5.3.1 General

An S1-S2 system is in theory a very appealing method for a number of different reasons. Among the most important are

- Low computational cost compared to 3D CFD.
- Flow past blades can be studied in detail.
- Blade design can be tailored by CFD.

- Natural step in between SLC and 3D CFD methods for design and analysis.

Considering these advantages, it is still a fact that the results obtained in this work not are good enough to be included in a design process, even though they show good potential. This raises the question whenever the S1-S2 approach is worth to continue working with.

To begin with, it should be noted that S1-S2 systems have been implemented before with very good results, Calvert and Stapleton 1994. Therefore, considering the advantages listed above, the author would argue that some coupling of the S1 and S2 surfaces still is a good approach. If this is to be done, there is still the option of automating this coupling or not.

Non automated coupling

There is the option of doing a non automated coupling between the S1 and S2 surfaces when designing a compressor. This can be achieved by first specifying a desired loss and distribution for each blade, and then letting the SLC code calculate the compressor performance based on this input. This further means that no correlations are needed. After this, a blade-to-blade method can be used to design the blades to meet the requirements set up in terms of work and loss. The SLC solution can further be used to obtain boundary conditions for the blade-to-blade method. If it is found that the specified blade performance can not be met, the input for the SLC method must be revised, and the process restarted since new streamtube shapes and boundary conditions for the blade-to-blade method is obtained. The blade design in itself could further be coupled with an optimization system, that automates the design towards the requirements set. This approach is clearly more suited for obtaining new designs, rather than analyzing existing designs. It also requires an experienced designer to set up realistic parameters for the compressor.

Automated coupling

The option of automating the coupling gives the advantage of being able to directly obtain the performance of a given design. It can also be used for design purposes, but in this case the program would work in the opposite direction compared to non automated coupling. This means that the blade design is initially set, and the performance in terms of loss and work becomes a function of it. This requires that the blades are continuously redesigned until the performance sought is obtained. If the computational time is kept low, the program could also be coupled with an optimization tool that redesigns the blades until the whole compressor meets the requirements set.

5.3.2 Implementation

The implementation of the coupling was done in the Python 3 programming language. This proved to be a very good choice, since the language is very well suited for scripting as well as passing and processing data.

The structure of the program is fairly straight forward, and no major changes are therefore found necessary. Also, since the majority of the computational time is spent by the CFD code, there is no need to optimize the code any further. This further justifies the use of a language like Python 3, that has many built in functions and libraries compared to faster languages like C and Fortran.

5.3.3 Results

In this part, the results obtained will be briefly discussed. This includes both the results for the compressor performance as well as convergence of the results.

Characteristic Map

The characteristic map shows that the mass flow and pressure ratio are roughly 4 respectively 9% off at the operating point. This should be considered acceptable, considering that little time for improvement and tuning has been available. The results also shows that the polytropic efficiency is very well predicted within a percent of 3D CFD. Even though extensive validation has not been performed, this indicates that the correct amount of losses are predicted by the S1-S2 system.

The characteristic map also reflects the difficulty of converging the program. The speedlines predicted are far from as smooth as would be expected, indicating that a stable point is hard to find. This could probably

be much improved if a better algorithm for finding the intersection between the speedline and the current operating line would be implemented.

Spanwise profiles

The predicted spanwise profiles generally shows the same trends as 3D CFD, but as noted before are often to some extent off in terms of absolute values. In addition to this, the results are generally better in the first stages of the compressor. This is much due to that the errors introduced at each component amplifies throughout the machine, creating increasingly bad boundary conditions etc for the blade-to-blade calculations in latter stages.

Since the loss and deviation was corrected by the blade-to-blade calculations in the S1-S2 system, these will be discussed in some more detail below.

Loss The loss is the parameter among the two that has been predicted best. For the majority of the components, both the magnitude and the overall shape agrees well with 3D CFD. Furthermore, the correlations for secondary losses appear to give reasonable increase in total loss close to the hub and shroud.

Deviation The magnitude of the deviation has been hard to predict for all components, even though the shape of the profiles agree well. One reason to why could be that the deviation is evaluated at the outlet of the blade-to-blade domain, whereas it should apply at the trailing edge of the component. Even though care has been taken to preserve angular momentum through extending the domain with constant radius, it might happen that this conservation is not exactly true. A possible remedy could be to perform the flux averaging at a plane closer to the trailing edge, that does not coincide with the actual outlet of the domain.

Convergence of S1-S2 Iterations

The convergence of the correction factors shows that the formulas for calculating and updating both the deviation and loss correction works. All factors appear to tend to some value, even though convergence problems prohibit them from completely stabilizing.

As noted before, the oscillations in the results reflect the problems for the program to converge towards a stable point along the operating line. In each iteration of the main program, the intersection between the speedline calculated by SC90C and the operating line set must be found. The algorithm implemented for this purpose is not to be considered good enough. This problem was identified late in the project, and there was consequently not much time to implement a better one. A better algorithm for this should both solve the problem of oscillations in the correction factors, as well as give a smoother slope of the speedline. It would probably not solve the problems with lower pressure ratio and mass flow though.

References

- Andersson, J. D. (2004). *Modern Compressible Flow: With Historical Perspective*. 3rd ed. McGraw-Hill Education. ISBN: 007-124136-1.
- Andersson, N. (2005). “A Study of Subsonic Turbulent Jets and Their Radiated Sound Using Large-Eddy-Simulation”. PhD Thesis. Gothenburg, Sweden: Department of Applied Mechanics, Chalmers University of Technology. ISBN: 91-7291-679-6.
- Burak, M. O. (2010). “Large Eddy Simulation for the Analysis of Supersonic Jet Noise Suppression Devices”. PhD Thesis. Gothenburg, Sweden: Department of Applied Mechanics, Chalmers University of Technology. ISBN: 978-91-7385-459-7.
- Calvert, W. J. and R. B. Ginder (1999). Transonic Fan and Compressor Design. *Proceedings of the Institution of Mechanical Engineers* **213.5**, 419–436. DOI: 10.1243/0954406991522671.
- Calvert, W. J. and A. W. Stapleton (1994). Detailed Flow Measurements and Predictions for a Three-Stage Transonic Fan. *Journal of Turbomachinery* **116.2**, 298–305. DOI: 10.1115/1.2928364.
- Casey, M. and C. Robinson (2010). A New Streamline Curvature Throughflow Method for Radial Turbomachinery. *Journal of Turbomachinery* **132.3**, 031021–1–031021–10. DOI: 10.1115/1.3151601.
- Denton, J. D. (1978). Throughflow Calculations for Transonic Axial Flow Turbines. *Journal of Engineering for Gas Turbines and Power* **100.2**, 212–218. DOI: 10.1115/1.3446336.
- Denton, J. D. and W. N. Dawes (1999). Computational Fluid Dynamics for Turbomachinery Design. *Proceedings of the Institution of Mechanical Engineers* **213.2**, 107–124. DOI: 10.1243/0954406991522211.
- Denton, J. D. and L. Xu (1999). The exploitation of three-dimensional flow in turbomachinery design. *Journal of Mechanical Engineering* **213.2**, 125–137. DOI: 10.1243/0954406991522220.
- Dixon, S. L. and C. A. Hall (2013). *Fluid Mechanics and Thermodynamics of Turbomachinery*. 7th ed. Butterworth-Heinemann. ISBN: 978-0-12-415954-9.
- Ellbrant, L. and L.-E. Eriksson (2014). *General 3D Streamtube CFD Solver*. Internal Report. Gothenburg: Dept. of Applied Mechanics, Chalmers University of Technology. To be published.
- Eriksson, L.-E. (1995). *Development and validation of highly modular flow solver versions in G2DFLOW and G3DFLOW*. Internal Report 9970-1162. Trollhättan: Volvo Aero Corporation.
- Gallimore, S. J. (1986). Spanwise Mixing in Multistage Axial Flow Compressors: Part II - Throughflow Calculations Including Mixing. *Journal of Turbomachinery* **108.1**, 10–16. DOI: 10.1115/1.3262009.
- Howard, M. A. and S. J. Gallimore (1993). Viscous Throughflow Modelling for Multistage Axial Compressor Design. *Journal of Turbomachinery* **115.2**, 296–304. DOI: 10.1115/1.2929235.
- Hu, J. F. et al. (2011a). An improved streamline curvature approach for transonic axial compressor performance prediction. *Proceedings of the Institution of Mechanical Engineers* **225.5**, 575–584. DOI: 10.1177/09544100JAERO772.
- (2011b). Performance prediction of transonic axial compressor based on streamline curvature method. *Journal of Mechanical Science and Technology* **25.12**, 3037–3045. DOI: 10.1007/s12206-011-0817-x.
- Korpela, S. A. (2011). *Principles of Turbomachinery*. John Wiley & Sons, Inc. ISBN: 978-0-470-53672-8.
- Miller, R. J. and J. D. Denton (2012). “Loss Mechanisms in Turbomachines”. *Cambridge Turbomachinery Course*. Vol. 1.
- Olausson, M. (2011). “Turbomachinery Aeroacoustic Calculations using Nonlinear Methods”. PhD Thesis. Gothenburg, Sweden: Department of Applied Mechanics, Chalmers University of Technology. ISBN: 978-91-7385-481-8.
- Pachidis, V. et al. (2007). Prediction of Engine Performance Under Compressor Inlet Flow Distortion Using Streamline Curvature. *Journal of Engineering for Gas Turbines and Power* **129.1**, 97–103. DOI: 10.1115/1.2363414.
- Pullan, G. (2012). “Introduction to Numerical Methods for Predicting Flow in Turbomachines”. *Cambridge Turbomachinery Course*. Vol. 2.
- SC90C (2011). *A streamline curvature program for axial flow compressors*. Version 8-0. PCA Engineers Ltd.
- Sonntag, R. E., C. Borgnakke, and G. J. Van Wylen (1998). *Fundamentals of Thermodynamics*. 5th ed. John Wiley and Sons, Inc. ISBN: 0-471-18361-X.
- Templalex, I. et al. (2011). Development of a Two-Dimensional Streamline Curvature Code. *Journal of Turbomachinery* **133.1**, 011003–1–011003–7. DOI: 10.1115/1.2720877.
- Versteeg, H. K. and W. Malalasekera (2007). *Computational Fluid Dynamics, The Finite Volume Method*. 2nd ed. Pearson Education Limited. ISBN: 978-0-13-127498-3.

Wilcox, D. C. (1998). *Turbulence Modeling for CFD*. 2nd ed. D C W Industries. ISBN: 978-0-96-360515-3.
Wright, P. I. and D. C. Miller (1991). *An Improved Compressor Performance Prediction Model*. Report C423/028.
Derby: Rolls-Royce plc.

A Flux Equivalent Flow Variables

In this appendix, the flux equivalent flow variables are derived.

A.1 Average Fluxes

The derivation starts by evaluating the average flux of mass, momentum, energy, turbulent kinetic energy and dissipation of turbulent kinetic energy across the boundary. This is done based on only the convective contribution to the total flux across the boundary. To simplify the derivation here, the normal vector to the boundary is assumed to be aligned with the x-axis. This is no infringement in this work, since all inlet and outlet boundaries satisfy this condition. The average mass flux across the boundary can then be calculated as

$$f_m = \frac{\sum_{k \in \partial\Omega_b} [\bar{\rho} \tilde{u}_x \cdot S]_k}{\sum_{k \in \partial\Omega_b} S_k}, \quad (\text{A.1})$$

where $\partial\Omega_b$ is the set of all cell faces belonging to the boundary and S_k the area of face k . Furthermore, the average flux of axial, tangential and radial momentum becomes

$$f_{p,x} = \frac{\sum_{k \in \partial\Omega_b} [(\bar{\rho} \tilde{u}_x^2 + p) \cdot S]_k}{\sum_{k \in \partial\Omega_b} S_k}, \quad (\text{A.2})$$

$$f_{p,\theta} = \frac{\sum_{k \in \partial\Omega_b} [\bar{\rho} \tilde{u}_x \tilde{u}_\theta \cdot S]_k}{\sum_{k \in \partial\Omega_b} S_k}, \quad (\text{A.3})$$

$$f_{p,r} = \frac{\sum_{k \in \partial\Omega_b} [\bar{\rho} \tilde{u}_x \tilde{u}_r \cdot S]_k}{\sum_{k \in \partial\Omega_b} S_k}. \quad (\text{A.4})$$

The velocities at the cell face in the tangential and radial direction can be obtained by converting the Cartesian coordinates used in the solver. Next the average energy flux across the boundary is calculated as

$$f_e = \frac{\sum_{k \in \partial\Omega_b} [(\bar{\rho} \tilde{e}_0 \tilde{u}_x + \bar{p} \tilde{u}_x) \cdot S]_k}{\sum_{k \in \partial\Omega_b} S_k}. \quad (\text{A.5})$$

Finally, the average flux of turbulent kinetic energy and the dissipation of turbulent kinetic energy becomes

$$f_k = \frac{\sum_{k \in \partial\Omega_b} [\bar{\rho} \tilde{u}_x k \cdot S]_k}{\sum_{k \in \partial\Omega_b} S_k}, \quad (\text{A.6})$$

$$f_\varepsilon = \frac{\sum_{k \in \partial\Omega_b} [\bar{\rho} \tilde{u}_x \varepsilon \cdot S]_k}{\sum_{k \in \partial\Omega_b} S_k}. \quad (\text{A.7})$$

The average fluxes are evaluated directly in the CFD code and will be used to calculate the flux equivalent properties, as will be presented next.

A.2 Flux Equivalent Properties

The flux equivalent properties are defined in terms of the average fluxes according to

$$f_m = \hat{\rho} \hat{u}_x, \quad (\text{A.8})$$

$$f_{p,x} = \hat{\rho} \hat{u}_x^2 + \hat{p}, \quad (\text{A.9})$$

$$f_{p,\theta} = \hat{\rho} \hat{u}_x \hat{u}_\theta, \quad (\text{A.10})$$

$$f_{p,r} = \hat{\rho} \hat{u}_x \hat{u}_r, \quad (\text{A.11})$$

$$f_e = \hat{\rho} \left(\hat{e} + \frac{\hat{u}_k \hat{u}_k}{2} + \hat{k} \right) \hat{u}_x + \hat{p} \hat{u}_x. \quad (\text{A.12})$$

$$f_k = \hat{\rho} \hat{u}_x \hat{k}, \quad (\text{A.13})$$

$$f_\varepsilon = \hat{\rho} \hat{u}_x \hat{\varepsilon}. \quad (\text{A.14})$$

The ideal gas law (2.8) together with the equations for the internal energy (2.13) and the specific heat (2.12) can be used to rewrite the internal energy in (A.12) in terms of the flux equivalent density and pressure. The remaining system of equations can be used to form a quadratic equation for $\hat{\rho}$, which has the following two solutions

$$\hat{\rho}_1 = \frac{1}{2} \frac{\xi_2}{\xi_1} + \sqrt{\frac{1}{4} \left(\frac{\xi_2}{\xi_1} \right)^2 - \frac{\xi_3}{\xi_1}}, \quad (\text{A.15})$$

$$\hat{\rho}_2 = \frac{1}{2} \frac{\xi_2}{\xi_1} - \sqrt{\frac{1}{4} \left(\frac{\xi_2}{\xi_1} \right)^2 - \frac{\xi_3}{\xi_1}}, \quad (\text{A.16})$$

where

$$\xi_1 = \frac{f_e}{f_m} - \frac{1}{2} \left(\left(\frac{f_{p,r}}{f_m} \right)^2 + \left(\frac{f_{p,\theta}}{f_m} \right)^2 \right) - \hat{k}, \quad (\text{A.17})$$

$$\xi_2 = f_{p,x} \left(\frac{\gamma}{\gamma - 1} \right), \quad (\text{A.18})$$

$$\xi_3 = f_m^2 \left(\frac{\gamma}{\gamma - 1} - \frac{1}{2} \right). \quad (\text{A.19})$$

Two solutions are also obtained for the remaining properties, reading

$$\hat{u}_{x,i} = \frac{f_m}{\hat{\rho}_i}, \quad (\text{A.20})$$

$$\hat{u}_{\theta,i} = \frac{f_{p,\theta}}{f_m}, \quad (\text{A.21})$$

$$\hat{u}_{r,i} = \frac{f_{p,r}}{f_m}, \quad (\text{A.22})$$

$$\hat{p}_i = f_{p,x} - \frac{f_m^2}{\hat{\rho}_i}, \quad (\text{A.23})$$

$$\hat{k}_i = \frac{f_k}{f_m}, \quad (\text{A.24})$$

$$\hat{\varepsilon}_i = \frac{f_\varepsilon}{f_m}, \quad (\text{A.25})$$

where $i = 1, 2$ denotes either the first or second solution. The two solutions represent a subsonic and a supersonic one. In cases where the flow is subsonic in the normal direction of the boundary, the first solution is valid. In the opposite case, where the flow is supersonic, the second solution is valid.

The flux equivalent stagnation enthalpy can be obtained directly according to

$$\begin{aligned} \hat{h}_{0,i} &= \hat{e} + \frac{\hat{p}}{\hat{\rho}} + \frac{\hat{u}_k \hat{u}_k}{2} + \hat{k} \\ &= \frac{f_e}{f_m}. \end{aligned} \quad (\text{A.26})$$

The static enthalpy is calculated by subtracting the kinetic energy (mean + turbulent) from the stagnation enthalpy. The flux equivalent stagnation temperature and pressure are obtained from the corresponding enthalpy via (2.14) and the ideal gas law (2.8). Furthermore, the flux equivalent speed of sound can be calculated from (2.49) which in turn can be used to calculate the Mach number using (2.48). Finally, the stagnation pressure can be obtained from (2.53).